Human visual-vestibular interaction during curvilinear motion in VR

A thesis

submitted in fulfilment

of the requirements for the degree

of

Doctor of Philosophy in Psychology

at

The University of Waikato

by

Aden C. Garnett

THE UNIVERSITY OF
WAIKATO
Te Whare Wānanga o Waikato

2020

Abstract

When people move through the world they use retinal image motion to form an estimate of self-motion, although how this is achieved is not yet fully understood. Furthermore, the process is not fool-proof and many conditions create incorrect percepts of self-motion. In particular, experiencing rotation makes it difficult for humans to correctly perceive heading during movement from visual input alone.

Here we re-examined human perception of rotation during true and simulated curvilinear motion. Broadly, this was done by simulating movement along various paths using currently available head-mounted stereoscopic virtual reality displays. These displays overcome many of the shortcomings of historical equipment but also represent a significant departure from established setups. As such, the first two experiments, presented together in Chapter 2, replicated experiments from Banks, Ehrlich, Backus, and Crowell (1996) and Crowell, Banks, Shenoy, and Andersen (1998). This was to aid in determining the suitability of consumer-grade virtual reality headsets for self-motion perception research and to provide a point of comparison between this thesis and historical works.

Following confirmation that the VR devices were suitable for research we developed a virtual line-based bendable response tool. This tool made use of tracked hand controllers to facilitate fast and intuitive reporting of self-motion perception without confounding heading and rotation perception errors. Using this tool we confirmed reports of curvilinear motion perception during linear travel with rotation. We then measured perception of heading and curvature during travel on linear paths of increasingly eccentric heading, finding that eccentric headings elicited perceptions of curvature. We also measured perceptions of travel along curvilinear paths so that a model of human visual-vestibular interaction (Perrone, 2018) as it applies to heading perception could be tested against participant per-

formance. Finally, predictions from this model prompted us to measure curvilinear path perception while using a rotating chair that allowed us to provide a rough congruent vestibular signal.

Overall, we found consistent large individual differences in perception across all motion types, although each individual's perceptions were internally consistent. Furthermore, we found that participants perceived curvature while travelling on not only curvilinear paths, but also on linear paths with rotation and linear paths with eccentric headings. The tested model, as implemented, matched participant results well, proving able to explain the majority of the individual differences. Finally, we found that providing a rough congruent vestibular signal resulted in participants perceiving less curved paths compared to when the vestibular signal indicated no rotation.

Acknowledgements

Thank you Ma and Dad for your support throughout my entire journey. Thank you John for being a fantastic supervisor – it has helped made my research so far incredibly fun and interesting. Thank you Robert for your positive input on my progress. Thank you to the School of Psychology staff for handling so many of the details that I wouldn't know how to do myself.

Thank you to the University of Waikato, the Traffic and Road Safety research group, the Claude McCarthy Fellowship, and, through John, the MBIE Endeavour fund, for providing the scholarships, funding, and equipment that made this thesis possible.

Contents

List of Figures

Introduction

Humans are are capable of skilfully moving through the world. We avoid obstacles, intercept targets, negotiate tight curves, and spin while dancing. While doing this we manage to keep track of where we are and where we are going. Successfully doing so requires accurate perception of self-motion. How we achieve this is not yet fully understood, but in order to develop this perception we rely on information provided by our senses.

1.1 What we see

The key sense for human navigation is vision. Patterns of light falling on the retinae provide information about the location and movement of objects in the environment. When the observer moves, these patterns of light change as the navigator alters their position relative to objects in the world.

Different movements produce different patterns over time, but in the mid-nineteen-hundreds Gibson (1950, 1966) demonstrated that the simplest case – *linear translation* (moving in a straight line) – produces an image where points in the scene expand radially out from the direction of travel over time. An example of this can be seen in Figure 1.1(a). In this example, the observer is travelling in a straight line towards the orange circle while looking towards the blue cross. All other points in the image, depicted by the origin of each arrow, appear to be moving out from the orange circle at a rate proportional to their arrow length. The corresponding top-down view of this motion can be seen in Figure 1.2(a).

Gibson termed this time varying change in the pattern of light falling on the retinae *optic flow*, and the point from which all others appeared to radiate the *focus of expansion* (FOE). Furthermore, in the course of his analysis, he proved

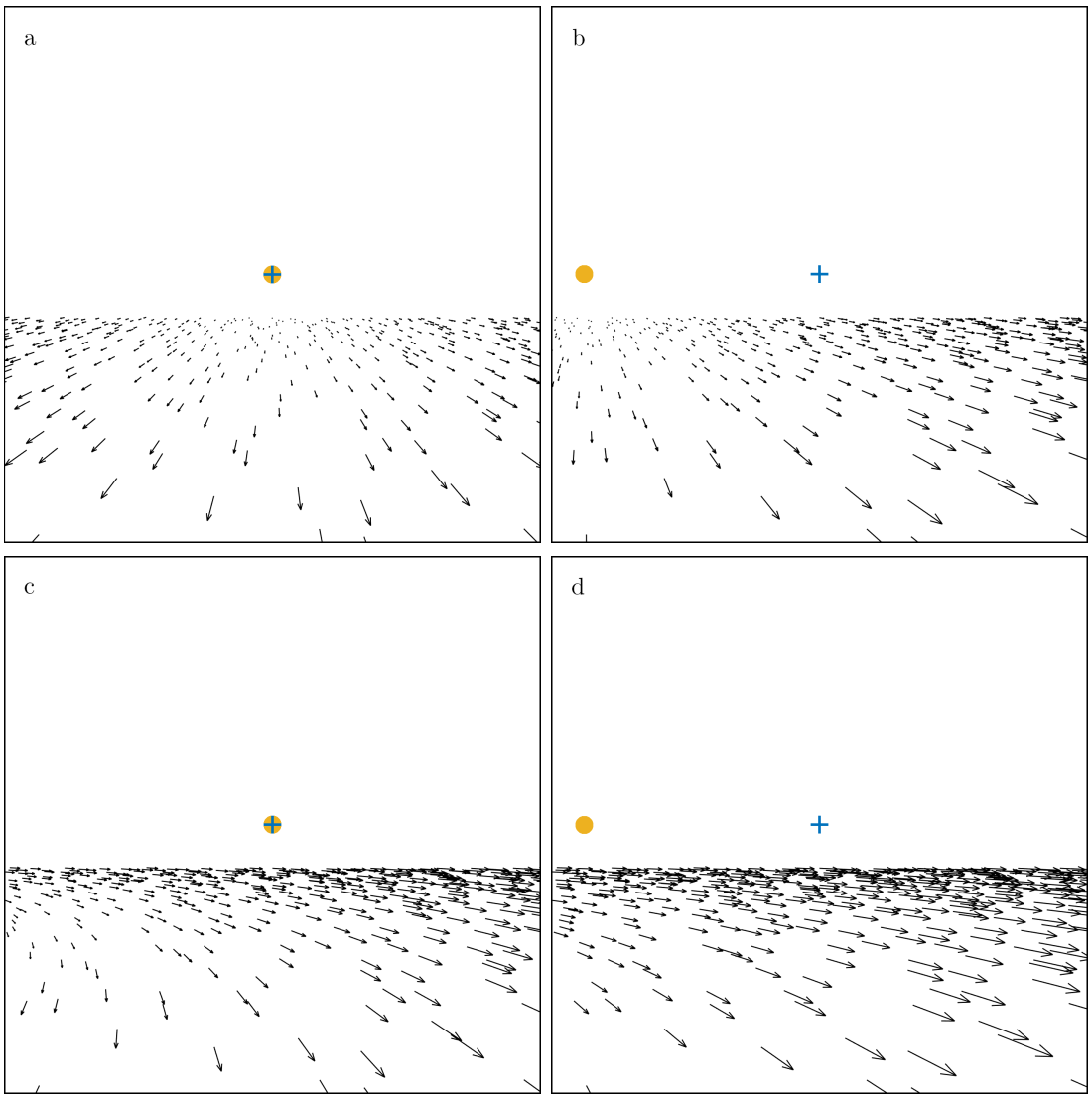

Figure 1.1: Example flow fields: (a) Linear translation with either (b) heading displaced 20° left of view direction, (c) rotation counter-clockwise at $7.5^{\circ}s^{-1}$, or (d) both.

for linear translation that the optic flow field contains sufficient information to determine observer heading. This holds even where the direction of travel does not coincide with the view direction, as can be seen in Figures 1.1(b) and 1.2(b). Here, even though the direction of travel is displaced 20° left from the gaze direction all points in the scene still appear to radiate out from the direction of travel. Whether or not the navigator can actually determine heading from this flow field is of interest because an estimate of *instantaneous heading* (heading at a particular point in time) is required for obstacle avoidance and depth estimation. Subsequent work (Cutting, 1986; Rieger & Toet, 1985; Stone & Perrone, 1997; W. H. Warren,

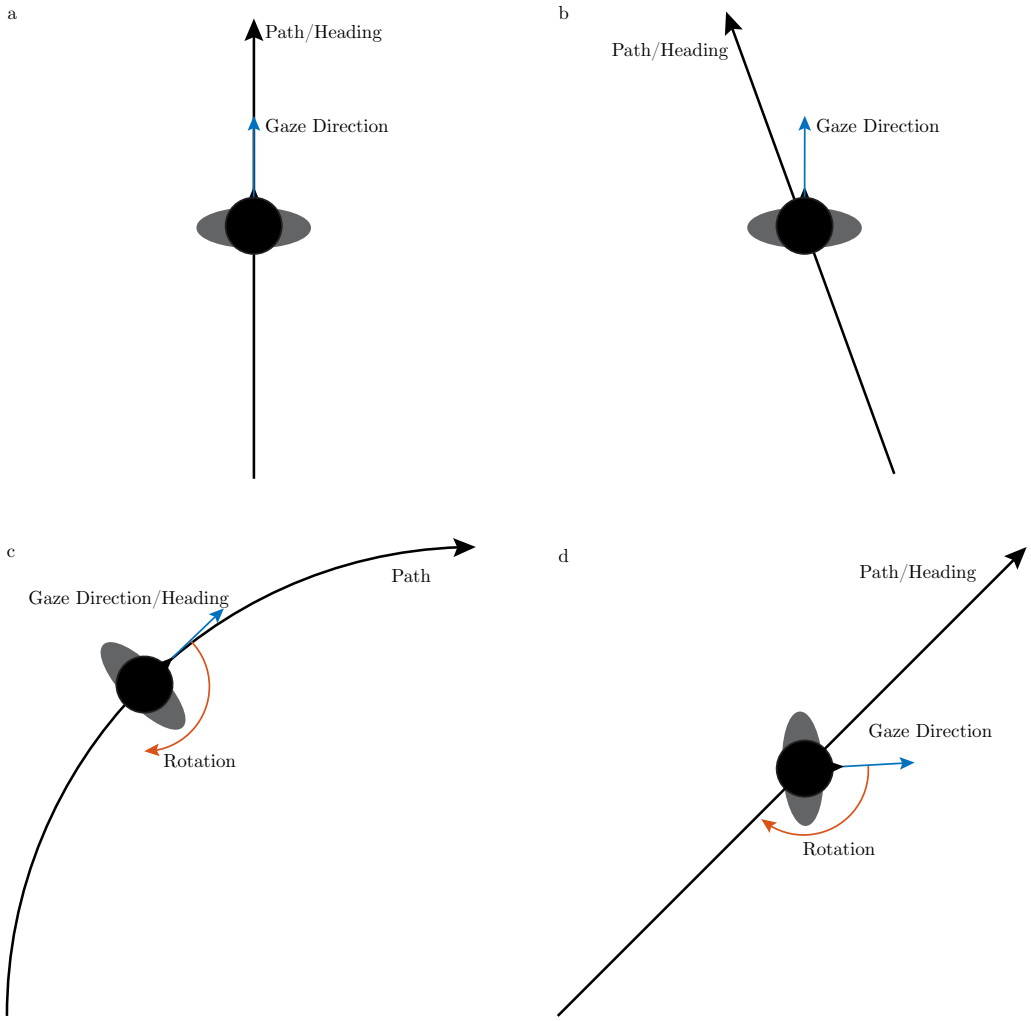

Figure 1.2: (a) Example linear path, (b) linear path with eccentric heading, (c) curvilinear path and (d) linear path with rotation.

Morris, & Kalish, 1988) confirmed that humans, using only visual cues, could indeed determine their heading with reasonable accuracy during linear translation.

The process of determining heading is complicated, however, by the presence of eye and head rotations as well as by full body turns (e.g. Figure 1.2(d)). When these rotations occur the optic flow field is distorted and, as a result, the FOE no longer coincides with the direction of travel (Priest, Cutting, Torrey, & Regan, 1985; Regan & Beverley, 1982; Van den Berg, 1992; Royden, 1994; W. H. Warren et al., 1988; W. H. Warren & Hannon, 1990). Examples of this distortion can be found in Figures 1.1(c) and (d). In these examples the observer is still travelling in the same direction and at the same speed as in the previous examples (Figures

1.1(a) and (b) respectively). However, with the addition of a rotation component vectors in the flow field no longer radiate out from a single point in the image. The same issue occurs with travel around a curved path as seen in Figure 1.2(c) as the instantaneous flow field is identical for both cases. This means that heading is not immediately available through finding the point from which the flow field radiates as this point no longer exists. Heading, therefore, has to be determined by some other method. This is what is known as the *rotation problem*, a problem that remains unsolved. There have been, however, numerous attempts to develop a model of how the brain could obtain heading from visual signals in isolation.

1.1.1 Models of visual navigation

Historically, models restricting themselves to only visual input have fallen into one of three broad groups based on the process of obtaining heading from the flow field. As one of the main hurdles to retrieving heading is the presence of rotation in the scene these groupings are therefore broadly characterised by how they separate, or not, flow generated by rotation from flow generated by translation. These categories of model are vector decomposition, motion parallax, and error minimisation based models.

Vector decomposition models, assuming that the brain can derive motion vectors for points in the optic flow field, decompose said vectors into their rotational and translational components. There are various specific implementations of the process ranging from static comparison (e.g. Longuet-Higgins, 1981; Tsai & Huang, 1981; Weng, Huang, & Ahuja, 1989) to differential comparison (e.g. Crowell, Banks, & Royden, 1989; Hanada & Ejima, 2000; Hildreth, 1992; Royden, 1997). The general approach of these implementations, however, makes use of the invariance of the rotational component of vectors near each other in two-dimensional image space but at different depths in the world. Since rotation is common to all vectors and independent of depth, vector subtraction leaves only the translational component of the vector.

For example, if you take two vectors close in two-dimensional image space but originating with two points at different depths in the world, each with a translation

and a rotation component:

$$V_1 = T_1 + R_1$$

$$V_2 = T_2 + R_2$$

And the rotation component is uniform:

$$R_1 = R_2$$

Comparison of such vectors allows the cancellation of the rotational field component, leaving only the translational component of the two vectors.

$$\therefore \quad (T_1 + R_1) - (T_2 + R_2) = T_1 - T_2 = T$$

When this is repeated for all pairs of vectors in the flow field what remains is a field with half as many vectors that only contain a translational component. This flow field, therefore, has a FOE from which we can determine heading. This approach does have its limitations however. First, there are half as many vectors to use for determining heading. Furthermore, when there is little depth between V_1 and V_2 subtracting T_2 from T_1 results in a vector T that is approximately zero. This results in a loss of information, something that becomes particularly apparent in scenes where there is little to no depth (Perrone, 2018).

Motion parallax models also make use of differences in the three-dimensional depth of points from which vectors originate (Cutting, 1986; Eriksson, 1974). In this case, however, the models are interested in the relative differences in motion caused by motion parallax rather than the invariance of rotation across depth. Generally objects that are closer to the observer appear to move faster than those further away. By re-projecting the flow field into polar coordinates objects that are closer to the observer than the observer's fixation point appear to move away from the direction of travel while objects that are further than the fixation point appear to move towards the heading direction. By shifting their fixation point in the opposite direction of the fastest moving object the observer can find their heading without explicitly determining their rotation.

The third broad category of model is error minimisation. While error minimisation itself is not unique to a single class of models – a number of models include iterative error minimisation to achieve more accurate results (e.g. Heeger

& Jepson, 1992; Hildreth, 1992) – error minimisation is a defining feature of models that search the optic flow field for a solution as opposed to trying to find the FOE. One major category of error minimisation models are Template models. These template models have been based on properties of area dorsal Medial Superior Temporal (MSTd) neurones (Duffy & Wurtz, 1991; Britten, 2008; Britten, Shadlen, Newsome, & Movshon, 1992; Britten & van Wezel, 1998; Tanaka, Fukada, & Saito, 1989; Tanaka et al., 1986). Template models use assemblies of motion sensors arranged to form a 'template' that can extract heading directly from the flow field without first explicitly correcting for any rotation it contains (Beintema & Van den Berg, 1998; Perrone, 1992; Perrone & Stone, 1994; A. V. van den Berg & Beintema, 1997). The 'template' tests the optic flow field by projecting flow vectors onto a line originating from the test position through the origin of the vector and then summing these projected vectors. The position producing the peak response then is taken as the heading direction, although this can be influenced by the presence of rotation to give an incorrect heading. More recently a number of these models were fashioned with realistic front ends allowing testing with both natural and abstract flow fields as input (Browning, Grossberg, & Mingolla, 2009; Perrone, 2004, 2012).

For the most part, these models have performed well, typically achieving within one or two degrees of the true heading under test conditions (Browning et al., 2009). These models do have some limitations however.

1.1.2 Limitations of the visual only approach to modelling

Historically model performance has not matched human perception. While this is not necessarily a limitation with regards to a model's ability to accurately determine heading it is a limitation when the model purports to describe the human visual system. An example of the mismatch between model behaviour and human perception can be seen with vector decomposition models. These have been shown capable of determining heading from two or three frames of motion containing seven or fewer points (Longuet-Higgins, 1981; Tsai & Huang, 1981; Weng et al., 1989). Humans have not been able to replicate this performance in psychophysical experiments due to the sparseness of the flow field. On the other hand,

models using only a few points are not tolerant to noise in the input, while human performance remains good given even relatively noisy input (W. H. Warren, Blackwell, Kurtz, Hatsopoulos, & Kalish, 1991).

Furthermore, while these models can determine heading in the presence of rotation and while humans can determine heading in the presence of low ($<|1.2|^{\circ}s^{-1}$, i.e. walking around a gentle curve) rates of rotation (W. H. Warren & Hannon, 1988, 1990) it appears that, in contrast to vector decomposition models, humans cannot process high levels of visual rotation using visual stimuli alone (Royden, Banks, & Crowell, 1992).

1.1.3 Efference signals

While not always recognised as essential (W. H. Warren & Hannon, 1990), one well considered (Crowell et al., 1998; Holst & Mittelstaedt, 1950; Sperry, 1950; Bridgeman, 2007) explanation for part of this ability to determine heading in the presence of rotation is that the brain makes use of efference signals generated by active eye and head movements to compensate for eye and head rotations. These signals are generated alongside the motor commands for the eyes and neck (Perrone & Krauzlis, 2008; Sperry, 1950; Holst & Mittelstaedt, 1950) and it has been shown that the presence of the active movements that would generate these signals allows for consistently accurate performance during eye (Banks et al., 1996) and head (Crowell et al., 1998) rotations. Furthermore, performance is degraded in scenarios where participants view displays without moving their eyes and so produce no efference signals (Banks et al., 1996) thus challenging differential motion models which suggest that this should not occur. In light of human data some models have been expanded to include efference signals (Beintema & Van den Berg, 1998; Perrone & Krauzlis, 2008).

While the role of efference signals in visual navigation involving eye or head rotation is well established it is not so clear that efference signals can provide feedback on the expected flow changes generated while travelling around curved paths as in Figure 1.2(c) or while experiencing a skid as in Figure 1.2(d). When travelling along a curve the body rotates relative to the reference frame of the external world therefore efference copies generated by eye and head movement

are unavailable. Furthermore, the brain appears unable to use either the efference signals associated with lower body motion or the subsequent somatosensory and proprioceptive information in determining heading (Telford, Howard, & Ohmi, 1995). Since humans cannot accurately determine heading in the presence of rotation without some signal containing rotation information beyond what is provided by visual stimulus alone the rotation problem with respect to curvilinear motion remains unsolved.

1.2 The vestibular system

In the absence of a usable efference signal a suitable substitute input could be provided by the vestibular system. The vestibular system is already known to be associated with the visual system, for example in the form of the vestibulo-ocular reflex (Angelaki, 2004; Angelaki & Cullen, 2008). Recent neurophysiological work in monkeys also suggests that vestibular information is integrated with visual information during heading perception. Given this, the vestibular system presents a plausible source for the information required to correctly perceive travel around curved paths.

Capable of sensing inertial motion, the vestibular system and in particular the semi-circular canals respond in a predictable manner to rotation of the head (Angelaki & Cullen, 2008; Fitzpatrick, Butler, & Day, 2006). In addition, they are closely linked with the human ability to correctly sense (Ivanenko, Grasso, Israël, & Berthoz, 1997) and control (Fitzpatrick et al., 2006; Lepecq et al., 2006) motion through the world. However, while humans are capable to some degree of finding their heading in darkness using vestibular signals alone the precision of the vestibular system is inferior to that of the visual system even with clean supra-threshold accelerations (MacNeilage, Banks, DeAngelis, & Angelaki, 2010). In spite of this lower precision, however, the vestibular system could still facilitate an improvement in heading discrimination ability when combined with vision by providing an independent measure of rotation relative to the world.

Neurophysiological work provides strong support for the idea that vestibular signals are involved in the processing of visual input during heading determination. It has been shown in Rhesus monkeys that visual and vestibular information is

generally integrated such as would be expected in a system attempting to reduce the effect of world-centric rotations on the flow field (Takahashi et al., 2007). Also in Rhesus monkeys the MSTd area, understood to represent heading in the brain (Maciokas & Britten, 2010), receives vestibular input in addition to its primary visual input (Fetsch, DeAngelis, & Angelaki, 2010; Gu, Watkins, Angelaki, & DeAngelis, 2006; Takahashi et al., 2007). Even within this one overall area of the brain it has been shown that vestibular input has a range of effects at a neuronal level, improving heading selectivity in some cells and decreasing it in others (Fetsch et al., 2010). Furthermore, the ventral intraparietal (VIP) and visual posterior sylvian (VPS) areas in the visual pathway also respond to vestibular input (Chen, DeAngelis, & Angelaki, 2011a, 2011b). Notably, some cells in the VIP, which encode heading in a manner similar to that found in MSTd, tend to weigh vestibular input more heavily than visual input, representing an area of processing where information from the vestibular organs is more salient than information from the eyes (Maciokas & Britten, 2010).

Most recently, and of particular interest here, cells have been found in the Rhesus monkey Parietal cortex that primarily accept vestibular input and are tuned to curvilinear motion. These cells also have the ability to inhibit cells that display a similar tuning to linear paths even when rotation is present in the stimulus (Cheng & Gu, 2016).

1.3 A visual-vestibular model of human heading perception

As there is strong psychophysical and neurophysiological evidence that visual and vestibular inputs both inform perception of self-motion, models of self-motion should consider both of these sources of information. My supervisor has recently published such a model (Perrone, 2018), and it is on this model that chapters 7 and 8 are based. We discuss this model in depth in Chapter 7 where we use a restricted implementation to test the model against human data from Chapter 6.

Broadly, however, to determine perceived heading this model relies on determining the magnitude and angle of rotation present in the stimulus (R'). R' can

then be removed from the combined flow field generated by the observer translation and rotation ($T + R$) leaving a translation (T) only flow field from which heading can be determined. To find R' the model makes use of an imprecise vestibular estimate of rotation combined with a visual estimate of rotation in order to discard spurious solutions and improve overall accuracy beyond what either system can achieve alone.

1.4 Human perception and equipment choice

Historically the equipment available for use in heading perception experiments has been limited by the technology available. Early experiments made use of shadow projectors (e.g. Llewellyn, 1971). With these projector setups stimuli consisting of expanding patterns were created on rear-projection screens by moving a patterned piece of glass held between a point light and the screen closer to the light to evoke the perception of moving forward. It is difficult to directly compare these systems to the more recent digital computer systems, but their stimuli lacked motion parallax. Furthermore, individual shadows expanded in size as the glass approached the light, providing an undesirable depth cue.

Digital computer systems did, to some degree, solve these problems. Stimuli containing parallax information could be generated and, if desired, pixel sized points that did not expand as they approached the position of the viewer could be used. These digital systems introduced problems of their own however. Most historical systems required a trade-off of FOV, frame rate, and angular resolution. Examples include the displays of Rieger and Toet (1985) which achieved good angular pixel densities with each pixel subtending 0.039°and a good, for the time, refresh rate of 40Hz at the cost of a small 20×20°FOV. Similar angular pixel densities were achieved by W. H. Warren and Hannon (1990) and W. H. Warren, Mestre, Blackwell, and Morris (1991) (0.031 degrees per pixel) with a larger FOV, 40×32°however this was at the cost of a 15Hz frame rate. Royden, Crowell, and Banks (1994) achieved similar, albeit more balanced, specifications to previous experiments; 0.04 degrees per pixel, 30×30°FOV and 33Hz refresh rate, but as a result the equipment was not particularly outstanding by any specific measure.

Banks et al. (1996) achieved higher frame rate (75Hz) and FOV (64×64°)

but comparably low angular pixel density (0.115 degrees per pixel) compared to previous experiments. Stone and Perrone (1997) reported two displays, one with 30×22°FOV at 15Hz with high resolution (2024×2024°) and another lower resolution (1024×1024°) display with 45×45°FOV at 76Hz refresh rate. Li and Warren (2000) used a display with 112×95°FOV, 0.7°per pixel but the stimulus updated at only 30Hz.

Some experiments have made use of stereoscopic displays, with Ehrlich, Beck, Crowell, Freeman, and Banks (1998) presenting stimuli monopticly, synoptically, and stereoscopically at 75Hz with a 60×55°FOV using a red/green anaglyph display. Cuturi and MacNeilage (2013) using a 60Hz polarised light display with 0.056 degrees per pixel and and 107×75°FOV but this display had visible edges and required blurring to obscure individual pixels. Further, this device required an additional separate screen for the response interface, and this screen was of different aspect ratio to the display necessitating scaling of participant responses. Virtual reality (VR) devices have also been used previously with Bertin, Israël, and Lappe (2000) using a head-mounted VR display capable of 60Hz refresh but this suffered from particularly poor FOV for the time at 40×36°and a maximum render distance of 15m for stimuli. This device too, required a separate response interface, in the form of a tracking pad and tracked object that the participant held in their lap but this proved difficult to use, often requiring several attempts before participants were satisfied that the path they drew matched their perception.

The equipment available is largely the product of technological progress and cost of acquirement. This is not directly in the control of the researcher and similar criticisms will be levelled at the currently available technology in the future, however, these limitations and trade-offs are of consequence. There exists evidence of bias in heading perception towards the centre of the screen that worsens with smaller FOVs (Johnston, White, & Cumming, 1973; Llewellyn, 1971; W. H. Warren & Saunders, 1995). This calls into question the reliability of experiments conducted on low FOV displays. Additionally, frame rate has a strong impact on the apparent smoothness of motion, especially when displayed motion is fast, rendered objects are near the viewer, or the display is of high resolution (Watson, Ahumada, & Farrell, 1986) - all of which occur frequently in heading

perception experiments.

In addition to the limitations imposed directly by display performance many previous experiments use points in the world as a reference for when participants reported their perception of motion. For example participants could be asked to move a marker in a pointing task (Banks et al., 1996; Ehrlich et al., 1998). Alternatively, participants could also be asked to judge how they are moving relative to a post in the scene (Crowell et al., 1998). Using a point in the world as a reference like this is less than ideal if the observer perceives a curved path. If during a given trial their task is to make some judgement about their future path through the world then measured 'heading error' is going to be dependant on the perceived depth of the response marker in the scene (Ehrlich et al., 1998). This is clearly an issue for testing perception of curved paths, but it also has implications for eccentric headings and simulated rotation as participants have reported perceptions of curvature under these conditions.

Modern VR systems go some way to overcoming these limitations, with comparable pixel densities, wide FOVs and relatively high refresh rates and as such it is worth revisiting some of the historical experiments with this new equipment.

1.5 New hardware

On the 29th March 2013, with the release of the Oculus Rift DK1 a new generation of VR devices became available. Followed by the DK2 (July 2014) and Vive Pre (2015) these were each initial development kits for game designers. These devices were provided so that said designers could test games in production before improved consumer devices arrived so that games were ready to launch with the headsets, providing content for the new platform from release.

These development devices had only basic head tracking and low-resolution screens. They did, however, offer relatively large fields of view, reasonable refresh rates, obfuscated screen edges, binocular stereoscopic displays, and some ability to move the head and body without additional equipment exclusively designed to facilitate this. Having the display fixed to the head reduces the need to immobilise the head as moving the head no longer creates a perspective error for the viewed stimulus. Perhaps most importantly for this thesis, using these headsets increases

the variety and quality of vestibular and proprioceptive stimuli that we can provide in our experiments.

These devices did have several shortcomings however. Screens designed for phones and not for VR devices combined with the optics required for viewing a screen so close to the eyes created a 'screen door effect' when viewing scenes in the headset. This effect manifested as the separation of pixels in the image by visible vertical and horizontal bands of darkness, similar to what one might see when viewing the outside world through a screen door. This effect was quite noticeable when viewing complete scenes but was unnoticeable when viewing a point cloud consisting of single pixel sized points. The tracking was also fairly limited, especially for the Oculus devices which, for the DK2, required the wearer to be looking mostly forward towards a single camera and in a volume restricted to a rectangular cone 2.5m deep and 72°h×52°v directly out from the tracking camera. Additionally, this position tracking was not as precise as for mechanical motion platform such as the one used by Nooij, Nesti, Bülthoff, and Pretto (2016)

Following the initial experiments using the Oculus DK2 confirming the suitability of these VR devices for use in heading experiments (see Chapter 2) consumer head-mounted devices from Oculus (the CV1) and HTC Valve (the Vive) became available to us. Over and above the development versions, the new consumer headsets offered several major benefits. Lower latency tracking was standard with head rotation updating at 1000Hz and translation at 60Hz. Larger tracking volumes, a 3.5m cube of tracked space for the Vive, came standard. Higher resolution screens, 2160×1200 pixels compared to the 1920×1080 pixels of the DK2, with notably reduced pixel separation distances provided clearer images with a lessened screen door effect. Refresh rates improved by 50% to 90Hz and when combined with lower persistence displays this reduced screen blur and motion sickness. Additionally, more developed APIs were available, making it easier to control headset behaviour and thus code experiments.

Since the newly available headsets further improved on desirable features while addressing the major shortcomings of the development devices it made sense to upgrade to a newer headset. We selected the HTC Vive to replace our DK2 as while the consumer devices from both HTC Valve and Oculus were similar we deemed it the better device. The new Vive headset presented a higher and wider field of view

at practical (10mm) viewing distances compared to its competitor. Although both manufacturers list the same nominal FOV for their headset - 110°(*VIVE Specs*, 2018; *Oculus Rift specifications*, 2018) - this constitutes a simplified picture of the situation. In use, the Vive achieves wider horizontal binocular and vertical fields of view (108°h x 113°v at 10 mm) at practical eye-lens separation distances than the Rift (94°h x 93°v at 10 mm). The Rift does, however, achieve a greater diagonal field of view at these distances due to differences in lens geometry (Kreylos, 2015). The Vive device came with hand-held controllers from release. It also produced a clearer image and, while rather subjective, seemed the more comfortable headset during extended use.

1.6 This thesis

This thesis revisits a selection of historical experiments using new head-mounted VR systems to re-examine human perception of heading, rotation, and path. As part of this process, a new tool for measuring these perceptions was developed that makes use of the stereoscopic depth and world immersion provided by the new systems as well as the intuitiveness of the associated input devices. This new tool is applied in experiments not only concerning travel around a curved path but also along linear paths with rotation and travel on eccentric headings. Linear paths with rotation are examined as participants in past experiments have reported the perception of curved paths but experimenters have lacked the ability to satisfactorily measure this perception. Eccentric headings are examined as the model presented in Perrone (2018) indicates that the flow field generated by eccentric headings can be interpreted as containing a rotational component. As such, it is possible that travel on eccentric headings may be misperceived as travel on a curved path and this may contribute to observations, such as the centre screen bias, that are currently unexplained.

This thesis opens up new tools and equipment for use in heading perception experiments. In doing so it advances our understanding of how the human visual and vestibular systems operate and interact. It does this with a particular focus on perceptual responses and visual-vestibular system characteristics and interactions when observers are experiencing curvilinear motion – an area that has received

relatively little attention. It will also aid in the refinement of a biologically based model of how this system works. As a consequence of this, we will be able to make improved inferences as to the purpose of groups of motion sensitive neurons.

Ultimately, in conjunction with other work in the field, the work done here is applicable to the future development of tools and processes for the prediction, assessment, avoidance and treatment of visual and vestibular disorders thus improving outlook for those experiencing medical conditions, injury, or surgery for these disorders. New knowledge on how humans use visual and vestibular information to navigate also means that this work has immediate relevance to both the development of control systems in self-navigating robotics and the use of inertial motion systems (particularly low-fidelity inertial motion systems) in long duration navigational tasks, both fields where more research is required.

1.6.1 Notes

Video: For most experiments described in this thesis an example video depicting the main condition of interest has been included. These videos are part of Figures 2.1, 2.4, 4.2, 5.1, and 6.1. The embedded mp4 video in these figures should play automatically on loop if viewed in Adobe Acrobat 9 or later with the most recent Flash plugins installed. If you are viewing this thesis as a printed document or in an incompatible viewer then you will see instead a static image of the stimulus as seen by the participant at the start of the trial.

Due to differences in rendering, screen size, and FOV the point clouds used in the experiments presented in Chapter 2, while clearly visible in the Rift, display and print poorly. As such, the point cloud videos presented in figures 2.1 and 2.4 have been edited to increase the brightness of the point cloud and fixation cues. Consequently, these figures should be taken as examples rather than true-to-view replications.

An electronic copy of this thesis can be obtained from (place-holder:waiting on library) if you wish to view the video.

Graphs and statistical significance: Test statistics are not reported in this thesis when significance (or lack thereof) is demonstrated in graphs of results. This is done primarily to streamline the reading experience and is possible as the

precise p-values are not required for and, arguably (e.g. Aarts, Winkens, & van Den Akker, 2012; Lang, Rothman, & Cann, 1998; Poole, 2001; Stang, Poole, & Kuss, 2010; Stang & Rothman, 2011), add nothing to the interpretation of the data presented here.

Error bars used in this thesis represent the 95% confidence interval of the standard error of the mean for group averages or the standard error for individual data. As such, where the error bars of any two means do not overlap they can be understood as significantly different vis-à-vis a two-tailed t-test (paired or otherwise) uncorrected for multiple comparisons and with a significance level of $p<0.05$. Conversely, where the errorbars of either or both means overlap the other mean the pair would be recognised as non-significant under the same test.

Heading detection in consumer virtual reality

The gaming focus of current generation VR displays suggests that before conducting new experiments we should first verify that the devices are suitable for use in visual heading self-motion perception experiments. Furthermore, if the headsets prove suitable then comparability of results obtained using this new system and results from previous works should be assessed. To fulfil both of these purposes we chose to first replicate experiment one from Banks et al. (1996) and then, in a second separate experiment, the simulated and active head pursuit conditions from Crowell et al. (1998). The first of these experiments tests how heading is perceived during both real and simulated rotation of the eyes. The second tests the same, but with real and simulated head turns.

These experiments were chosen because they are key experiments in the field and contain conditions we are interested in investigating further. They were also relatively simple to recreate with respect to the coding required to generate stimuli and obtain responses from participants. Banks et al. (1996) examined the effect of varying the ratio between simulated and real eye rotation on heading perception and found that greater heading errors occurred as the portion of simulated rotation in the stimulus increased. Crowell et al. (1998) compared heading perception across, amongst other conditions, simulated rotation and active rotation of the head. This experiment found similar errors as Banks et al. (1996) under the simulated rotation condition and accurate heading perception regardless of rotation rate during active head rotation.

2.1 Heading in VR with eye rotation

2.1.1 Method

Participants

Twenty naive participants (eight male) with normal or corrected-to-normal vision completed the experiment. Fourteen of these were recruited from undergraduate psychology classes and received a one percent course credit for participating. This experiment was approved by the University of Waikato Psychology Research and Ethics Committee.

Equipment

Stimuli were presented on an Oculus Rift DK2 virtual reality head-mounted display (Rift). Display resolution was 960h×1080v pixels per eye (1920h×1080v overall), providing a 94°h × 104°v combined field of view (FOV). Pixel centre-to-centre angular separation was approximately 0.097°h × 0.096°v. Note that there is a small apparent discrepancy between the approximate horizontal angular pixel density and the horizontal resolution per eye when compared to the horizontal FOV. This is because the reported FOV is the combined binocular FOV. As the FOV for each eye partially overlaps that of the other eye the per eye FOV differs from the total FOV. For the Rift, the monocular horizontal FOV at a 10mm viewing distance is 93°.

Image persistence was 2ms and display refresh rate was 75Hz, with rotation tracking updating at 1000Hz and positional tracking updating at 60Hz. Motion to photon latency, the time between the user moving and that motion being reflected in the stimulus, was 60ms. Unit weight was 440g, the majority of which sat forward of and level with the eyes. Further details can be found in the *Oculus Rift DK2 specifications* (2018). Stimuli were rendered in real time using a computer running Windows 8.1v6.3 64-bit with an Intel Core i7-4790 CPU, 16GB RAM, and an NVidia GTX960 GPU. The controlling code was written using C++ and DirectX 11.0.

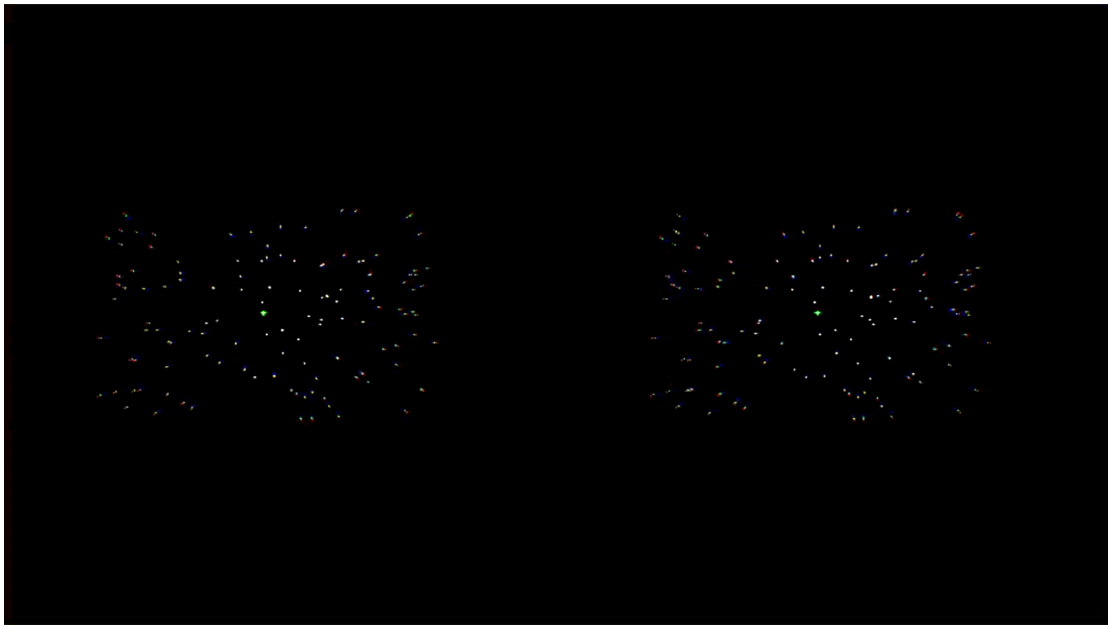

Figure 2.1: Example stimulus depicting linear travel at 1.5ms^{-1} through a point cloud. The observer maintains fixation on the green cross as it tracks to the left at 7.5°s^{-1}.

Trial design

The experiment consisted of travel through a star field. This field was 30h×30v degrees, initially beginning 0.18m from the observer and extending 5.0m in depth, and containing 64 randomly positioned stars. This meant the stars filled a volume in the shape of a truncated pyramid matching the virtual world used in the Banks et al. (1996) experiments. The screen depicting space outside of this volume was unlit. At the end of each trial at least ten of the stars remained visible. Each trial lasted for 1.5 seconds, with only the fixation point moving for the first 0.15 seconds to assist participants in establishing smooth pursuit before the trial began proper. During each trial participants observed linear travel at 1.5ms^{-1} on the horizontal plane along one of three headings (0°, ±3°– see Figure 2.2(a)) relative to the initial viewing direction. Additionally, participants observed rotation totalling one of 0, ±0.6, ±1.25, ±2.5, ±5.0, or ±7.5°s^{-1}. An example trial can be seen in Figure 2.1.

This total observed rotation consisted of two separate components – real rotation and simulated rotation – generated simultaneously. The relative ratio of simulated to real rotation in any given trial was one of 0, 0.25, 0.5, 0.75, or 1, with zero indicating the stimulus contained only real rotation and one indicating the rotation was entirely simulated. Simulated rotation was generated by rotating the

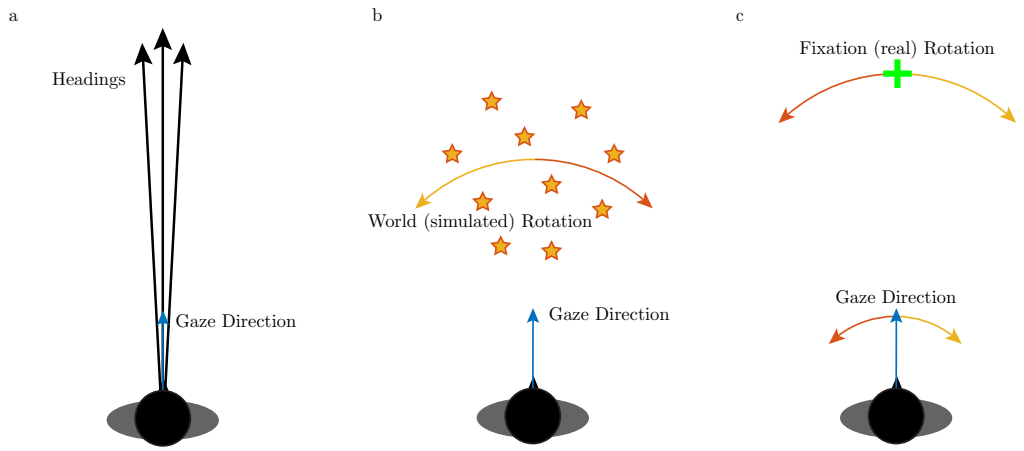

Figure 2.2: Individual sub-conditions for heading in VR with eye rotation. Sub-plot (a) shows the different headings. Sub-plot (b) shows how simulated rotation is generated by moving the star field around the participant. Sub-plot (c) shows how real rotation is generated by having the participant fixate on the cross as it rotates about the participant. Orange arrows represent counter-clockwise rotation of the observer, yellow arrows represent clockwise rotation of the observer.

star field about the participant's vertical axis as depicted in Figure 2.2(b). Real rotation was generated by having participants track the fixation point as it rotated about their vertical axis 10m distant from their viewing position as depicted in Figure 2.2(c). For example consider rotation at $7.5^{\circ}s^{-1}$ at a ratio of 0.5, where there is an equal contribution to the total rotation from both the real and simulated rotational components. In this case the fixation cross rotates at $3.25^{\circ}s^{-1}$ (counter-clockwise) and the star field rotates at $-3.25^{\circ}s^{-1}$ (clockwise). Note that the apparent change in rotation direction is correct - when the participant rotates their eyes to the left the star field appears to rotate to the right.

Ten trials were used per condition resulting in a total of 1650 trials. At the conclusion of each trial a small cross appeared 10.1m distant, such that it would pass behind the fixation point, from the participant and displaced from their viewing direction by a pseudorandomly selected value between $\pm 15^{\circ}$. Participants then used a mouse to move this cross into alignment with their perceived heading on the horizontal plane. For a sub-sample of eight participants, we used electrooculogram (EOG) recordings to measure eye rotation and thus verify that they were smoothly and accurately tracking the fixation point. All participants tested in

this manner were able to accurately complete the task, and these participants were divided equally between the two response groups discussed below.

2.1.2 Results

Accuracy of heading perception was equivalent across all three tested heading directions, so this condition was collapsed into a single set for analysis. Ten participants produced results indicating significant (p ¡ .001 for each participant) interaction between rotation rate and the ratio of real to simulated rotation in the stimulus. The mean results for these participants are shown in Figure 2.3(a). For these participants the green line, representing trials where all stimulus rotation was generated by active pursuit of the fixation point by the eyes, shows that they could accurately determine heading regardless of rotation rate when an efference signal was available. Conversely, the blue line, representing trials where all stimulus rotation was simulated by rotating the star field around the participant, shows that with the absence of an efference signal these participants produced large errors in heading perception. For these participants an increase in simulated rotation rate resulted in an increased heading bias in the direction of the rotation but an increase in real rotation did not. Furthermore, heading error was proportional to the magnitude of the simulated rotation independent of real eye rotation in the scene. Visual comparison with Figure 2.3(c), Figure 3 from Banks et al. (1996) reproduced here for ease of comparison, shows that results from this group of participants are substantially similar to the results from participants in experiment one from Banks et al. (1996), even though the original experiment used a desktop display and not VR.

The remainder of the participants (a further 10 individuals) produced results displaying no significant interaction (p ¿ .25 for each participant) between rotation rate and ratio of real to simulated rotation. Furthermore, for these participants there was no significant difference in perceived heading between the simulated and real rotation conditions. The mean results for these participants are shown in Figure 2.3(b). For these participants the effect of increasing total rotation was more pronounced at lower rates of rotation. Increasing the rotation rate beyond $2.5^{\circ}s^{-1}$ had no significant effect for any of the tested simulated to real rotation ratios. Ad-

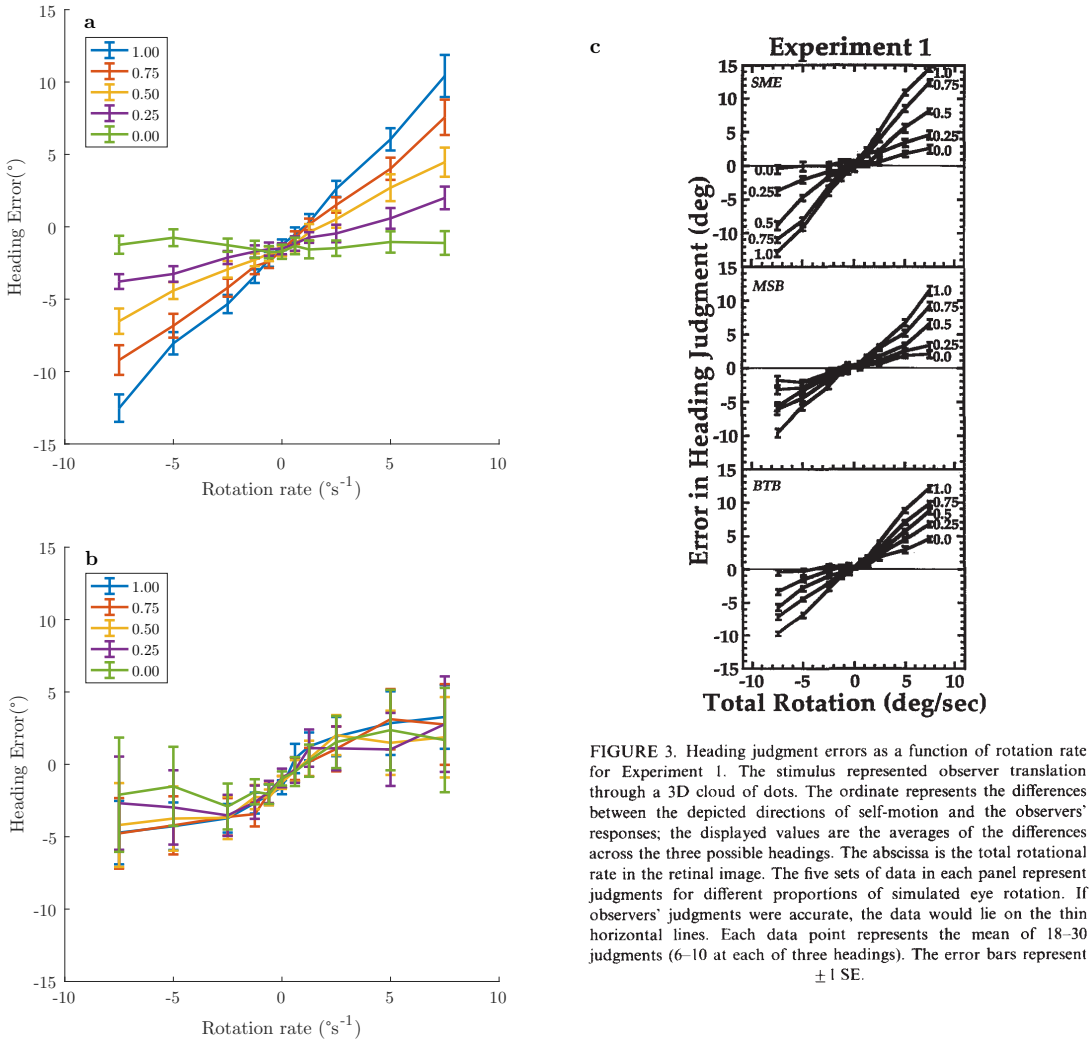

FIGURE 3. Heading judgment errors as a function of rotation rate for Experiment 1. The stimulus represented observer translation through a 3D cloud of dots. The ordinate represents the differences between the depicted directions of self-motion and the observers' responses; the displayed values are the averages of the differences across the three possible headings. The abscissa is the total rotational rate in the retinal image. The five sets of data in each panel represent judgments for different proportions of simulated eye rotation. If observers' judgments were accurate, the data would lie on the thin horizontal lines. Each data point represents the mean of 18–30 judgments (6–10 at each of three headings). The error bars represent ±1 SE.

Figure 2.3: Mean heading perception in VR. Plot (a) shows the mean perception for participants who followed the expected pattern of responding. Plot (b) shows the mean perception for those who did not. Legend indicates the portion of total rotation in the stimulus attributable to simulated rotation. Plot (c) shows individual results from experiment one of Banks, M. S., Ehrlich, S. M., Backus, B. T., & Crowell, J. A. (1996). Estimating heading during real and simulated eye movements. Vision research, 36 (3), 431–443. reproduced for ease of comparison.

ditionally, the degree to which rotation contained by the stimulus was simulated had no effect on heading perception – participants perceived simulated rotation and real rotation the same way. The results produced by these participants are quite different from what has been seen previously. Even without efference signals the participants who fell into this group were able to produce reasonably accurate heading estimates compared to those seen in Banks et al. (1996).

Additionally, and not directly related to the recorded participant responses, at approximately two seconds per trial the experiment took around 55 minutes to complete. The slowest participant took 1 hour 8 minutes to finish all trials. For many of the first time virtual reality users in the group this proved to be too long. While no participant reported motion sickness, and only two accepted the offered mid-experiment break many commented post-experiment that the experiment was too long to be completed in a single sitting without discomfort. From this we decided that for now VR based experiments should favour sessions of shorter duration to help ensure peak participant performance and comfort are maintained over the entire experiment. This recommendation may change however as more comfortable headsets are developed and as the participant pool becomes more familiar with the increasingly available technology.

2.2 Heading in VR with head turns

2.2.1 Justifications

A preliminary answer to the question of whether the Oculus Rift virtual reality system is suitable for use during heading detection experiments has been established. In the previous section replication of experiment one from Banks et al. (1996) has shown that perception of heading with simulated and real eye rotation can be substantially similar in the Rift as when viewed on a regular 2-D computer display screen. This answer could be extended and confirmed by testing under additional conditions however. One such condition that is of particular interest is the active head rotation examined in Crowell et al. (1998).

Using the new head-mounted displays makes it fast and easy to implement test conditions where the participant actively turns their head as there is little further setup required beyond setting up the head-mounted display itself. Previous heading experiments looking at the role of head rotations needed special equipment for measuring and sometimes constraining head movement and participants had to move their head relative to a fixed screen reducing the FOV and changing the perspective of the stimulus. With VR headsets the display device is already fixed relative to the head and remains so under safe operating conditions. Furthermore,

the virtual world is fixed relative to the outside world using the built in tracking capabilities of the headset. The only additional requirement is the generation of some kind of cue or guide for participant head turning.

Testing perception of heading during head turns is of particular interest as previous experiments investigating active head turns have reported only a single style of responding. It would be interesting to know if the two styles of responding found in 2.1.2 with eye turn tasks are also present with head turn tasks.

2.2.2 Method

Participants

Eight naive participants (four male) with normal or corrected-to-normal vision completed the experiment. Six of these were recruited from undergraduate psychology classes and received a one percent course credit for participating. This experiment was approved by the University of Waikato Psychology Research and Ethics Committee.

Equipment

This experiment was conducted using the same equipment as described in Section 2.1.1.

Trial design

This second experiment, run to assess consumer VR suitability for head rotation experiments, used stimuli similar to those described in Section 2.1.1. It differed only in having a mechanism to control head rotation instead of eye rotation and had a smaller number of trials. The star field, and the simulated rotation conditions, were the same as previous.

The method to control head rotation made use of a red fixation point. This fixation point was always straight ahead relative to the direction the head was facing. Additional to the fixation point there was also a small green circle, subtending 1°, initially 10m directly forward from the participant at eye height. This served as a target within which the participant was required to keep the fixation point. Participants did so by tracking this circle with their whole head, in

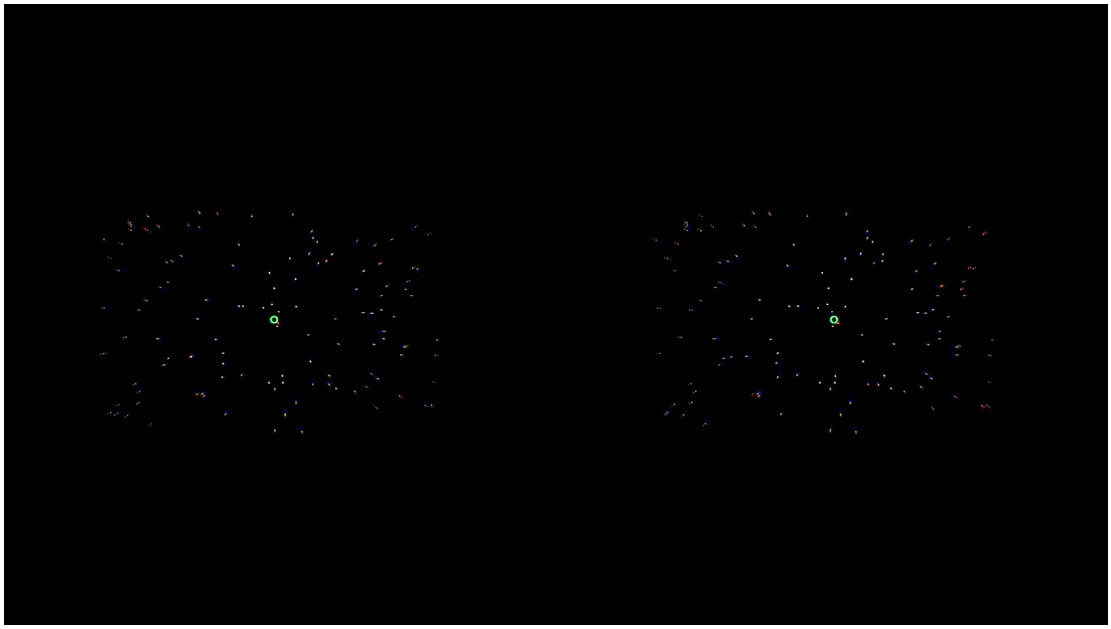

Figure 2.4: Example stimulus depicting linear travel at 1.5ms^{-1} through a point cloud while the observer keeps fixation point (red) inside a target (green).

the process providing their sensory systems with efference, proprioceptive, and vestibular signals. During each trial the green circle could track to either the left or the right at 7.5°s^{-1} or remain stationary. As the fixation point was fixed relative to the head this tracking ensures that the head rotates at approximately the correct speed. Failure to maintain tracking resulted in the system discarding response data for the current trial and shuffling that trial back into the remaining trials to be taken again later. Participants were not told that they had failed to track adequately and were allowed to respond as per usual for that trial. Several participants commented that they believed they had failed in such a manner on at least one occasion but this belief was not confirmed. All participants repeated at least one trial in this manner, but no participant repeated more than four.

Only a subset of the trials from the previous experiment in 2.1.1 were tested. The trials tested were the 0 and ± 7.5°s^{-1} rotation rate trials for ratios of simulated rotation of either 0 or 1. Each combination was tested with headings 0 and ±3°s^{-1} relative to initial facing direction. Because the ratio of simulated to real rotation does not matter if there is not any rotation only one set of trials was done for the zero rotation condition. Data from these trials were used when the rotation rate was zero for both the real and simulated conditions. Each condition was

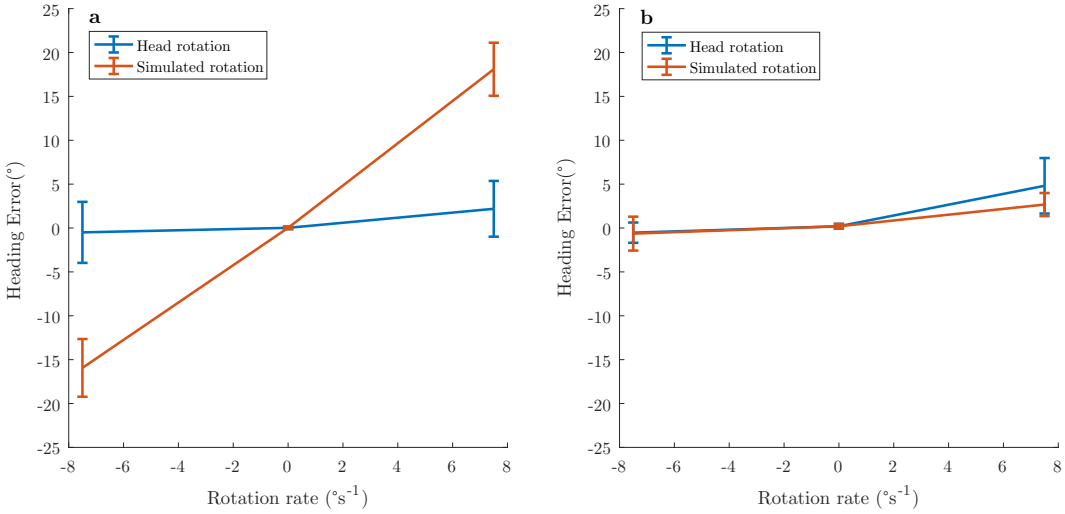

Figure 2.5: Mean heading perception for participants in VR with head turns. Plot (a) shows the mean perception for half of the participants (n = 4) who followed the expected pattern of responding. Plot (b) shows the mean perception for those who did not.

tested in 15 separate trials giving a total of 225 trials. This limited selection of trials was chosen in order to decrease the duration of the experiment so that it was easier on first time virtual reality users. The consequent loss of information was deemed acceptable based on the approximate linearity of response magnitude across rotation rate seen in the previous experiment. Requiring participants to precisely move and position their head significantly increased the time between responding and the participant being ready to commence the next trial. Even so, with the reduced number of trials participants took between 12 and 16 minutes to complete the experiment. First time virtual reality users reported no discomfort with this duration when asked.

2.2.3 Results

There was no significant difference in heading error across the 0° and ±3° conditions therefore results for all three heading conditions were collapsed together.

For four participants there was a significant difference in heading perception between the simulated and head rotation conditions at 7.5°s^{-1}. Participants heading bias here was dependent on simulated rotation and invariant under real rotation. Simulated rotation produced a heading bias in the same direction as the

rotation. The average of these responses can be seen in Figure 2.5(a). In this plot the blue line represents heading perception during active head rotation trials. Under this condition, these participants produced accurate estimates of heading, consistent with the idea that having a reliable efference and vestibular signals allows accurate determination of heading as per Crowell et al. (1998). The orange line represents data during the simulated condition and shows that participants made significant errors in heading perception when efference and vestibular signals were absent. This effect was similar in magnitude to that seen in 2.3 under the fully simulated condition, as should be expected considering the stimuli were equivalent.

The remaining four participants perceived no significant difference in heading between the simulated rotation and active head turn conditions. Additionally, perceived heading was not significantly different from true heading. The mean results for these participants can be seen in Figure 2.5(b). These participants were equally accurate when estimating heading with or without extra-retinal cues.

2.3 Overall comments

We saw much greater interpersonal variation in these two experiments than the two replicated experiments found. Half of the participants here were able to accurately determine heading when presented with linear paths and rotation (see Figure 1.2d) in the absence of congruent extra-retinal cues. The other half were not. This was unexpected as the two experiments we were attempting to replicate found only that the accuracy of participant perception was degraded by rotation in the absence of extra-retinal cues. It is worth noting however that finding large interpersonal differences is not wholly unprecedented. Distinctly different response patterns have been seen in heading experiments before (e.g. A. van den Berg, 1996). Compared to the replicated experiments we tested a relatively large number of participants. Furthermore, these participants were untrained, unfamiliar with the field, and ignorant of any expectations as to performance. In comparison, the participants in Banks et al. (1996) were only three in number. These differences could explain why we found such striking individual differences while the replicated studies did not.

Unfortunately, as the existence of two distinct perceptions was unexpected insufficient additional information was collected to determine a reason or reasons for the differences. Once the existence of two different styles of responding became apparent we asked participants a short series of questions during post-experiment conversation. The answers to these questions suggest that the difference is not obviously due to experience with video games or driving, nor related to age or gender. Furthermore, it is unlikely to be due to experience with VR devices as only a single participant across both experiments had previously used a VR device.

One possible explanation for this difference in perception is that some individuals are capable of accurately determining their rotation from visual stimuli alone, perhaps using a system of curvilinear detectors. If this can be done then these individuals would not need to rely on vestibular or efference signals to determine their rotation even when they were available, leading to no change in performance across the two conditions. This would be a useful ability to discover, or train, in individuals as situations where navigation occurs primarily in the absence of congruent extra-retinal information – e.g. drone piloting, gaming and remote inspection – are becoming increasingly more common.

Overall, however, and in spite of the differences between our results and the results from the experiments we were replicating, we determined that it was both possible and useful to run heading perception experiments using the current generation of stereoscopic head-mounted virtual reality. Half of the participants here produced results substantially similar to those seen in the previous works suggesting that the gaming focus of these VR devices does not introduce some fundamental perceptual difference. Furthermore, the current generation of VR headsets has proven both versatile and easy to use. Physical movements can be quickly integrated into experiments without requiring additional equipment and in particular, compliance with required head and body movements can be accurately measured using the built in tracking systems. All this can also be done without ill effect provided participant lack of experience with VR is kept in mind. Additionally, another major advantage is that VR systems are currently novel, and thus an exciting draw for participants making it easy to recruit volunteers.

A new tool for measuring curvilinear paths

The previous two experiments, described in Sections 2.1 and 2.2, considered heading perception as a function of view rotation and linear translation. This was largely with an eye to comparing results obtained using the new VR headsets with data from historical works. As such the experiments used a simple pointing task common to early heading experiments. With a new system, however, comes new possibilities for measuring the perception of self-motion. Previous experimental setups have been limited by both the available displays and the available response interfaces. Here we present a new response tool making use of the features provided by the Vive HMD system.

3.1 Path, heading, and rotation

Together rotation rate and linear velocity sufficiently define a curvilinear path. Furthermore, for a given curvilinear path it is possible to create a linear path that is instantaneously indistinguishable (Whittaker, 1988)) from that curvilinear path although this path does diverge over time (Rieger, 1983). Creating this matched path is done by having the observer travel in a straight line at equal *speed* while rotating about their vertical axis at the same rate as for the curvilinear path. Figure 1.2d provides an example of this linear motion with rotation as compared to true curvilinear motion (1.2c).

These two paths diverge over time and thus should be distinguishable. In spite of this, individuals participating in heading perception experiments involving linear motion with rotation have historically reported perceiving curvilinear paths

(Banks et al., 1996; Ehrlich et al., 1998; Li & Warren, 2000, 2004; Royden et al., 1994; A. van den Berg, 1996). Unfortunately it has been difficult to measure this perception.

Bertin et al. (2000) used a drawing task where participants, after viewing a trial as many times as required for them to feel confident in their answer, reported their perceived path by moving a model hovercar over a recording surface. While this did successfully capture participant perceptions of curvilinear motion there were a few issues with the method. Participants sometimes required multiple attempts at drawing their path, in addition to multiple views of the stimuli while doing so, suggesting that the tool was relatively difficult to use. More importantly, however, it is difficult to quantitatively analyse the data produced by the drawn responses as in most cases the curvature and headings of the drawn paths are changing in a non-constant manner.

Another approach to the measurement of curvilinear perceptions was taken by W. H. Warren, Mestre, et al. (1991). Observers presented with stimuli depicting curvilinear motion were asked to judge whether they would pass to the left or right of a target at 16 meters. While this approach provided a quick and easy response procedure for participants it does not distinguish errors in heading perception from errors in curvature perception.

Since these difficulties with measuring human perception of paths exist a tool that could measure both heading and perceived path simultaneously and in a quick and intuitive manner is desirable. Such a tool could also potentially serve as an indirect measure of rotation perception.

3.2 The response tool

The new response tool proposed and tested here consists of a thin 15-meter-long, initially straight, line on a plane parallel to and 0.5m above the ground plane and projecting from the centre of the participants chest in stereoscopic 3D virtual reality. The stereoscopic 3D environment should render such a line more useful compared to a 2D display due to the availability of stereoscopic depth cues. These cues make it easy to determine the location of the line relative to the ground plane. This line is only visible during the response period, and not during the motion

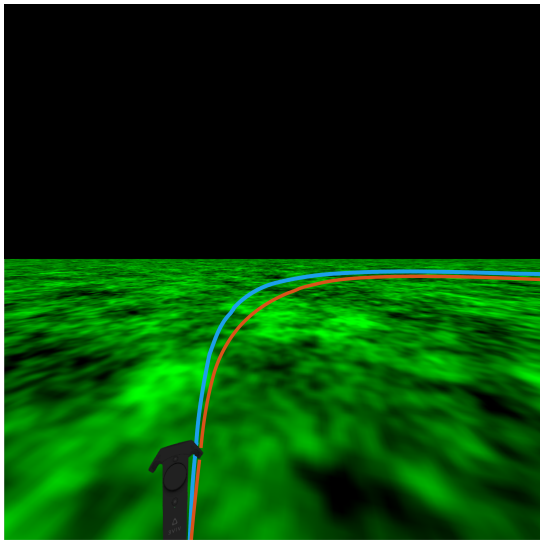

Figure 3.1: Static illustration of the response tool as presented to the left eye. The blue line represents the response line manipulated by the participant, thickened for visibility in this figure. The orange line, not visible to the participant but shown here for reference, depicts the circular path of radius 11.5m along which the participant was travelling. Note that neither line appears to depict a circular path in this image due the to image distortion necessary to correct for lens effects in the headset.

period, of the trial so as to not provide additional cues beyond those being tested.

When providing a response participants can modify the tangent of this line at the point where it intersects them by pointing with one of the Vive controllers. This starting tangent aligns with the line between the centre of the controller (and thus the participants hand) and the point where the line intersects the participants centre of mass. This forms the measure of perceived heading.

Additionally, participants can modify the curvature of the line. This is carried out by the participant pulling on the controller triggers, with the rate of change in curvature proportional to the degree of trigger depression. The left and right trigger each bend the line to the left and right respectively. This linear ramp in trigger effect allows precise control of path curvature with slight depression of the triggers, particularly useful when responding with a low curvature path or distinguishing between two similar paths while still allowing the participant to quickly set large amounts of curvature by fully depressing the triggers. Once the participant has matched the line to their perceived path a final thumb button press saves the curvature and initial angle (heading) of the line.

In the following experiments presented here the response line is coloured cyan (RGB – 0, 225, 225). This choice of color was not entirely arbitrary, but the color itself doesn't matter to the tool and can be changed as required. Cyan was chosen because it was clearly visible above the green and black ground plane while still maintaining relatively low average contrast. This minimised the appearance of visible crepuscular rays when the tool was used with devices containing Fresnel

style optics.

3.3 Overall comments

While the current iteration of the tool can only handle paths of constant curvature on a single (here horizontal) plane it is not technically difficult to modify the tool to allow for non-constant curvatures or paths on any number of planes. Unfortunately, the greater the number of degrees of freedom in the tool the greater the number of input options required for the user to access all possibilities. With the current controller setup, it seems unlikely that these required additional inputs could be manipulated in an accurate, timely, and intuitive manner. As such, the biggest hurdle to using the tool with more complex motion is to design a more efficient input method.

Linear paths with rotation

Before the new measurement tool is applied under novel conditions its performance needs to be compared to that of previous response tools. Consequently, the first experiment conducted using the new tool again examines participant perception of linear motion with rotation about the participants vertical axis. This condition is of particular interest as a point of comparison. Historically, participants have made anecdotal reports of curvilinear path perception under these conditions but have been unable to reliably report such using the response tools made available to them.

Because of these anecdotal reports we expect to see participants make use of the new opportunity to respond with curvilinear paths under these conditions. In particular, we expect to see participants reporting more strongly curved paths, alongside the previously seen increasingly large heading errors, as rotation rate increases. This makes these conditions a good test of how intuitive the tool is and how quickly relatively complex responses can be made by participants.

As linear travel with rotation provides no extra-retinal cues expecting the perception of curved paths means we expect to see behaviour consistent with models of heading perception that require extra-retinal cues. Models that suggest R' can be removed from $T + R$ using visual input alone predict that participants should perceive a straight path and the correct heading. On the other hand, models that suggest extra-retinal cues are required would predict that participants will prove unable to correctly determine R' as no extra-retinal cues are available to the static observer. Participants would thus fail to compensate for scene rotation resulting in the perception of a curved path.

In particular, if we see behaviour consistent with a complete failure to compensate for rotation then participants should report curvatures consistent with

the curvature of the *equivalent circle*. That is, consistent with the circle requiring rotation of the given magnitude for the trial in order to maintain view direction along the tangent of the circle while translating along the circumference of the circle at 1.5 ms^{-1}. On the other hand, if we see behaviour consistent with partial or complete compensation (i.e. $0 < R' \leq R$), perhaps driven by visual estimates of rotation at low rates of rotation, then participants should report perceived curvatures between the curvature of the equivalent circle and a straight line.

4.1 Method

4.1.1 Participants

Eighteen participants, ten male, with normal or corrected to normal vision completed the experiment. This experiment was approved by the University of Waikato Psychology Research and Ethics Committee.

4.1.2 Equipment

Stimuli were presented on the HTC Vive stereoscopic head mounted display (Vive). Resolution was 1080 h x 1200 v pixels per eye (2160 h x 1200 v overall), and eye relief was set such that the display provided a 108°by 113°combined field of view with each pixel subtending approximately 0.092°h x 0.094°v at a 10 mm viewing distance. As with the Rift DK2 previously, the per eye field of view differs from the total binocular field of view. The per-eye horizontal field of view for the Vive headset at a 10 mm viewing distance is 100°.

Image persistence was 1.9 ms and display refresh rate was 90 Hz, with rotation tracking refreshing at 1000 Hz and positional tracking updating at 60 Hz. Motion to photon latency was 11 ms. Unit weight was 555 g, with most of this centred forward of and between the eyes. Further details can be found at (*VIVE Specs*, 2018).

Stimuli were rendered in real time using a computer running Windows 10v1607 64-bit with an Intel Core i7-4790 CPU, 16 GB ram, and an NVidia GeForce GTX1080 GPU. The experiment was programmed using C++ and OpenGL 4.5.

The Vive as a research tool

Because the Vive is primarily intended as a consumer gaming device it includes contingencies designed to maximise player immersion when the device is used with sub-optimal computer systems or physical setups. One of these contingencies is the software re-projection of frames into the video stream should the renderer fail to meet the presentation deadline for a new frame. This has the benefit of maintaining frame rate and thus reducing motion sickness. Unfortunately, it also has undesirable side effects when the device is used in an experimental setting, and especially so when the device is used for motion perception experiments.

While this reprojection process provides sufficient accuracy for casual gaming, where motion has occurred between frames the motion apparent in the re-projected image differs from that which would have been shown by the incomplete frame replaced by the reprojection. This divergence increases significantly over several frames. As such, frame presentation was monitored during experiments to ensure that only freshly rendered frames were presented. No re-projected frames were shown during any trial or to any participant.

We did not repeat the experiments presented in Chapter 2 conducted using the DK1 after receiving the HTC Vive. We decided that in principle that although the differences between the development devices and the consumer devices were substantial, they were generally straight upgrades to the features desirable for our experiments and not fundamental changes to the device itself. The one notable change in device configuration was a change in lens structure. The development kit HMDs use conventional lenses, while the consumer versions use Fresnel lenses to allow for greater field of view, reduced weight, and reduced impact of the screen door effect. Unfortunately, this introduces the possibility of apparent crepuscular rays (also known as 'God rays'). While these rays were not as visible in the Vive when compared to the Rift, due largely to the smaller number of lens segments used in the Vive lenses (Kreylos, 2015), they were still apparent. Fortunately this effect can be easily managed through scene selection by limiting high contrast edges. As such, rays were not noticeable in the final stimuli presented and this one change did not adversely affect the suitability of the devices for use in heading experiments.

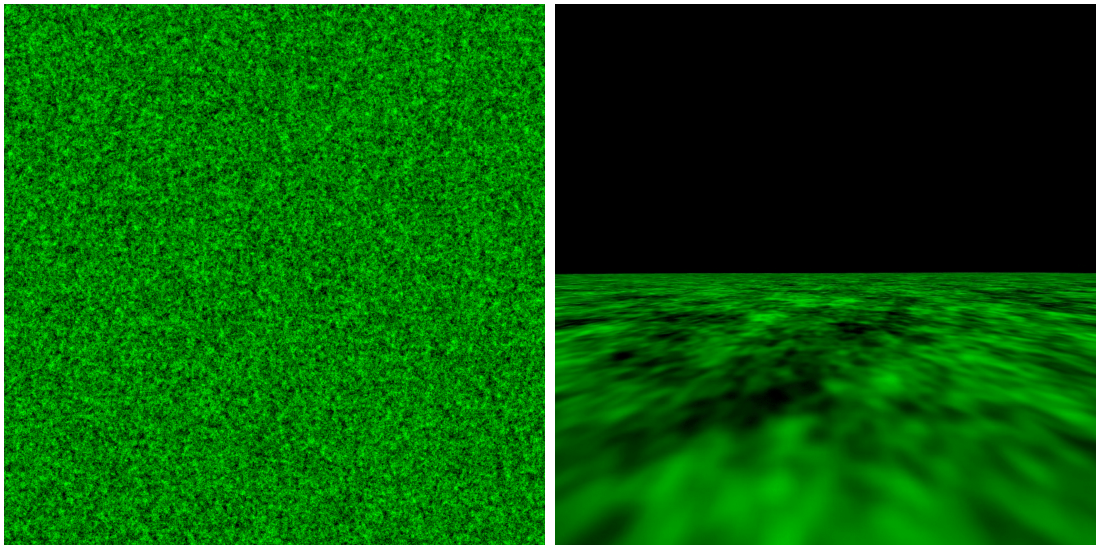

Figure 4.1: Views of an example ground plane used during a trial. Left shows an aerial view of the complete texture. Right shows the observers view of the texture.

4.1.3 Trial design

Each participant completed 165 two-second-long trials. Each trial consisted of linear motion straight ahead relative to the starting heading at 1.5 ms^{-1} with an additional visually simulated rotation about the vertical axis. There were 11 trials for each of the rotation rates 0, ± 0.6, ± 1.25, ± 2.5, ± 5.0, and $\pm 7.5°s^{-1}$. These trials were presented in a random order. At the end of each trial participants reported their perceived path using the response tool described in 3.2.

Movement during each trial was over a flat ground plane ending one kilometre from the participants position in all directions. A randomly generated noise texture with spectral power density proportional to $\frac{1}{f^2}$ (per Li & Warren, 2000), an example of which is seen in Figure 4.1, was applied to the ground plane to mimic the information available in natural scenes. Texture colour varied between green (0, 255, 0) and black (0, 0, 0,). Viewing height was 1.5 m. This ground plane was used for the experiment described in this chapter and additionally for those described in chapters 5, 6, and 8.

Before beginning the experimental trials participants also completed 33 practise trials to familiarise themselves with responding using the unfamiliar controller input. These trials were the same in all respects to the experimental trials, excepting that the actual motion shown differed. Participants saw, in order, linear

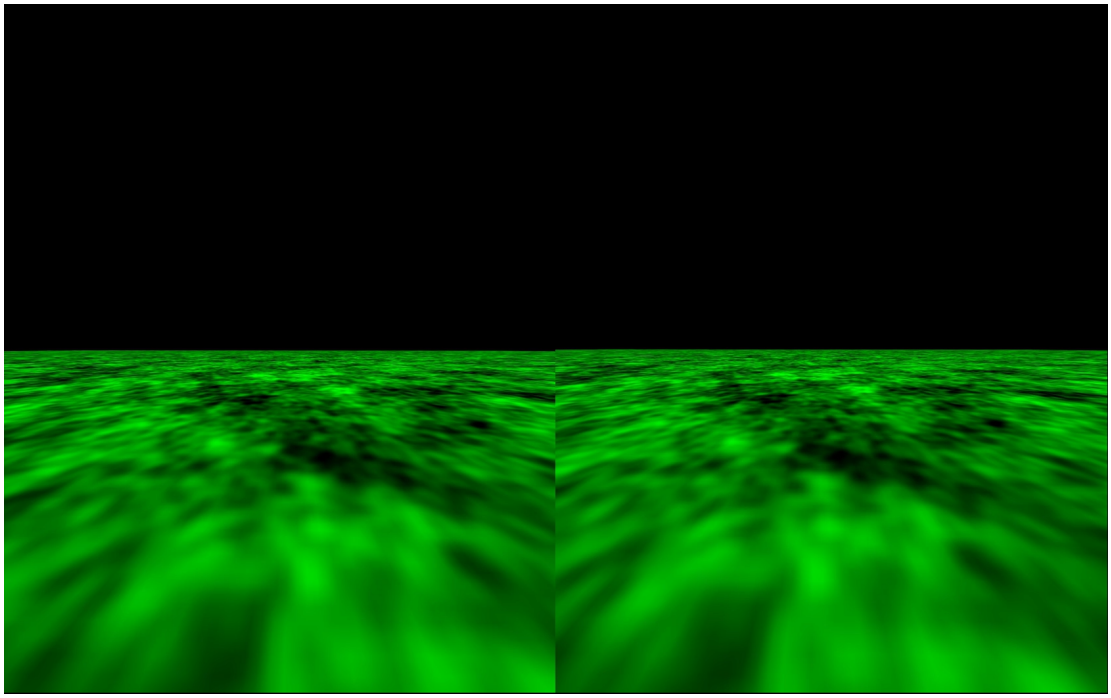

Figure 4.2: Example stimulus depicting linear translation at $1.5\,\mathrm{ms}^{-1}$ with an additional anticlockwise rotation about the vertical axis at $7.5^{\circ}\mathrm{s}^{-1}$.

motion with heading varying between $\pm 50^{\circ}$ in ten-degree steps followed by curvilinear motion with curvature varying between ± 0.175 in steps matching $3^{\circ}\mathrm{s}^{-1}$ steps in apparent rotation. The sequence was completed by travel along a linear path with rotation (the same condition as seen in the experiment) between $\pm 15^{\circ}\mathrm{s}^{-1}$ in $3^{\circ}\mathrm{s}^{-1}$ steps. Feedback was given only when participants asked for clarification of control mapping. At no point were participants advised as to the 'correctness' of their responses. Furthermore, at no point before or during the experiment (or in any other experiment presented in this thesis) were the actual path characteristics discussed with participants as this has been shown to affect perception (Royden, Cahill, & Conti, 2006).

4.2 Results and discussion

4.2.1 Curvature

All individuals perceived consistently curved paths despite movement being along a straight path, with two examples of this to be found in Figures 4.3a(18) and

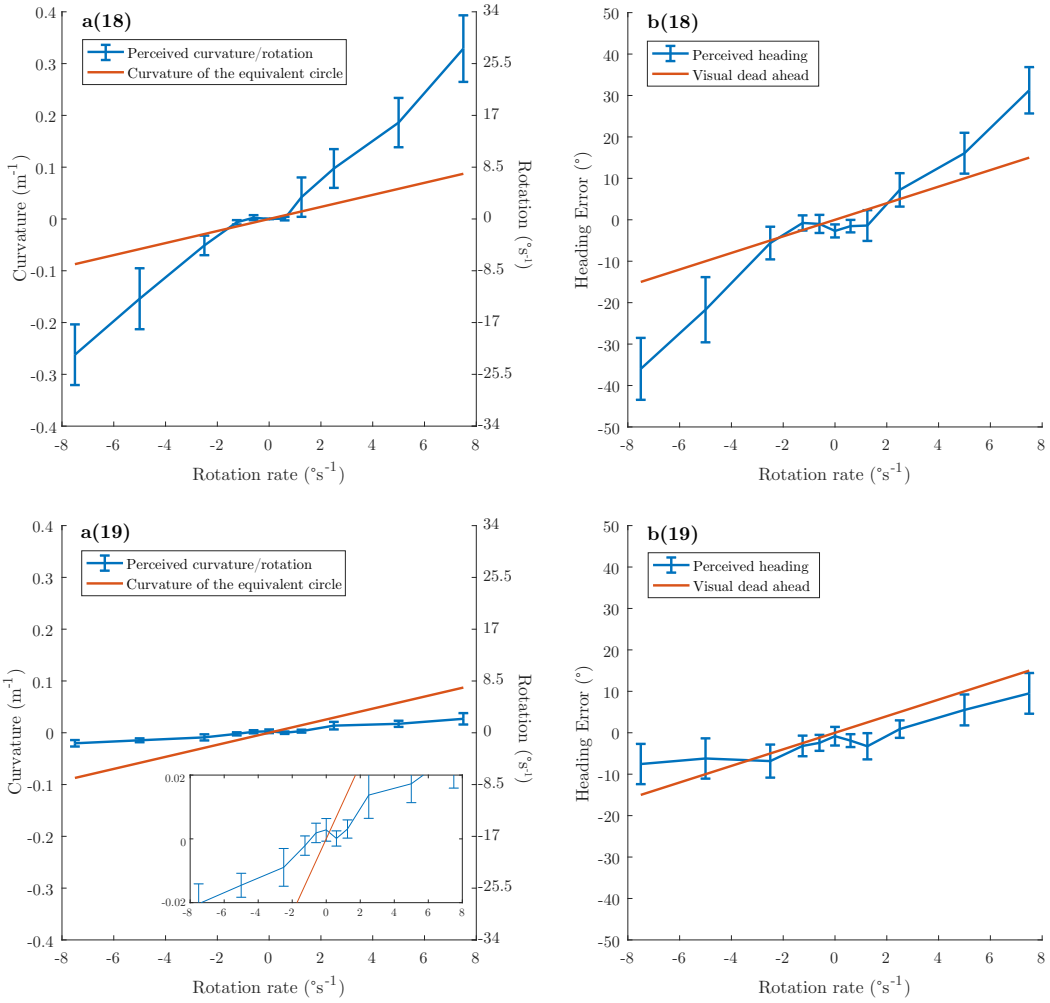

Figure 4.3: Individual perceptions of linear motion with rotation representative of the two different patterns in responding. Sub-figures a(18,19) represent perceived curvature for participants 18 and 19. These sub-figures also include an alternative y-axis scale. This shows the rotation generated by travel on a path of the curvature given in the matched point on the curvature scale if the observer is travailing at 1.5ms^{-1}. Sub-figures b(18,19) represent perceived heading relative to true heading for the same.

a(19). The responses of individual participants showed greater variation at higher rates of rotation however. There were also large interpersonal differences in responding, as can be seen by comparing Figures 4.3a(18) and a(19). These differences were broadly a matter of scale, with some participants reporting perception of tighter curves that might be expected given the simulated rotation rate while others reported much straighter, but still significantly curved, paths.

Regardless of scale, participants produced results demonstrating a significant

non-linearity over the full range of rotation rates. There was a plateau at low rates of rotation - typically at or below $\pm 1.25°s^{-1}$. This interesting feature can be seen clearly in the data from participants who generally overestimated curvature such as seen in Figure 4.3a(18). This participant underestimated curvature, relative to the equivalent circle, at rotation rates between -1.25 and $0.6°s^{-1}$, in spite of overestimating curvature at higher rates of rotation.

This pattern of responding was also found in the responses of curvature underestimators however. Here, in spite of the much smaller absolute difference in perceived curvature as rotation rate increased, there was still a significant plateau at low rates of rotation. An example of this can be seen in the Figure 4.3a(19) insert. This insert shows, with close y-axis zoom, that perceived curvature for tested rotation rates between $\pm 1.25°s^{-1}$ inclusive was not significantly different from that of any other tested point in the range or from zero perceived curvature, but was significantly different for perceived curvature for values outside this range. For both cases then, this represents an underestimation of curvature relative to their responding at other rates of rotation and generally indicated the correct perception of a path not significantly curved.

The presence of this plateau is not unprecedented. Previous experiments have shown that for low rates of rotation humans can correctly perceive heading (e.g. W. H. Warren & Hannon, 1988) and the presence of this plateau provides support for the argument that there is a process correcting for small rotations in the visual stimulus without vestibular input but that this process fails at higher rates of rotation.

Overall, mean perceived curvature across all participants was consistent with the curvature of the equivalent circle for any given rotation rate except for $\pm 0.6°s^{-1}$ rotation, where there was a small but significant underestimation of curvature. This can be seen in Figure 4.4.

4.2.2 Heading

In all cases true heading was zero degrees relative to the initial viewing direction at the start of the trial. Heading error therefore indicates participants perceived heading relative to their starting direction. Visual dead ahead represents the

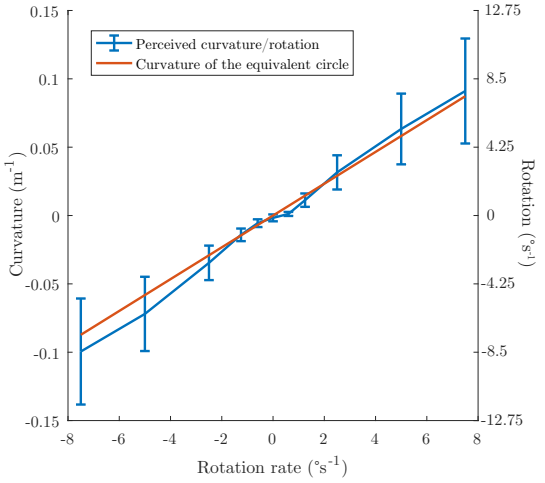

Figure 4.4: Average perceived curvature.

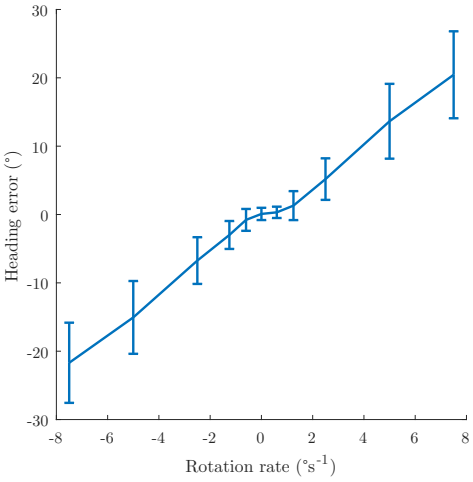

Figure 4.5: Average perceived heading error.

facing direction of participants relative to their starting direction at the completion of each trail post simulated rotation.

The change in heading error as rotation rate increased was also non-linear when averaged over all participants as per Figure 4.5. This means that overall, heading was determined accurately at rotation rates less than $|1.25|°s^{-1}$ but that there was a large and significant misperception of heading outside this range. This pattern did not hold for all individuals participating in the experiment however.

Figure 4.3b(18) shows an example participant who's pattern of responding, particularly with regard to the non-linearity at low rates of rotation, was similar to the overall average. Most participants produced results like this with only differences in scale between them. However, eight participants produced results similar to those seen in Figure 4.3b(19) where perceived heading, while significantly different from the true heading of zero degrees, was a lot closer to true heading and appeared linear across the range of rotation rates tested.

4.2.3 Heading and curvature

Perceived heading and perceived curvature appear to be closely related. On an individual by individual level perceived heading error was proportional to perceived curvature with the perception of increasingly curved paths being accompanied by larger heading errors. This pattern is apparent in the overall means, where an increase in perceived curvature is associated with an increase in heading error

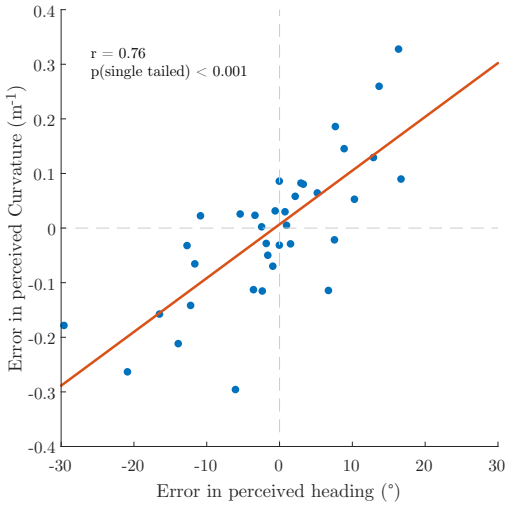

Figure 4.6: Mean error in perceived heading vs mean error in perceived curvature at $\pm 7.5^{\circ}s^{-1}$ simulated rotation for all participants. The orange line represents the best linear fit from the sum of squared errors. Mean error in perceived heading and mean error in perceived curvature were strongly correlated, $r(34) = 0.76$, $p < 0.001$.

(compare Figures 4.4 and 4.5). Furthermore, for any given tested magnitude of rotation mean error in heading perception and mean error in curvature perception were strongly correlated. For an example of this see Figure 4.6 where error in perception is compared across all participants for the rotation rates $\pm 7.5^{\circ}s^{-1}$. Here we found a strong correlation $r(34) = 0.76$, $p < 0.001$.

Individual variation in the presence of an overall relationship could suggest some sort of compensatory mechanism, where detected rotation is removed before heading is determined. The stimulus presented to participants consisted of $T + R$, and extracting the translation component requires an estimate of R, R', to be removed from $T + R$. If $R' = R$ then only T remains and heading error should be zero. When R' does not equal R then T is not correctly recovered. Examples of this can be seen by comparing the alternate y-axis scale to the true rotation rate shown on the x-axis of Figure 4.3. The perceived rotation in these figures represents residual rotation not accounted for in R'. Where perceived rotation is low (e.g. Figure 4.3a(19)) participants perceive heading relatively accurately. On the other hand, where perceived rotation is high heading error is correspondingly high. The underestimation of R' therefore manifests as the perception of a curved path, where the simulated rotation has not been detected using visual means alone and is thus misinterpreted in the absence of extra-retinal cues. This mechanism is discussed in further depth in Chapter 7.

4.2.4 Anecdotal reports of forgetting

While it was not recorded, some participants reported forgetting what path they were on when they failed to enter a response within two seconds post-trial due to distraction. This usually occurred during the familiarisation period, and the delay was often due to fumbling of the controls. Each of the participants for whom this occurred reported resorting to guessing to complete the trial. This short period of memory availability bears some resemblance to sensory memory processes and may be worth investigating further.

4.3 Overall comments

The overall agreement between the heading errors we recorded and those seen in past experiments, both in pattern and relative magnitude, suggest that the new response tool is producing data that are usefully comparable to that from previous experiments. The short response times seen during pilot testing persisted when the tool was used by a wider selection of participants confirmed is suitability for rapidly and efficiently acquiring simultaneous estimates of heading and curvature. Participant ability consistently produce precise estimates with the tool, even while operating at speed, combined with the low familiarisation requirements confirm the assertion that the tool is intuitive. Altogether, this makes it useful for testing predictions about curvilinear path perception made by models of curvilinear motion estimation.

Anecdotal reports on the rapid decay of participant memory for path also provides some support for the use of our tool over existing slower tools. When participants are likely to forget exactly how they perceived the motion after a short delay tools that allow them to respond quickly have an advantage. While the current tool does not allow responding during a trial it does allow participants to record a complete response in less than a second which is shorter than the elapsed time before participants began to report forgetting how they perceived their movement. That said, delay effects on path memory are unconfirmed. Future work could include a parametric study manipulating response delay time to better quantify any effects.

Linear paths

The new line tool should prove as useful for measuring perception of linear paths as it is for measuring perception of curvilinear paths. When translations are correctly perceived observers can respond by using the line as a pointing tool, disregarding their ability to curve the line. In this respect using the tool is like using a cursor to report perceived heading, different only in that it extends from the observer to a distant point instead of existing at only the distant point in the world.

This tool provides a benefit beyond replicating the utility of pointing tools however. It allows participants to indicate a curved path should they perceive so. One condition where it seems likely that participants could perceive such a curved path is during linear translation at increasingly eccentric headings. Heading directions that are not along the viewing direction bias the flow field such that there is an increasingly strong influence of sideways motion on the flow field as heading eccentricity increases (Perrone, 2018). Indeed, although motion parallax has an effect, a heading of $\pm 90^{\circ}$ to the view direction the instantaneous flow field is quite similar to a flow field generated by pure rotation in that all vectors point in the same direction.

It has been proposed that this uniform direction of motion shared by sideways motion and rotation sideways could be the cause of the centre screen bias reported throughout the history of heading perception experiments (Perrone, 2018). Perrone (2018) suggests as an explanation the erroneous detection of rotation driven by curvilinear path detectors in combination with a lack of vestibular input. When this occurs rotation is incorrectly estimated to be greater than zero and therefore compensating for this detected rotation causes a heading bias. If this is the case then we would expect to see increasingly strong perceptions of

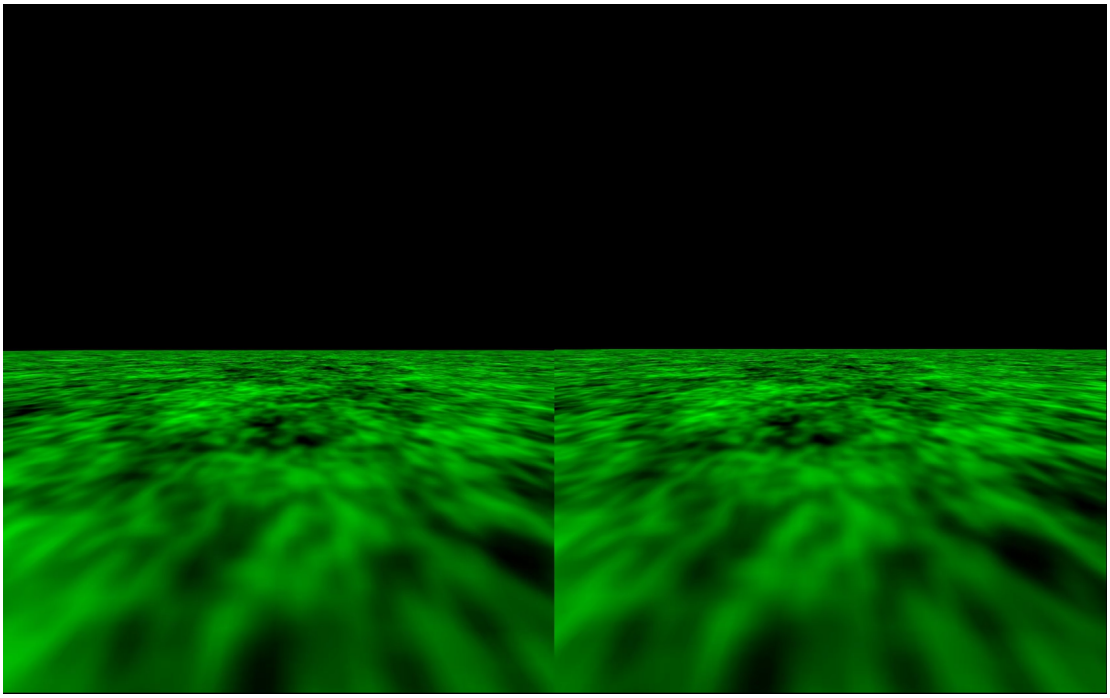

Figure 5.1: An example stimulus depicting travel at 1.5ms^{-1} in a straight line with a heading displaced 20° left from the initial viewing direction.

curvature as absolute heading angle increases.

5.1 Method

5.1.1 Participants

Twenty-five undergraduate psychology students, 18 female, aged 17 to 47, with normal or corrected to normal vision participated in the experiment. This experiment was approved by the University of Waikato Psychology Research and Ethics Committee.

5.1.2 Equipment

Stimuli were presented using the same virtual reality equipment and computer system as described in 4.1.2.

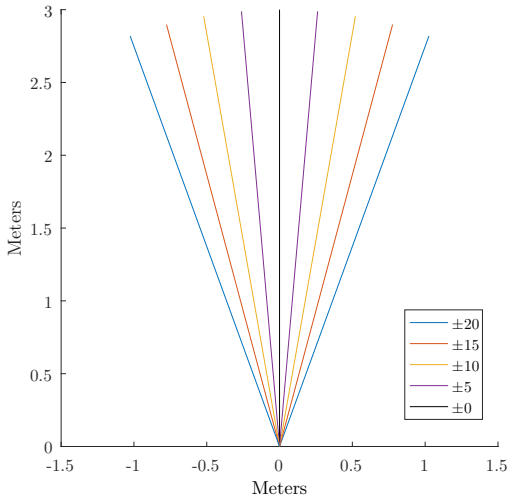

Figure 5.2: A birds-eye- and to-scale-view of the linear paths used in this experiment. The legend shows path angle in degrees. Negative values represent angles to the right. All paths start at the origin [0, 0].

5.1.3 Trial design

Each participant completed 90 trials, ten each for the headings between ±20° in 5° steps relative to view direction, presented in a random order. A visual depiction of the paths used can be seen in Figure 5.2. View direction was always straight ahead relative to the starting position. Each trial started when the participant indicated that they were ready by pressing a button on the controller. Once started, a trial consisted of two seconds of motion along a linear path at 1.5ms^{-1} followed by an unlimited but typically less than 1.5-second-long period of responding. An example of a trial where heading was displaced 20° to the left can be seen in Figure 5.1. All participants were told they could take a short break between any two trials if they required, but only one participant did so. That participant recommenced the experiment after three minutes. All participants completed all trials within ten minutes.

Movement during each trial was over a flat ground plane as described in Subsection 4.1.3. At the end of each trial participants reported their perceived path using the response tool described in Section 3.2.

Before beginning the experimental trials participants also completed 33 practise trials to familiarise themselves with responding using the unfamiliar controller input as per the previous linear with rotation perception experiment and described in Section 4.1.3.

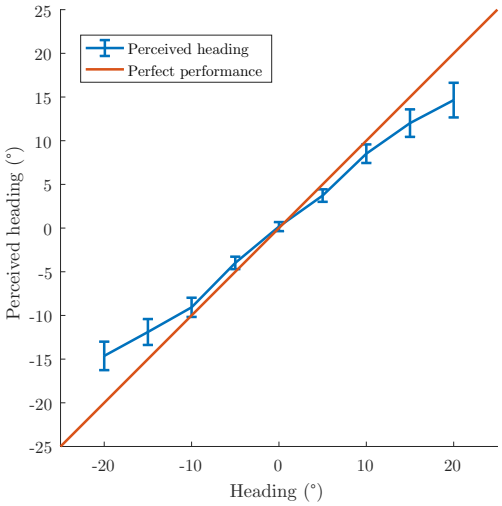

Figure 5.3: Average perceived heading during linear translation.

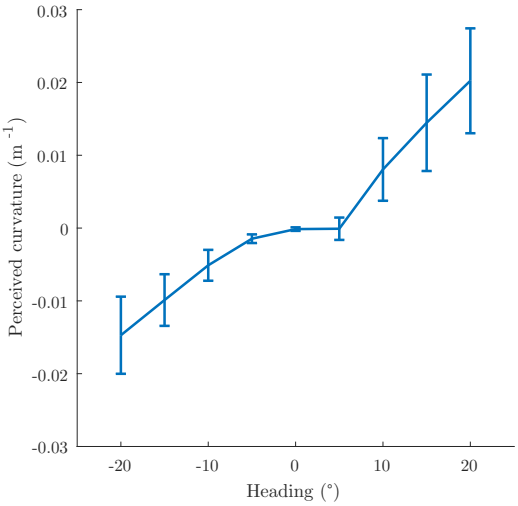

Figure 5.4: Average perceived curvature during linear translation.

5.2 Results and discussion

5.2.1 Heading

Across all participants a broad range of responses were recorded. The two extremes of this range can be seen in 5.6. Sub-figure a(4) shows data for a participant with near perfect perception of heading regardless of heading angle. Sub-figure a(25) however shows a very different pattern of response where the participant believed their heading was always straight ahead relative to their gaze direction regardless of their true heading. Most participants tended towards the average seen in Figure 5.3 however, presenting an increasingly large underestimation of heading as true heading increased. This overall result is congruent with previous findings showing a centre screen bias effect (W. H. Warren, 2003).

5.2.2 Curvature

All participants perceived significant curvature at a heading eccentricity of $|20|°$ and most participants also perceived this curvature at headings equal to or greater than $|10|°$. On average participants generally perceived curved paths when heading was equal or greater than $|10|°$ and straight paths at lesser heading excentricities as can be seen in Figure 5.4. Degree of perceived curvature was relatively variable

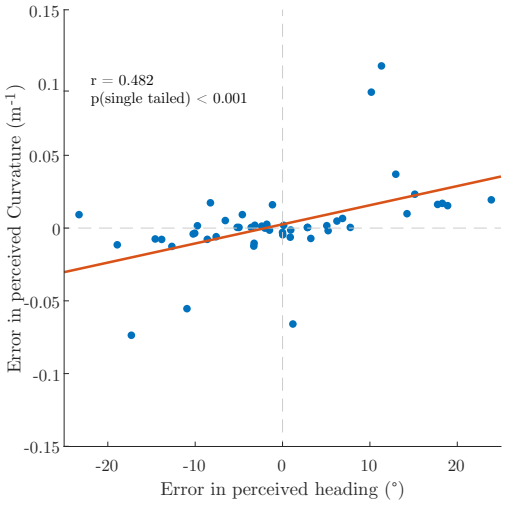

Figure 5.5: Mean error in perceived heading vs mean error in perceived curvature at ±20°heading eccentricity for all participants. The orange line represents the best linear fit from the sum of squared errors. Mean error in perceived heading and mean error in perceived curvature were weakly, but significantly, correlated, $r(48) = 0.482$, $p < 0.001$.

across participants however. Also, while participants did perceive a significant degree of curvature, perceived curvature was generally an order of magnitude less than that seen when participants were presented with a combination of linear translation and rotation as can be seen by comparing Figures 5.4 and 4.4.

5.2.3 Heading and curvature

Notably, errors in heading perception were accompanied by significant perceptions of curvature even though stimuli consisted of pure linear translation. Much like the relationship between error in perceived heading and curvature reported in in Subsection 4.2.3, this relationship shows in the mean data (compare Figures 5.3. It is also visible as a moderately weak but significant, $r(48) = 0.482$, $p > 0.001$, correlation (see Figure 5.5) between error in perceived heading and error in perceived curvature for heading eccentricities of ±20°across all participants. This suggests that the flow field bias created by eccentric headings may be misperceived as curvature.

5.3 Overall comments

Testing perception of heading during linear translation using the new tool showed that participants tended to misperceive linear paths on eccentric headings as curved paths. This was seen alongside a heading bias similar to the center screen

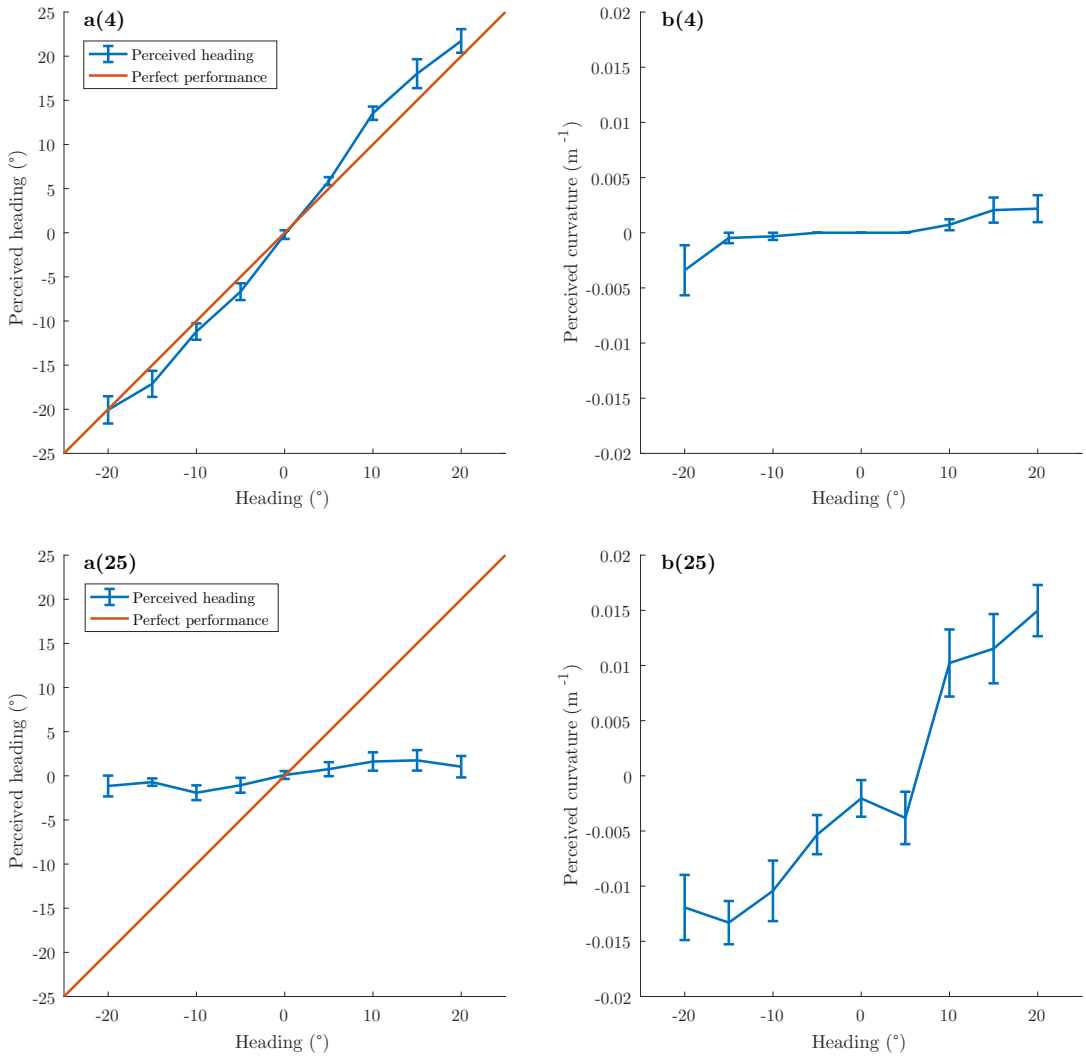

Figure 5.6: Example individual perceptions of linear motion. Sub-figures a(4) and a(25) depict perceived heading as a function of trial heading. Sub-figures b(4) and b(25) show perceived curvature as a function of trial heading.

bias seen in many (e.g. D'Avossa & Kersten, 1996; Llewellyn, 1971; W. H. Warren & Saunders, 1995; Johnston et al., 1973), although not all (e.g. R. Warren, 1976) previous studies. This bias was observed even with the relatively wide FOV of the Vive headset when previous studies have suggested that perhaps increased FOV could decrease the effect. This suggests the possibility that the centre screen bias may not be an artefact of display type but a consequence of the visual system misperceiving the sideways flow generated by eccentric headings as rotation (Perrone, 2018).

True curvilinear paths

Given identical starting conditions, travel around a true curvilinear path while maintaining gaze direction along the tangent of the curve (see Figure 1.2a) produces an instantaneous flow field identical to that created by linear translation with rotation. However, because the paths followed during each movement diverge over time the flow fields produced evolve differently. The extra information provided by this divergence could be used to more accurately determine heading and rotation.

As a consequence of this instantaneous equivalence if humans rely solely on the instantaneous flow field to determine heading and rotation then we would expect perception of true curvilinear paths to be similar, if not identical, to perception of linear paths with rotation. This is because the stimuli for both cases would be functionally identical. On the other hand, if humans make use of the flow field evolution over time then we would expect to see different perceptions arise from the two types of motion. In either case, however, previous work suggests a high degree of heading accuracy is unlikely given the absence of extra-retinal rotation signals and the incongruent vestibular signal, indicating zero rotation, that is available to static observers.

The tool for measuring path and heading presented in Section 3.2 seems ideal for measuring perception of these curved paths compared when compared to previous measures. Unlike pointing alone, or asking which side of a post one is going to pass on, it does not confound errors in heading perception and errors in curvature perception. As such, an experiment was devised to measure participant perception of curved paths using this tool.

6.1 Method

6.1.1 Participants

Twenty-seven individuals aged 17 to 47 with normal or corrected to normal vision completed the experiment. Of these 25 were the same individuals recruited for the previous experiment described in chapter 5. Participants from this group completed this experiment in the same session as they completed the previous experiment. The remaining two participants completed only this experiment. All participants completing both experiments in the same session were permitted a rest break between experiments so that they could remove the headset and walk around. Participants variously took breaks of five to 15 minutes. This experiment was approved by the University of Waikato Psychology Research and Ethics Committee.

6.1.2 Equipment

Visual stimuli were presented using the same virtual reality equipment and computer system as described in 4.1.2.

6.1.3 Trial design

Each participant completed 130 randomly ordered trials over the course of up to 14 minutes. Each trial started after the participant indicated they were ready and consisted of a two-second-long period of motion along a constantly curved path at 1.5ms^{-1} followed by an unlimited but typically less than 1.5 second long period of responding. Participants were told they could take a short break between any two trials if they required but none did so. There were 10 trials for each of the radii ±11.46, ±17.19, ±34.38, ±68.76, ±143.2 m. There were an additional 10 trials for each of three linear (curvature = 0m^{-1}) paths with headings 0 and ±5°. A graphical depiction of the different paths can be seen in Figure 6.2.

Travel on circular paths of these radii while viewing instantaneous heading direction (i.e. the tangent to the curve) created rotations respectively equal to those – ±7.5, ±5.0, ±2.5, ±1.25, ±0.6, and 0°s^{-1} – seen in the previous experiments where rotation was directly manipulated. Each of the three blocks of zero

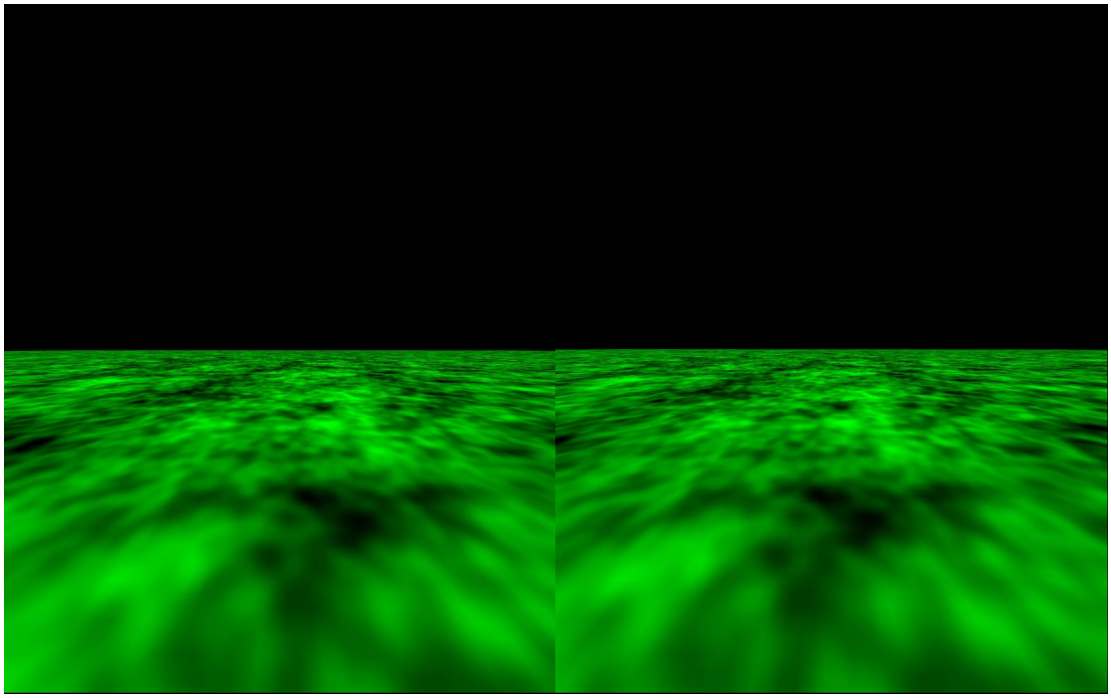

Figure 6.1: An example stimulus depicting travel on a curved path of radius 11.46m at 1.5ms^{-1} while looking down the tangent to the path (the instantaneous heading). This combination results in a vertical axis rotation of 7.5˚s^{-1}, making it the true curvilinear equivalent to the 7.5˚s^{-1} simulated condition shown in figure 4.2.

curvature presented trials with different headings. Headings tested were ±5°, and 0°. This was done as a check to ensure that participants could and were pointing using the new response tool during trials where only a small movement was required. Motion during each trial was over a flat ground plane as described in section 4.1.3. At the end of each trial participants reported perceived curvature using the line response tool as described in 3.2.

Before beginning the experimental trials participants who had not previously completed the linear motion perception experiment described in chapter 5 also completed 33 practise trials to familiarise themselves with responding using the unfamiliar controller input as per the previous linear motion with rotation perception experiment and described in section 4.1.3.

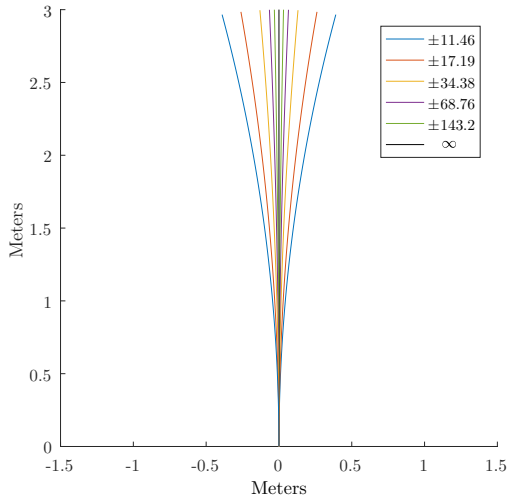

Figure 6.2: A birds-eye- and to-scale-view of the paths used in this experiment. The legend shows path radius in meters. Negative values represent curves to the right. All paths begin at the origin [0, 0].

6.2 Results and discussion

6.2.1 Curvature

Again, continuing with the theme of the results for the previous experiments in this thesis, there was a broad range of participant responses. Seen in Figure 6.3 there were participants who significantly over estimated curvature as per sub-figure a(7) and those who significantly underestimated curvature as per sub-figure a(13).

Participants covered the full range of heading perceptions between a(7) and a(13), though most fell close to the average. Overall tendency, therefore, was for participants to slightly overestimate curvature at higher degrees of curvature while accurately indicating curvature for paths of radius greater than 68 m. This can be seen in Figure 6.4.

6.2.2 Heading

Participants generally displayed some degree of heading misperception as can be seen in 6.3 b(7) and b(13). Furthermore, these errors, while significant, tended to be relatively small, and subject to greater variation than heading errors for linear paths that resulted in perceived headings of similar magnitude.

Heading for test trials of ±5° linear translation were perceived accurately by all participants but headings for straight paths of zero heading were significantly

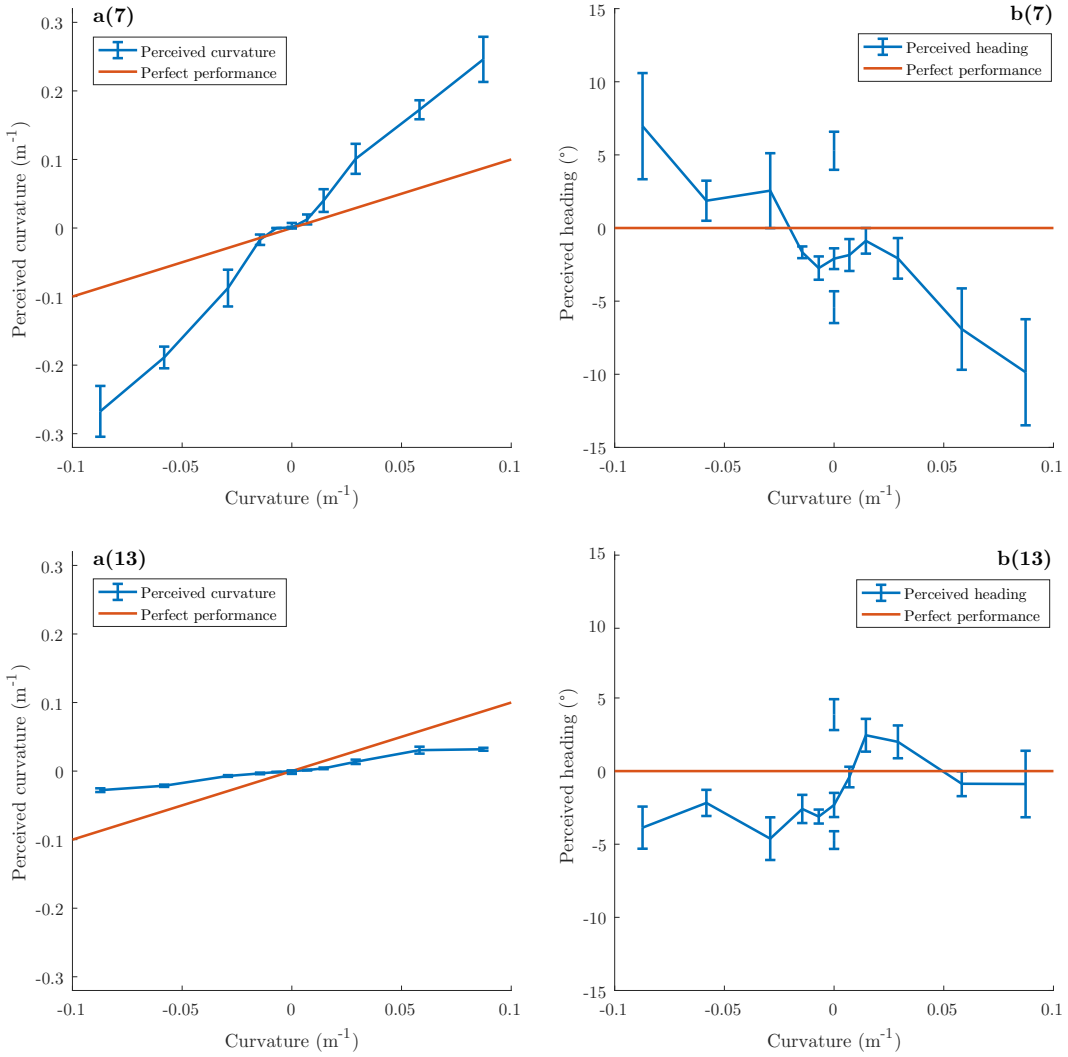

Figure 6.3: Example individual perceptions of curvilinear motion. Sub-figures a(4) and a(25) depict perceived curvature as a function of trial curvature. Sub-figures b(4) and b(25) show perceived heading as a function of trial curvature.

misperceived by all participants even though curvature was perceived correctly.

Average perceived heading across all participants was unusual, and not only in that it changed non-linearly with degree of curvature. This non-linearity was somewhat expected after seeing the results of the previous two experiments. What stands out is that here heading does not change monotonically. For paths of greater curvature perceived heading was biased towards the edge of the screen in the direction of rotation, towards the inside of the curve. For low but non-zero path curvatures heading perception was biased towards the other side of the screen, on the outside of the curve. Heading perception was therefore accurate at

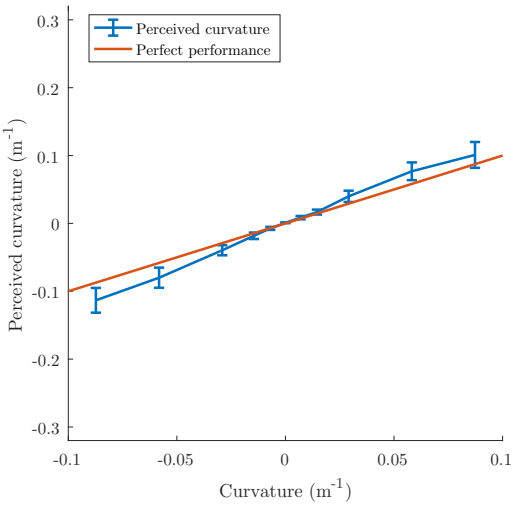

Figure 6.4: Average perceived curvature during curvilinear motion.

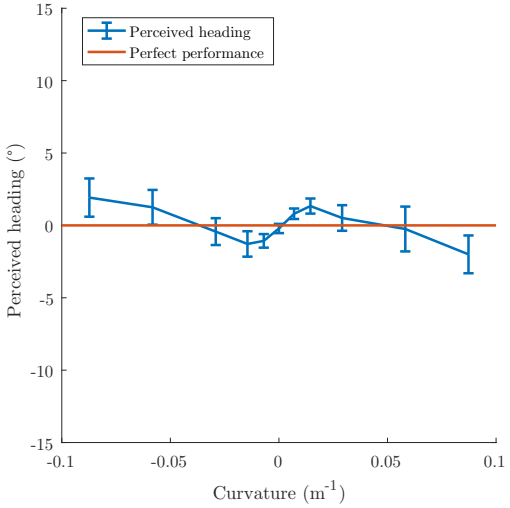

Figure 6.5: Average perceived heading during curvilinear motion.

three separate points across the range of curvatures tested, not being significantly different from true heading for the radii ±34.38 and ∞ meters. This reversal could be caused by the mechanism driving the plateau seen in heading data from Chapters 4 and 5 responding more strongly to the stimulus here.

6.2.3 Curvature and heading

For individual participants, those who overestimated curvature tended to have perceived heading errors of opposite sign to those participants who underestimated curvature. An example of this can be seen in comparison of Subfigures 6.3 b(7) and b(13). The relationship between average perceived curvature and average heading is less clear however. Possible reasons for this are discussed in Chapter 7.

6.3 Overall comments

The overestimation of curvature seen here is similar in magnitude to the overestimation of curvature, relative to the curvature of the equivalent circle, seen in Chapter 4. Additionally, as before, two similar groups of response style were seen. Overall, however, individual participants were more precise in their responding

and the difference between the two groups was less pronounced.

This increased consistency could indicate greater familiarity with curvilinear motion compared to linear motion with rotation as it corresponds to the much more common travel around a curved path rather than the less common skid. On the other hand, the increased consistency, both in individual responses and between observers, could instead be a consequence of reduced conflict between the perceived path and the rotation in the visual stimulus.

This consistency, or its lack, is of interest. Perception of each trial depends partially on both how long the participant takes to make a judgement and when during a given trial the judgement is made. The information required to determine heading is available over very short time scales while the trials presented here are comparatively long. As such, one might see increased consistency in heading and path judgements during linear motion with rotation when using shorter trials.

Modelling visual-vestibular integration

We now have data recording heading and curvilinear path perception during both simulated rotation with translation and curvilinear motion as well as evidence for the perception of curved paths when translating eccentric to view direction. As such, we can begin comparing the predictions of a model presented by Perrone (2018) to participant performance. The Perrone (2018) model suggests that a vestibular estimate of rotation is needed in order for R' to match R. It also suggests that where $R' \neq R$ there will be heading bias, with values of R' greater than R resulting in heading bias in the direction of the perceived rotation while values of R' less than R result in bias of the opposite direction.

Each of the experiments presented in this thesis has explicitly used visual stimuli to elicit perception of self-motion. At the same time, however, because participants remained stationary, the experiments provided a vestibular stimulus indicating no rotation during every trial. While this vestibular stimulus is common to many historical heading perception experiments it is nevertheless incongruent with the presented visual stimuli. This means that we will be modelling participant behaviour when the vestibular signal indicates zero rotation. This chapter compares model predictions to data from the true curvilinear motion experiment in Chapter 6. In particular, it compares participants perceived rotation to model predictions for perceived rotation generated on the assumption that the vestibular system is reporting rotation distributed around no rotation and the visual system is reporting rotation distributed around true rotation.

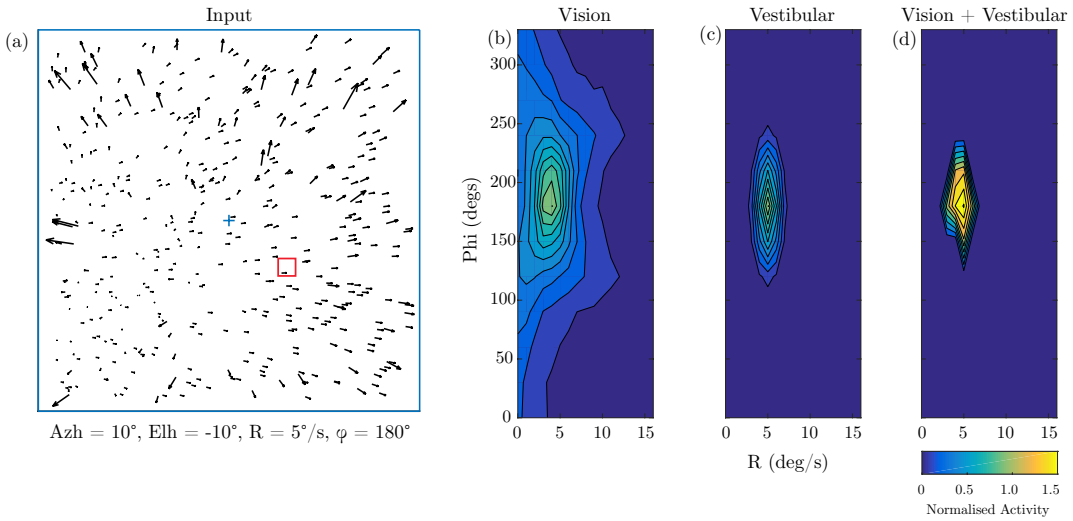

Figure 7.1: (a) Input flow field generated by travel at 1.5ms^{-1} along a curved path of radius = 17.2m, instantaneous heading towards azimuth = 10°, elevation = -10° relative to view direction. Travel on this path results in counter-clockwise rotation at 5°s^{-1}. (b) Normalised activity map for vision only rotation detectors. (c) Vestibular signal centred on the correct rotation. (d) Combined visual and vestibular distributions.

7.1 The model

The Perrone (2018) model produces a vision based estimate of rotation by sampling the flow field across a range of possible headings and for each of these potential headings calculating the range of rotation rate and directions that could produce the given vector if one was travelling in that direction. By then binning the calculated rates and direction pairs into a set of candidate rate and direction pairs it determines the most commonly occurring pair, in the process producing a distribution of activity across rate and angle values, forming the visual estimate of rotation. An example of this can be seen in Figure 7.1, where the flow field from sub-plot (a) is processed as described resulting in the distribution of possible rotation rates and pairs as seen in sub-plot(b). Here, with the relatively large number of vectors, the distribution peak is centred roughly at the correct value, although the standard deviation of the distribution in each dimension is quite broad.

This vision based estimate of rotation alone is not enough to explain human perception however. Achieving human level heading perception accuracy of

within one degree from true heading requires a rotation discrimination threshold of $0.2°s^{-1}$ (Perrone, 2018). This makes visual estimates of rotation, with their rotation discrimination threshold of approximately $1°s^{-1}$, a poor basis for estimating rotation. Further, vision only rotation estimation can result in substantial errors. When only a few vectors are available the rotation estimation mechanism presented in Perrone (2018) can produce a distribution peak of displaced significantly from the true rotation. If the most probable peak is incorrect then using the rotation angle and rate it indicates to compensate for rotation in the flow field will result in an inaccurate estimation of heading.

A potential solution to the shortcomings of visual only rotation estimation comes in the form of a vestibular rotation estimate. As with visual estimates of rotation, however, vestibular estimates alone are insufficient to explain human heading perception performance. While the vestibular system does not suffer from the possibility of multiple probable rates and angles the vestibular system rotation threshold of $1°s^{-1}$ (MacNeilage, Banks, et al., 2010) is insufficiently precise to explain human heading perception performance. Nevertheless, the visual distribution can be combined with information from the vestibular system. By applying a two-dimensional Gaussian distribution centred on the vestibular estimate of rotation rate and angle with the Gaussian standard deviations equivalent to human discrimination thresholds for rate and angle such as seen in Figure 7.1(c) the Perrone (2018) model down weights visual solutions that fall outside the window of solutions considered possible by the vestibular system. Combining the visual and vestibular estimates in this way results in a better defined peak in a distribution that now excludes the most unlikely incorrect response. For the example here this combined distribution can be seen in Figure 7.1(d). This better defined peak and reduced deviation results in a more accurate estimate of rotation rate and angle and therefore more accurate rotation compensation, to a degree sufficient to allow human level performance in heading perception tasks.

7.2 Implementing the model

7.2.1 Distribution creation

Visual distributions were created to represent possible rotation rate estimates that the visual rotation estimation stage could arrive at given a specific rotation rate as input. Vestibular distributions were created to represent the possible rotation rate estimates from the vestibular system given zero rotation and human level vestibular rotation thresholds. For both types of distribution only two possible phi angles were modelled – zero degrees, representing clockwise rotation on the horizontal plane and 180 degrees, representing counter-clockwise rotation on the horizontal plane. This is because the experimental data we have contains only information regarding perceived rotation on the horizontal plane.

All distributions were calculated across the range $\pm 15^{\circ}$ regardless of their shape or position. In all modelled cases this allowed each distribution to be calculated out to at least four standard deviations from its mean. Changing the location parameter does not change the shape of the distribution.

The visual distribution

Figure 7.2(a) shows a set histograms depicting normalised detector activity across rotation rate for three angles of rotation. These histograms represent 'slices' of the contour plot in Figure 7.1(b) for Phi values of 150°, 180°, and 210°, illustrating the skew towards higher rates of rotation seen in vision only model estimates of rotation at any particular angle. To match the skew of these distributions the visual distributions for this model implementation were constructed as skew normal distributions of the form

$$f(x) = \frac{2}{\omega}\varphi\left(\frac{x-\zeta}{\omega}\right)\Phi\left(\alpha\left(\frac{x-\zeta}{\omega}\right)\right)$$

where

$$\varphi(x) = \frac{1}{\sqrt{2\pi}}e^{-\frac{x^2}{2}}, \quad \Phi(ax) = \int_{-\infty}^{ax}\varphi(t)\,\mathrm{d}t.$$

with the parameters scale ω, location ζ, and skew α. The effect of changing scale and shape parameters is depicted in Figure 7.3. The skew normal distribution is generally considered a good distribution for modelling data where the skewed

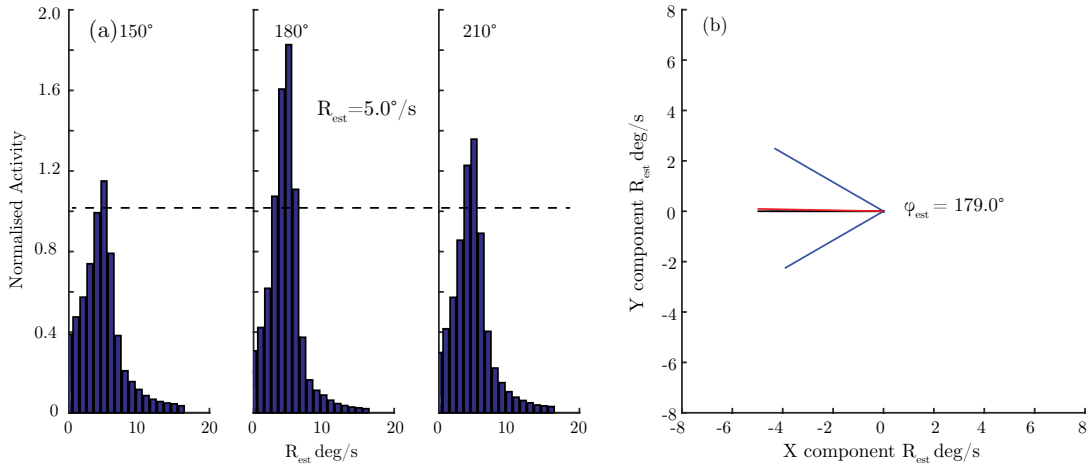

Figure 7.2: (a) Normalised rotation detector activity by angle, taken from Figure 7.1(b) and most notable for showing the long tail towards higher rates of rotation. The dashed line represents the threshold applied before the centroid estimation of rotation rate (see Section 7.2.2). (b) Centroid estimation of rotation rate based on the three distributions in (a), where blue lines represent each sub-figure in (a) and the red line represents the centroid of all three responses.

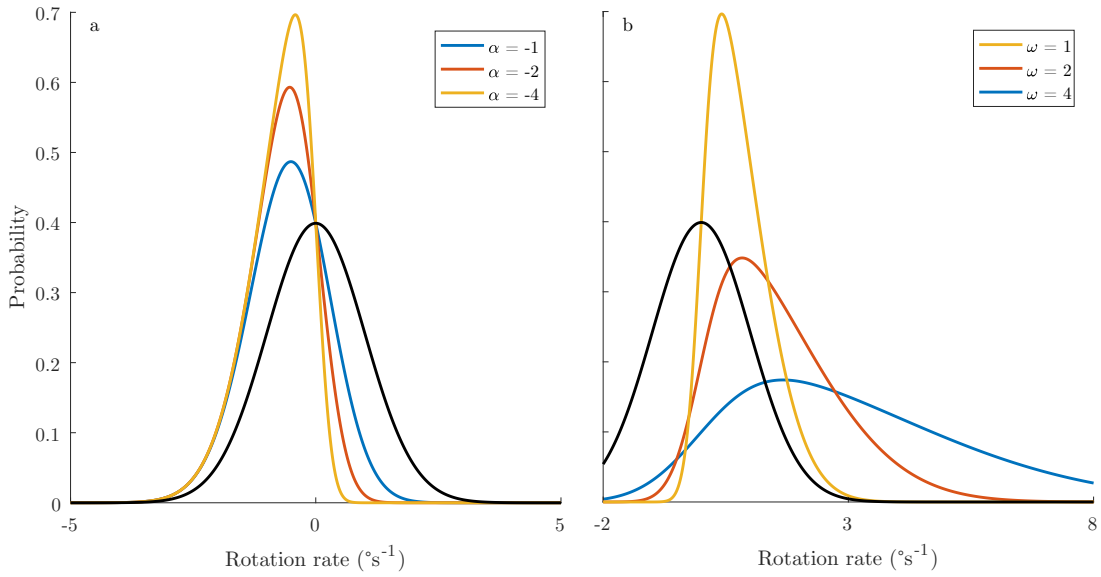

Figure 7.3: Skew-normal distributions demonstrating the effect of changing (a) shape(α) with fixed scale(ω) = 1 and (b) scale(ω) with fixed shape(α) = 4. All functions are located at the origin. The normal distribution (i.e. $\alpha = 0$, $\omega = 1$; in black) is provided for reference.

distribution still has normal-like properties, most notably low incidence of outliers, in the direction of the skew and where further complex manipulations of the distribution are not required by the analysis. Further details on the distribution can be found in *"The skew-normal and related families"* (Azzalini, 2013).

Location of the distribution was varied with the rotation rate required to maintain view direction along the tangent of the path such that the mean of the normal probability density function was equal to the test rotation rate. Shape was scaled linearly with rotation magnitude such that it was 0 (i.e. normal) at zero rotation and increasingly skewed at higher rates of rotation. To achieve this a fixed skew value determined by best fit was multiplied by the true visual rotation rate. This modelled the increased skew in model estimates as rotation rate increased.

The vestibular distribution

The vestibular distributions were normal distributions of the form

$$f(x) = \frac{1}{\sqrt{2\pi\sigma^2}} e^{-\frac{(x-\mu)^2}{2\sigma^2}}$$

where σ is the standard deviation of the distribution and μ is both the mean of the distribution and the location parameter. The mean for each vestibular distribution was always equal to zero - i.e. no rotation, the true physical situation. The standard deviation of the vestibular distribution is inversely proportional to its relative hight compared to the visual distribution such that where the maximum probability rotation rates for the visual and vestibular solutions were equal the standard deviation of the vestibular system was equal to one degree per second. This baseline standard deviation is roughly equivalent to average tested human performance, with MacNeilage, Turner, and Angelaki (2010) reporting human vestibular rotation threshold of $1.45°s^{-1}$ using a two-alternative forced-choice paradigm, then adjusted by dividing by $\sqrt{2}$ as per Green, Swets, et al. (1974) to provide the standard deviation of the underlying distribution approximately equal to $1.03°s^{-1}$.

7.2.2 Combining distributions

The process of combining visual and vestibular distributions for the range of considered rotation rates and arriving at a final prediction for perceived rotation rate involves four major steps. These are the summing of individual pairs of distributions, the thresholding of the combined distribution, finding the centroid of the threshold distribution, and repeating the process for each rotation rate of interest. These steps are based off of Perrone (2018) and represent the simplest method of combining information from the visual and vestibular systems and then deriving an estimate of rotation. While a range of different combination rules (Ernst & Banks, 2002; Fetsch et al., 2010; Landy, Maloney, Johnston, & Young, 1995; Rohde, van Dam, & Ernst, 2016) and methods of deriving an estimate (e.g. mean, peak) are possible the rules used here appear to sufficiently explain existing human perception data. A visual walkthrough of this process can be found in Figure 7.4.

Combination rules

The visual and vestibular distributions are combined as equally weighted components of a convex combination. This corresponds to Figure 7.4a.

Thresholding

The resultant distribution is normalised. Doing so allows the applied threshold, a number between zero and one, to be relative to the peak probability for any given test. This makes the threshold comparable across participants even though the combined distributions themselves may differ in peak magnitude. This threshold is applied by discarding the probability values for all possible perceived rates that have some probability less than the threshold value. This corresponds to Figure 7.4b.

Finding the centroid

The model estimate of perceived rotation for the tested real rate of rotation is then found by taking the centroid of remaining suprathreshold portion of the distribution. This corresponds to Figure 7.4c. The process is then repeated for

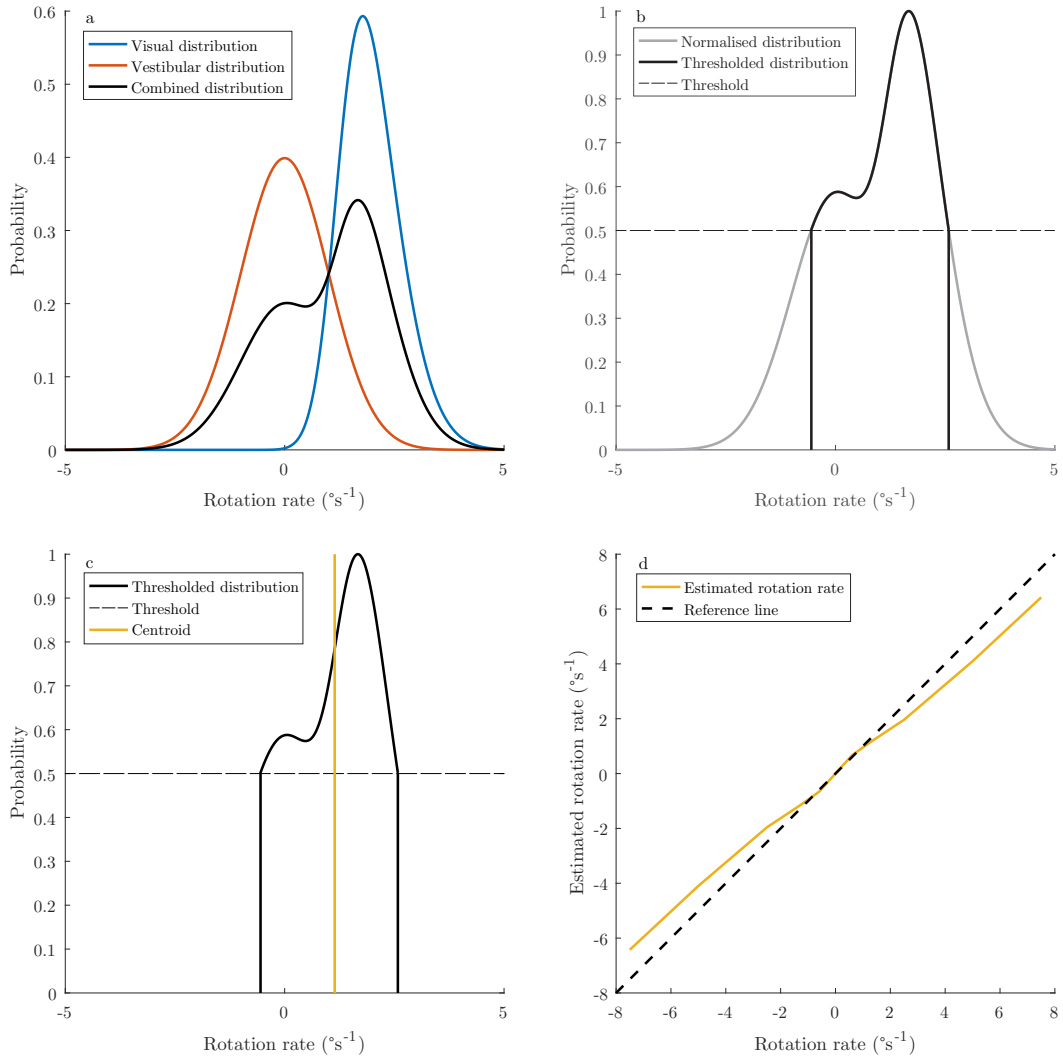

Figure 7.4: Example process for the calculation of model estimates where the visual system receives a stimulus indicating rotation at 1.25°s^{-1} while the vestibular system receives a stimulus indicating no rotation. (a) The combination of rate estimate distributions from each system. (b) Normalizing and thresholding the combined distribution. (c) Finding the centroid estimate from the final distribution. The value of the centroid estimate here (1.13°s^{-1}) is a slight underestimation of rotation rate compared to the visually simulated rotation due to the suprathreshold vestibular contribution. (d) Example plot showing model predictions for visual rotation rates between ±7.5°s^{-1} given a threshold value of 0.5, visual and vestibular distribution standard deviations of one, and a visual distribution shape parameter of 1.6.

all tested rotation rates, in this case 0, ±0.6, ±1.25, ±2.5, ±5.0, and ±7.5°s^{-1}. For the threshold and skew values chosen in the visual example this gives the perceived rotation rate estimation shown in Figure 7.4d.

7.2.3 Fitting the model to participant data

Model parameters to fit participant perception of true curvilinear motion as reported in Chapter 6 were determined using the *fminsearch()* search function from Matlab R2018b. *fminsearch()* is a multidimensional non-linear derivative-free minimiser using the Nelder-Mead simplex (direct search) method. An in-depth look at this algorithm can be found in Lagarias, Reeds, Wright, and Wright (1998).

Error functions

fminsearch() requires an error function which can be used to compare the target data to the successive calculated answers produced by the function. Two error functions were considered. Initially, a standard sum of squared errors term was used to produce an error estimate. At the time this did not seem sensitive enough to the observed non-linearities in participant rotation perception during movement along paths of low curvature. This was because it under-weights the large relative but small absolute errors usually found where both the estimate and the participant mean for a given curvature are close to zero.

An alternative was tested, the sum of squared standardised errors, which weights the absolute error for low variance estimates of rotation higher than the absolute error for noisy estimates of rotation. This is because, for any given absolute difference between the true and estimated rates of rotation, where participants responses were low variance the difference will represent a greater number of units of error than for an estimate with greater variance. Following finalisation of the distribution shapes and the selection of a skewed rather than symmetrical visual distribution, however, it was found that the simpler sum of squared errors now produced an acceptable fit and so, for a first pass, the simpler method prevailed.

Hard bounds

Because *fminseach()* does not by default support bounded searching of the problem space it was necessary to restrict some of the function parameters using the error function. These restrictions were implemented through the substitution of artificially large error function values in place of the calculated error function values. This caused *fminsearch()* to reject solutions containing out of bounds values. This was done to avoid the algorithm spending time testing and/or settling on nonsensical values (e.g. a threshold value lower than zero, the value of which already accepts the entire distribution and as such produces results no different to any negative value.).

Threshold restrictions: The first restriction applied was to limit the range of possible values that *threshold* could take to the range 0–1 inclusive. The upper limit was set at one because, when using a normalized distribution, a threshold value greater than one excludes all available information and results in undefined behaviour. With this restriction all cases must include some portion of the combined distributions when calculating the centroid estimate.

The lower limit of zero was chosen in order to improve comparability between model fits across participants. With this restriction all cases where the best estimate is found by including the full range of the distributions (i.e. $threshold \leq 0$) will settle on a *threshold* value of zero instead of a random value less than or equal to zero.

Vestibular ratio restrictions: The second restriction was to limit the values that *vratio* could take to > 0. Again, this is because the search function may attempt to use values less than zero. This would result in negative probability and a quasi-probability distribution of non-exclusive possibilities, which makes little sense if we assume that humans cannot be travelling in more than one direction at once.

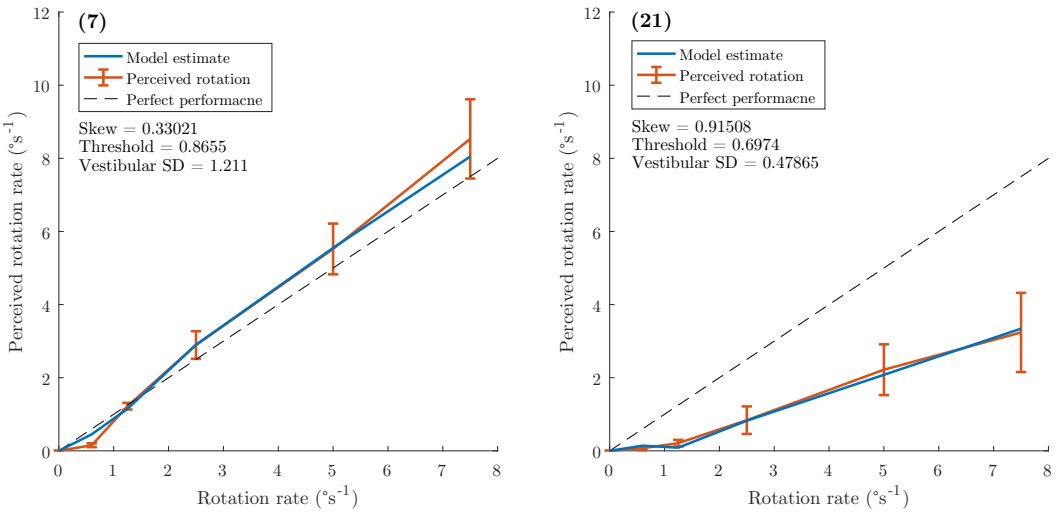

Figure 7.5: Example model fits for two participants curvature data from the experiment in Chapter 6 where the model successfully captures perception.

7.2.4 Final parameter count

In total the model has three manipulated parameters; skew, threshold, and vestibular standard deviation.

7.3 Results and discussion

Figures 7.5 and 7.6 show a selection of participant results from the experiment described in 6. For these figures the original data sets have had their means and 95% confidence intervals recalculated based on the absolute curvature. This was to remove asymmetries in the data that the model implementation cannot in its present state explain. Curvature was then recoded into rotation rate, based on the forward translation speed of 1.5ms^{-1} for ease of comparison against output from the model which produces an estimate of perceived rotation based on the parameters provided by the search function. These figures also contain numerical data listing the best fit parameters used by the model to produce the estimation. The complete set of numerical data for tested fits can be seen in Table 7.1.

Figure 7.5(7) shows the model fit for a participant with near accurate perception of curvature, only underestimating true rotation rate at $|0.6|°$. Overall this is a good fit with the search finding parameters that produced accurate estima-

Table 7.1: Model fit data for each participants perception of curvilinear motion. Fit itself is the sum of squared errors for the difference between model best fit and participant perception.

n	α_{vis}	Threshold	σ_{vest}	Fit
1	0.136	0.888	1.13	0.736
2	1.69	0.242	2.40	62.7
3	0.392	0.867	1.48	2438
4	0.480	0.761	1.14	635
5	0.516	0.755	1.24	412
6	0.584	0.952	1.02	311
7	0.330	0.866	1.21	0.661
8	1.68	0.418	0.223	2.17
9	0.446	0.891	0.460	5.38
10	1.29	0.498	0.339	0.623
11	0.789	0.651	0.883	11.4
12	1.29	0.587	0.542	0.873
13	0.756	0.598	0.890	0.994
14	0.479	0.761	1.14	133
15	1.17	0.480	0.416	0.110
16	0.363	0.809	1.97	127
17	1.05	0.704	0.743	3.10
18	1.15	0.567	0.510	0.492
19	0.915	0.790	1.14	26.6
20	0.986	0.516	0.932	0.393
21	0.915	0.697	0.479	0.0994
22	0.442	0.618	1.25	15.9
23	1.24	0.632	0.460	0.516
24	1.08	0.662	0.392	1.75
25	0.648	0.905	0.839	83.2
26	1.60	0.487	0.417	0.812
27	0.536	0.751	1.30	154
μ	0.850	0.678	0.924	163.8

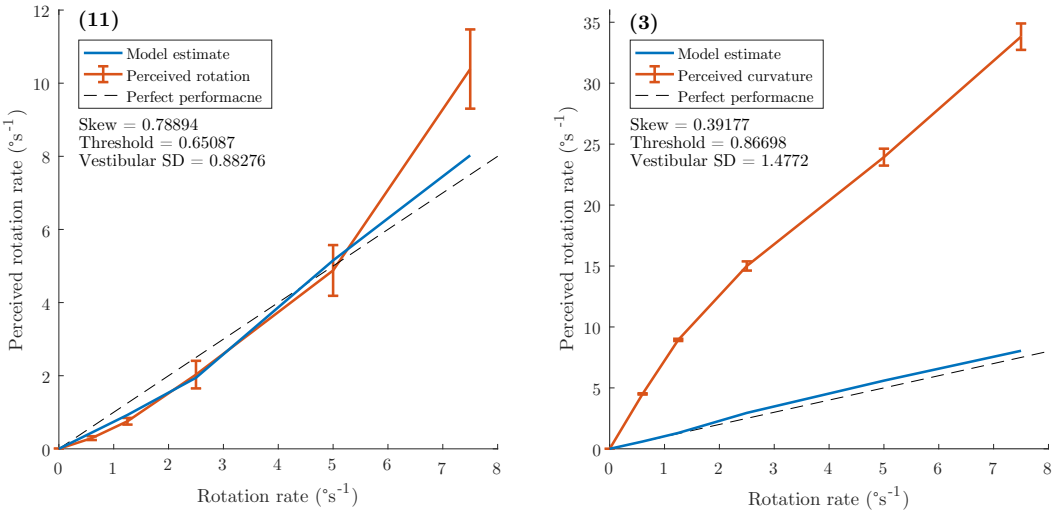

Figure 7.6: Example model fits for two participants curvature data from the experiment in Chapter 6 where the model failed to adequately capture perception. Sub-plot (11) shows inability to fit for a minor overestimation of rotation rate at high rates of rotation. Sub-plot (3) shows an inability to fit for major overestimation at all rates of rotation – note the change in scale. All cases where the model failed involved fitting to data that fell somewhere between these two cases.

tions for all rotation rates other than $0.6°s^{-1}$. Overall, for the model to match the performance of participants who estimated curvature with consistent accuracy the model fitting process settled on low skews, relatively high thresholds, and relatively large vestibular standard deviations. Low skew results in the visual distribution mean remaining close to the true rotation rate across all tested rates. Combined with the high thresholds, which further reduce the effect of skew, and the large vestibular standard deviations, which keep the vestibular contribution below threshold, this results in a model estimate based almost entirely off the visual estimate – especially at high rates of rotation. This can be seen in Figure 7.7 which shows the equivalent of sub-figures 7.4a and b overlaid for each of the rotation values tested and allows visual comparison of underlying numbers for different model fits. As we expect participants who can accurately perceive heading in the absence of congruent vestibular cues to pay little attention to the incongruent vestibular cues this matches the expected process for humans.

A better fit is seen in 7.5(21) which shows fit for an under-estimator of rotation, including a significant plateau near zero rotation. Here the model estimate is not

significantly different from the experimental results and indeed closely tracks the mean values for participant perception. Notably, this example shows the models ability to accurately match the plateau seen in many participant responses at low rates of rotation. In order to match these plateaus, the model tends to select very high skews, low thresholds, and low vestibular standard deviations. This combination causes the vestibular estimate to completely dominate the combined distribution at low rates of rotation but the high skew increases the vestibular contribution at higher rates of rotation. This can be seen in Figure 7.8.

Unfortunately, this implementation of the model is not capable of accurately matching all of the observed participant perceptions. Figure 7.6 demonstrates the failure mode for this implementation – the implementations inability to match large participant perceptions where they make large overestimations of of rotation rate. The model is unable to explain these large over-estimations due to limitations on the form of the underlying distributions. The underlying visual distributions were only evaluated out to $10°s^{-1}$ limiting the possible influence of any extended tail on the distribution. Furthermore, in an effort to limit free parameters the standard deviation of the visual distribution was fixed at one. This limited the relative magnitude of long skew tails. Additionally, for cases like this, the fitting process poorly matches observed values for lower rates of rotation relative to observation variance due to the least-squares fit prioritising attempts to close the large absolute difference between model expectations and observed values at high rates of rotation. In the most extreme cases, as for participant three shown in Figure 7.6(3), this results in parameter choices similar to those seen for accurate estimators of curvature (compare figures 7.9 and 7.7) with low skews, high thresholds, and high vestibular standard deviations. The difference for participant three however is that skew in the visual distribution is not, and as implemented can not be, sufficient to raise the final estimate by more than a degree per second and, as a result, the final distribution underestimates the participants perception.

Table 7.1 shows the complete model fit data set for all participants from Chapter 6. This table includes the visual distribution skew, cut-off threshold, and vestibular distribution underlying the model estimates, as per the graphs. Of particular interest here is that the mean vestibular standard deviation is very close to

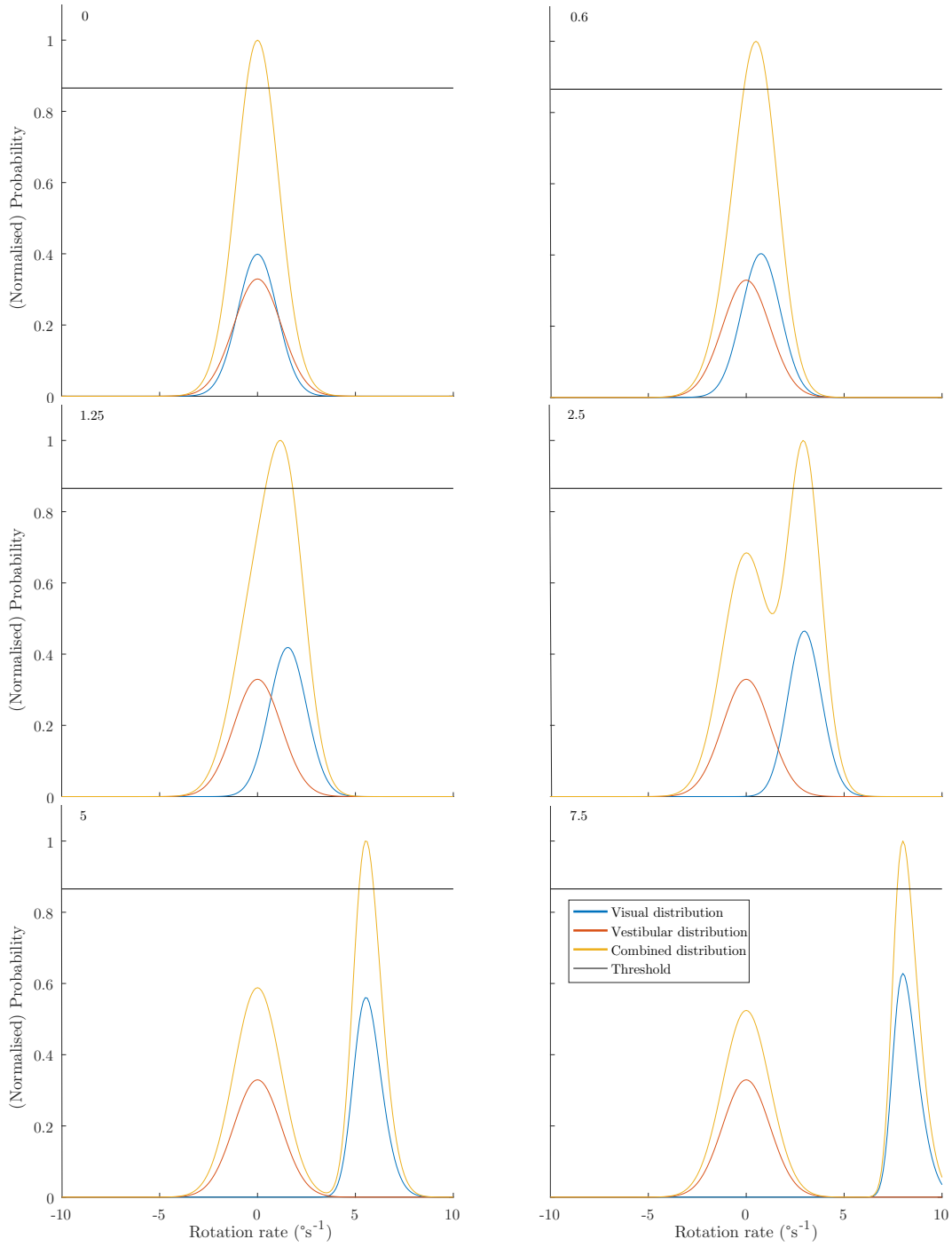

Figure 7.7: The distribution set for participant seven as seen in Figure 7.5(7). The number in the top right corner of each sub-plot indicates the visual distribution rotation rate for the plot. Each sub-plot corresponds to the perceived rotation data point from Figure 7.5(7) of equal rotation.

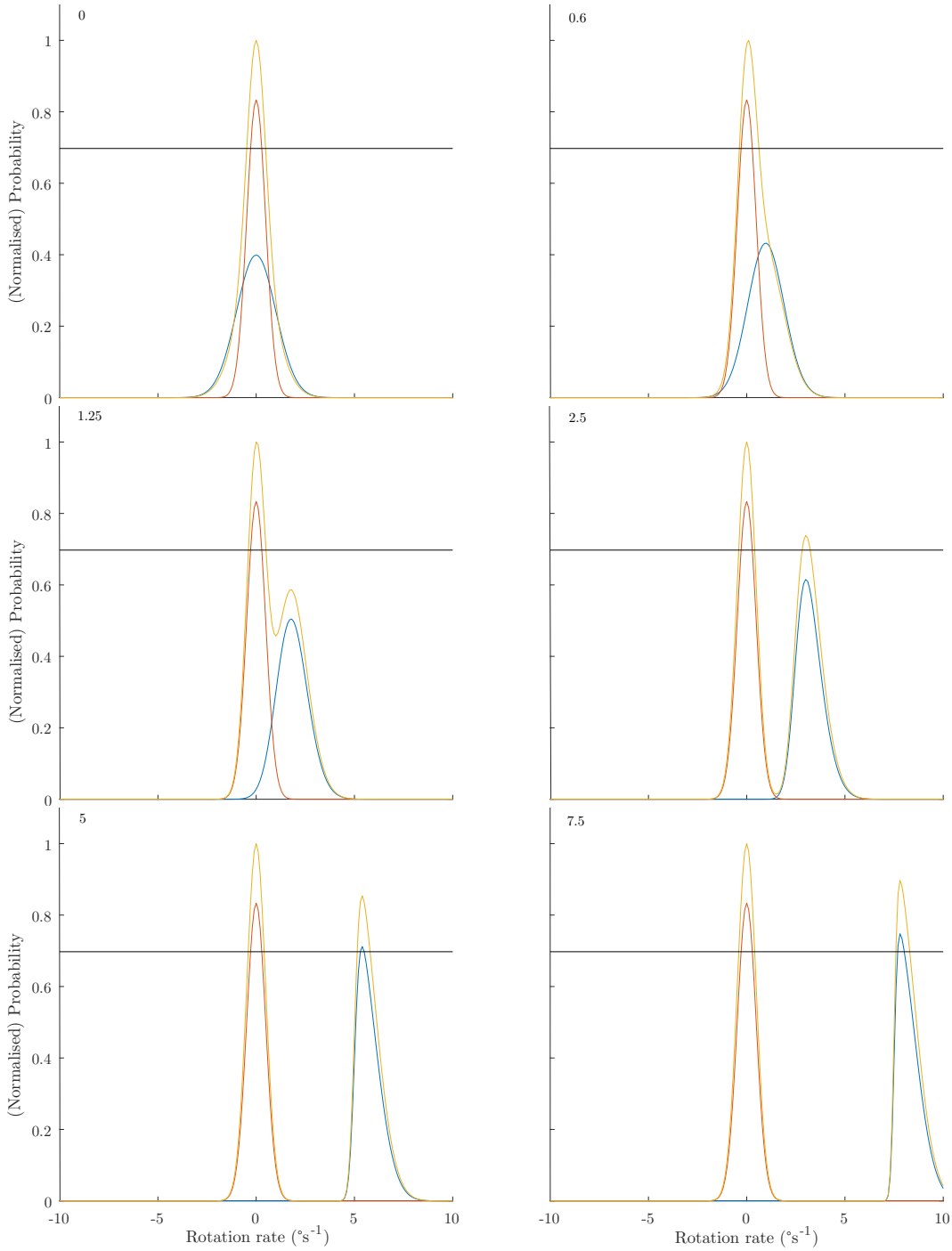

Figure 7.8: The distribution set for participant twenty-one as seen in Figure 7.5(21). The number in the top right corner of each sub-plot indicates the visual distribution rotation rate for the plot. Each sub-plot corresponds to the perceived rotation data point from Figure 7.5(21) of equal rotation.

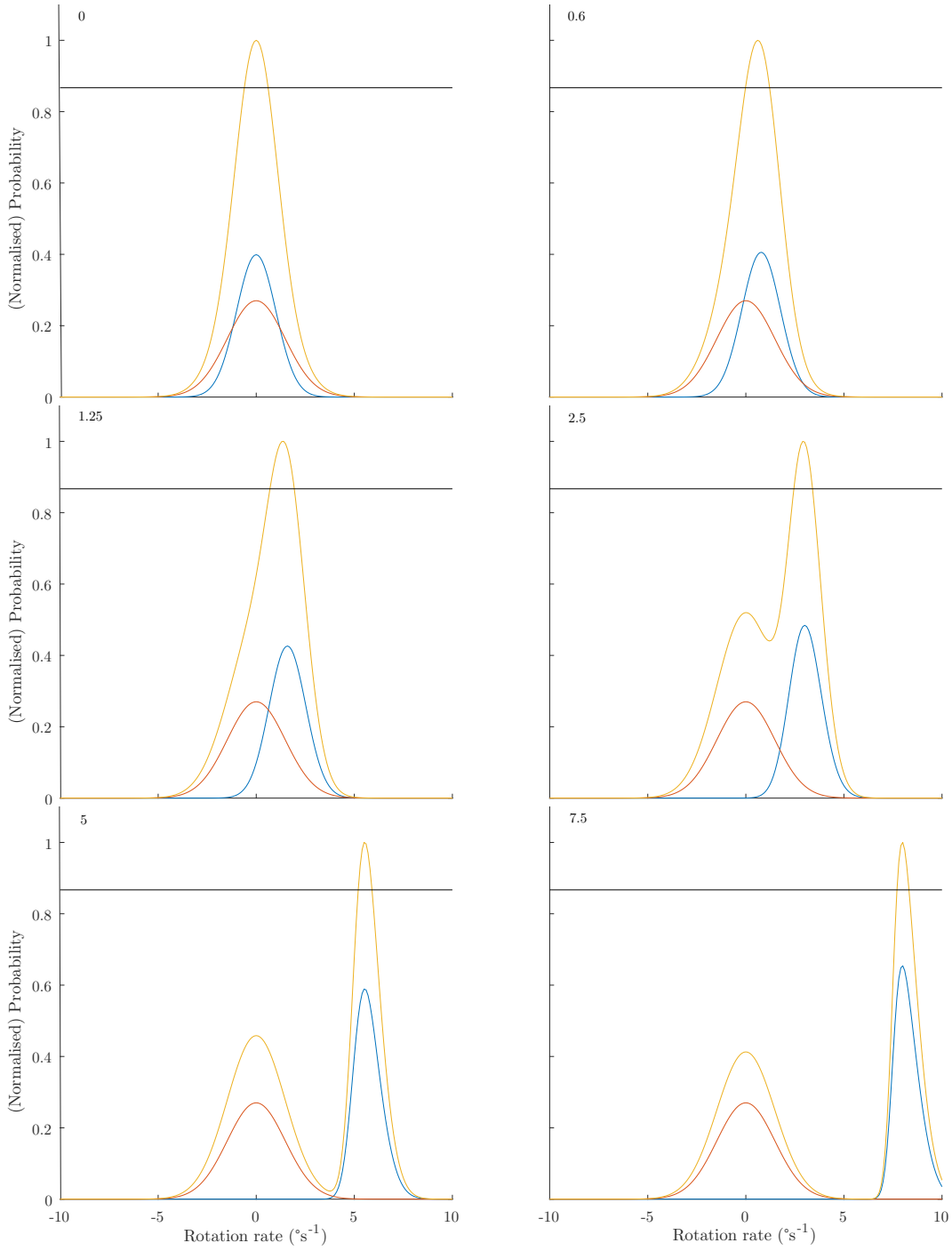

Figure 7.9: The distribution set for participant three as seen in Figure 7.5(b). The number in the top right corner of each sub-plot indicates the visual distribution rotation rate for the plot. Each sub-plot corresponds to the perceived rotation data point from Figure 7.5(b) of equal rotation.

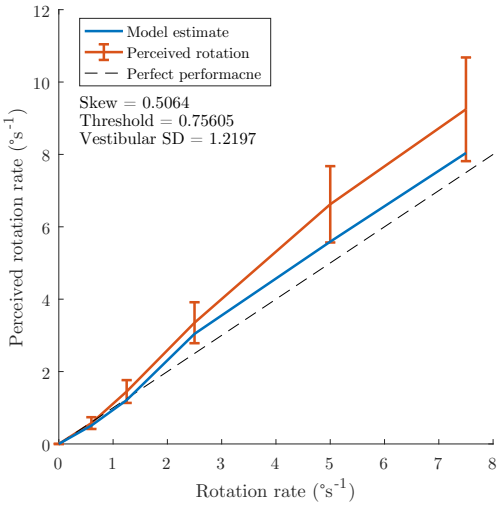

Figure 7.10: Model fit to the mean data from Chapter 6.

the vestibular system rotation threshold of $1°s^{-1}$ from MacNeilage, Banks, et al. (2010). Additionally, the table shows the overall sum-of-squared-errors fit value for each participant. There is a large range to these values and given how precise many of the fits are others look poor by comparison. In practice, however, any fit value below 160 indicates a good fit, with higher values generally indicating only a failure to match overestimations of rotation on higher curvature paths as is seen for participant 11 in Figure 7.6(11). Fits about this value were due to the same failure to fit large overestimations of rotation, but the difference tended to be both larger and present over the full range of tested values as for participant three seen in Figure 7.6(3).

Figure 7.10 depicts the best fit model for the mean overall rotation rate perception from the Chapter 6 experiment. This fit is technically good, in that it is not significantly different from the observed data. In particular the model does a good job of accurately matching observed data for lower rates of rotation. Unfortunately, model fit for higher rates of rotation still suffers from the same problem as the fit in Figure 7.6 in that it is not possible for the model implementation to explain the higher perceived rates of rotation at the higher levels of rotation due to the underlying distributions.

It is worth noting that when fitting data that included participant underestimation of rotation across part or all of the tested rates of rotation the fitting algorithm selected solutions with smaller vestibular distribution standard deviations and lower thresholds. This matches expected behaviour if the system is

maximising the vestibular contribution to the combined rotation as a smaller standard deviation results in a tighter distribution with a greater probability of no rotation, while a lower threshold up-weights the vestibular distribution by including a greater portion of the vestibular distribution relative to the increased inclusion of the visual distribution. The opposite is true of instances where the model has to fit data where the rotation rate has been wholly overestimated.

7.4 Overall comments

Overall, this implementation was capable of producing good to excellent matches to observed data for most participants using reasonable skew and threshold values and assuming biologically plausible vestibular distribution standard deviations. This would then suggest it captures the function of the biological systems underlying perception of curvilinear motion. The current implementation can not handle the occasionally seen extreme overestimation of rotation rate however and future work could stand to correct this.

Using skew normal distributions of unit deviation allows for modelling of slight overestimation, but more skewed distributions and larger deviations are required for greater over-estimations. This could potentially be implemented by allowing variable standard deviation for the visual distribution which would provide for dramatically longer tails away from zero. Allowing variable standard deviation for the visual distribution seems reasonable given the unlikeliness that participants display differences in perception based solely on differences in vestibular input processing. The process of implementing variable deviation vestibular distributions would with the current combination rules inherently down-weight the vestibular distribution relative to a vestibular distribution with a standard deviation of one however. As such, doing so would require a revision of the combination rules and threshold process, lest a modest vestibular input drown out the visual contribution. It is also worth noting that vestibular sensitivity varies over rotation frequency and the current implementation of the model fails to account for this as we assume a fixed vestibular standard deviation across all rotation rates.

Furthermore, in some cases, the search function ignores more valid solutions for points of low rotation in favour of closer fits for points at higher rotation,

even when an imprecise fit could be acceptable for the higher rate value based on increased variance in the observed value. This is an artefact of the least-squares fitting process which favours reducing large discrepancies without consideration for variance across the observed data. Weighting the model fit estimate by the variance associated with any particular measured value would solve this issue but the ideal system for doing so has not yet been determined.

Finally, it is worth noting that the model assumes that heading is determined over a relatively short interval of 200ms while the trials that produced the data we are trying to match with the model were relatively long at two seconds each. Unfortunately, the current methods for measuring human perception of motion do not provide a way to determine when during a relatively long trial participants make their judgement or how long it takes them to do so. This means that there may be some mismatch between the model assumptions and actual behaviour. Future work could include an investigation into how and when participants make heading judgements during trials, perhaps by using constantly changing paths and comparing participant judgements to the path over time.

Real rotation

Chapter 7 modelled participant behaviour based on the assumption that the vestibular system was signalling zero rotation and that this contributed to the overall perception of motion. This assumption puts the visual and vestibular cues in conflict but reflected reality as participants were not actually rotating while viewing the visual stimulus. Modelling participant perception in this way was successful in that it allowed the model to match most of the range of human performances observed well.

This success raises an obvious question however. How well can the model predict human performance when visual and vestibular measures of rotation are in agreement? Given how the model is implemented in this thesis the simplest method for making this prediction is to shift the mean of the vestibular distribution to the location of the visual distribution for each tested rotation and reproduce the remainder of the analysis. Unfortunately, the original participants were not available for a follow up experiment so specific individual predictions could not be tested. Performing the process of shifting the vestibular distribution and recalculating the rotation estimates in a more abstract sense does still produce a set of generalised predictions however.

8.1 Predictions

As described in Chapter 7, combining a visual and a vestibular estimate of rotation produces a combined distribution from which an estimation of true rotation can be taken. When the visual distribution indicates an approximation of true rotation rate and vestibular distribution indicates no rotation they produce a combined distribution that is skewed towards zero with a large standard deviation.

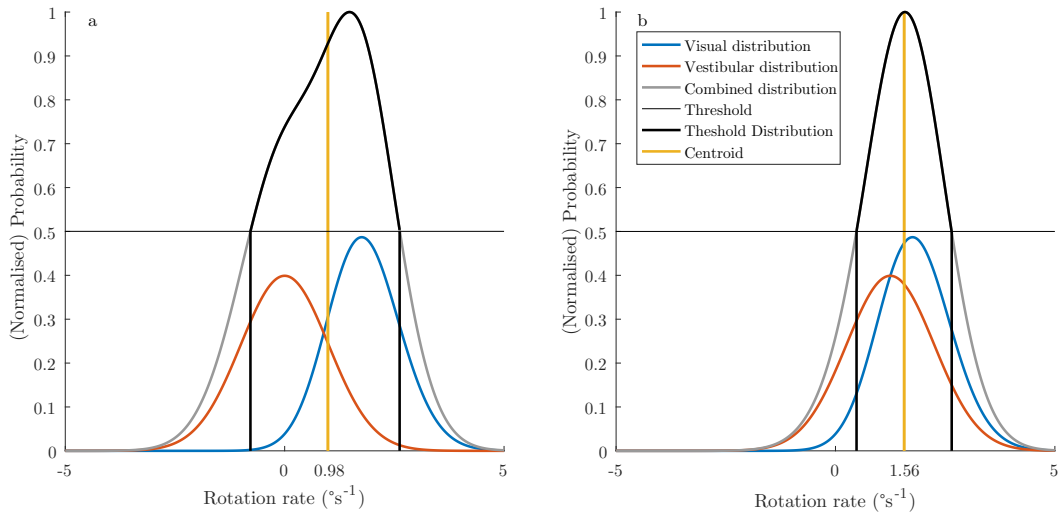

Figure 8.1: Figures showing the effect of visual-vestibular congruence on heading estimates. Plot (a) shows an example of incongruence, where the vestibular system is reporting no rotation while the visual system reports rotation at $1.25°s^{-1}$. Plot (b) differs only in that the vestibular system now also reports rotation at $1.25°s^{-1}$. Refer to 7.4 for clarification of individual plot components.

An example of this can be seen in Figure 8.1a. As a consequence of this skew and spread the system underestimates rotation, resulting in incomplete rotation compensation and thus heading misperception. This is a potential explanation for the results from the previous experiments in this thesis.

On the other hand, when the visual and vestibular distributions both indicate the same (correct) rate of rotation combining them produces a distribution with a smaller standard deviation. Furthermore, the skew of this combined distribution is now dominated by any skew in the visual estimate of rotation and not the incongruence of the two underlying distributions. This results in the system producing an estimate that ranges between correct, when the visual estimate of rotation is not skewed, and overestimated, when there is significant skew in the visual distribution. An example where overestimation occurs can be seen in Figure 8.1b. This situation, where the visual and vestibular estimates of rotation are in agreement, is expected to occur in this experiment where the vestibular system is stimulated by the physical rotation of the observer.

Consequently, we expect participants to produce an accurate estimate of rotation during each trial. This should result in the accurate perception of heading, as

in previous experiments where vestibular cues have been provided. However, as a consequence of the rotation compensation mechanism removing the estimated rotation (R') from the combined flow field ($T+R$) leaving only the translational flow field, if the model is effectively capturing human perception participants should report less curved paths. Indeed, if compensation is complete and accurate we would expect participants to report perception of linear paths in the direction of the correct heading.

8.2 Method

8.2.1 Participants

Six participants aged 18 to 26 with normal vision completed the experiment. Further participants were prevented from completing the experiment due to equipment failure. This experiment was approved by the University of Waikato Psychology Research and Ethics Committee.

8.2.2 Equipment

Visual stimuli were presented using the same virtual reality equipment as described in 4.1.2.

Physical rotation stimuli were presented using an electronically controlled rotating chair constructed from a rotating office chair with armrests, twelve volt DC motor, electronic speed controller and drive belt system. Instructions were sent to the chair from the experimental computer via serial connection and synchronised with stimulus presentation. The chair used a 360 segment optical position encoder with which it controlled its own speed and monitored its position relative to its starting position.

This chair was created from spare components for the purpose of providing an affordable, locally available, motion platform for pilot testing of physical rotation. Unfortunately, the chair did not perform as well as hoped. An example plot of the range of speeds obtained from, and the acceleration profile of, the chair can be seen in Figure 8.2. It is clearly visible in this figure that although the average rotation speed is close to the set speed averaged over several trials the chair was

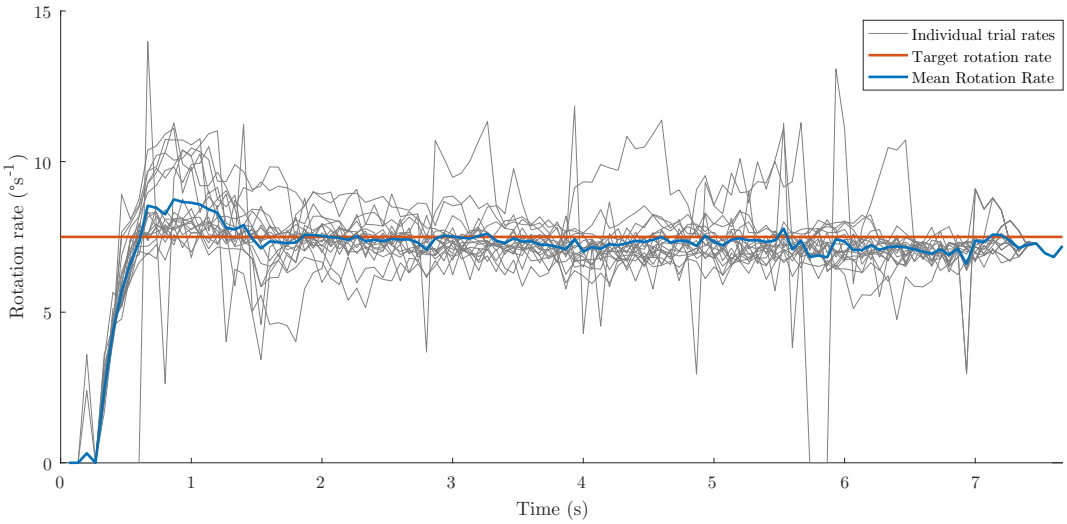

Figure 8.2: Motion characteristics of the rotating chair at a target rotation rate of 7.5°s^{-1} (shown in orange). The blue line shows average performance over 20 seven-second-long individual test trials (shown in grey). Instantaneous rate was reported by the chairs own motion controller. Some trials extended beyond the seven second mark due to command processing delays in the motion controller. Deceleration profiles were not captured as the motion controller did not report actual rotation values when the target value was zero.

generally unable to sustain a consistent speed over any given trial. Furthermore, there were significant delays between sending commands and having the chair execute the commands, and sudden changes in the motion of the chair caused its position to regularly shift. This had a noticeable effect on the consistency of the trials that included physical rotation. While the system as a whole ensured that the visual stimulus matched the physical one the unpredictability of the chair prevented the experiment from growing beyond the level of an exploratory pilot study.

8.2.3 Trial design

Each participant completed 60 randomly interleaved three-second-long trials from one of four 15 trial long blocks. Trials consisted of travel along a path of curvature $\pm 0.006981^{-1}$, two blocks for each sign. In one block for each sign participant view direction was maintained along the tangent of the curve by visually rotating the participant. Trials for these blocks were identical to those described in Chapter 6. In the other block for each sign view direction was maintained by physically rotat-

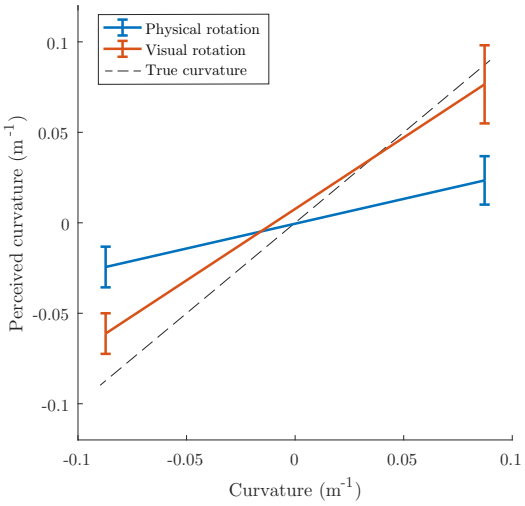

Figure 8.3: Average perceived curvature during physical and visual rotation.

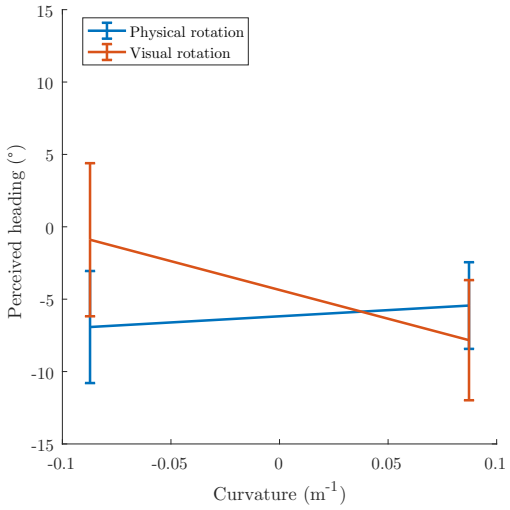

Figure 8.4: Average perceived heading during physical and visual rotation.

ing participants with an improvised motor driven electronically controlled chair. These trials differed in that participants experienced a half-second of rotation in the dark to allow the chair to accelerate to a stable seven and a half degrees per second before visual stimuli were displayed. Instantaneous rate during these trials was reported by the chairs own motion controller. Typical chair performance can be seen in Figure 8.2 which shows motion variability across 20 seven-second-long test trials. Some of these trials extended beyond the seven second mark due to command processing delays in the motion controller. Deceleration profiles were not captured as the motion controller did not report actual rotation values when the target value was zero. At the end of each trial participants reported perceived path and heading using the same response tool as described in 3.2.

As with the experiment presented in Chapter 4 before beginning the experimental trials participants also completed 33 practise trials to familiarise themselves with responding using the unfamiliar controller input. These trials were the same as described in 4.1.3, with the exception that linear path with rotation trials were replaced with true curvature trials where the rotation was provided by rotation of the chair.

8.3 Results and discussion

Mean participant curvature perception can be seen in Figure 8.3. Participants perceived significantly less curvature during trials where a congruent vestibular signal was provided by rotating the chair than when one was not. Perceived curvature for trials where only visual rotation was displayed and the participant was not physically rotated was not significantly different from that seen in the Chapter 4 which makes sense as this was the same condition as presented in that chapter.

Mean participant heading perception can be seen in Figure 8.4. This figure shows a noticeable bias in heading perception. Perceived heading is significantly different from zero for both positive and negative curvatures yet there is no significant difference between perception for the two paths. This bias was likely caused by mispositioning of the rotating chair which was difficult to position due to the cable and motor set-up. If this bias is ignored then it appears participants may have perceived heading more accurately during trials where they were physically rotated compared to when they were not, although this effect was not significant.

8.4 Overall comments

Given the limitations of the equipment used it is difficult to draw strong conclusions about participant perception of the motions presented. Participants did, however, perceive significantly straighter paths when the physical and visual rotation were congruent than when they were not. This is exciting, being that it was the main unique prediction of the model, and would appear to be worthy of further investigation.

Furthermore, the general pattern of heading error perception under visual-rotation-only condition appears to match that seen in high rotation rate conditions of the Chapter 6 experiment. This is difficult to assess with certainty due to the noise and bias in the heading measurements however, but the underlying conditions were the same in both cases, barring the uncertainly generated by chair misalignment. It is more interesting however that perception of congruent rotation, while not significantly different from perception of visual only rotation,

was not significantly different across the two directions tested whereas it was for the visual rotation condition. That heading perceptions were the same regardless of rotation suggests, bias aside, that heading was 'accurate' even in the presence of rotation.

That even under the poor conditions available participants perceived straighter paths and invariance of heading error suggests that the model may be making accurate predictions about human perception during physical rotation. Investigating this further is desirable but a more sophisticated and reliable motion platform would be required. The ability of the platform to maintain a constant speed while rotating would be essential, as would be the ability and to consistently return to the same starting position. This should eliminate the bias and noise seen in responses. The ability to maintain these characteristics over the full range of rotation rates tested in this thesis ($\pm 7.5^{\circ}s^{-1}$) would be useful to examine perceptions at low rates of rotation where this thesis has found significant non-linearities.

As the current iteration of the experiment should run on any up to date Vive system and handles matching the physical rotations to the displayed stimulus integration with an existing motion platform should be straightforward should one become available. Beyond physical arrangement of the devices only a method to communicate between the controlling computer and the motion platform would be required.

Closing Remarks

In this thesis perception of curvilinear motion was examined across a range of motions; linear, with and without simulated rotation, and curvilinear, with and without physical rotation. This was done using newly available virtual reality headsets and, after initially confirming the experimental suitability of said headsets through replication of historical experiments, a newly developed response tool. This chapter provides a summary of findings from these experiments, along with a discussion of the limitations of currently available virtual reality head-mounted displays and an exploration of potential future work.

9.1 Overview of findings

9.1.1 VR and heading perception

The currently available virtual reality headsets, although not designed for research use, possess a range of desirable features when it comes to their use in human self-motion perception experiments. They provide the high resolution screens and rapid refresh rates expected of modern display devices. Beyond this, however, they provide a wide field of view in a compact package, inherently obfuscated screen edges and easy to configure stereoscopic displays for improved depth perception. They also provide integrated high precision, low latency head motion tracking reducing the need for head stabilisation and making it easy to include both participant controlled and externally generated extra-retinal stimuli. Not least, they are also affordable, especially compared to historic virtual reality systems.

In Chapter 2 we replicated experiments from (Banks et al., 1996) and (Crowell et al., 1998). This was both to examine whether these devices were suitable for use in self-motion experiments and to provide, should the devices prove suit-

able, a point of comparison between the experiments in this thesis and those conducted using more conventional displays. We found that the virtual reality devices themselves did not distort participant perceptions, with half of the participants completing the experiments reporting perception errors equivalent to those seen in Banks et al. (1996) and Crowell et al. (1998). The remaining half of the participants unexpectedly reported accurate heading perception providing the first strong indicator that more than one style of responding was prevalent. We also discovered, however, that for many participants having to wear an unfamiliar virtual reality headset for an extended period was uncomfortable. While, against expectations, no participants reported feeling motion sick the discomfort sapped enthusiasm and generally rendered the experience less pleasant for all involved. From this it was determined that experiment duration should be kept to a minimum and that breaks should be provided, at least for so long as participants remain unfamiliar with virtual reality devices.

9.1.2 Curvilinear motion perception

During linear motion with and without rotation

In Chapter 4 we examined perception of linear motion with an additional rotation on the horizontal plane as the observer translated. With this experiment we confirmed historical reports (Banks et al., 1996; Bertin et al., 2000; Ehrlich et al., 1998; Li & Warren, 2000, 2004; Royden et al., 1994; A. van den Berg, 1996; W. H. Warren, Mestre, et al., 1991) of rotation causing participants to perceive curved paths. We determined that this misperception was individually consistent and linked this misperception to participant heading error. We found that on average participants perceived curvature equal to that of the equivalent circle. There was an interesting plateau around zero rotation for both perceived heading and curvature however. Within this range of $\pm 1.25^{\circ}s^{-1}$ both average path and heading perception and individual perceptions of path and heading were correct. This is consistent with previous findings suggesting humans can correctly perceive heading from visual stimuli alone at low rates of rotation (W. H. Warren & Hannon, 1988), and supports the idea that a mechanism for extracting rotation from optic flow exists. In this experiment we also found anecdotal evidence that path

memory decays rapidly over as little as two seconds. This suggested that methods allowing rapid response should be strongly favoured, but the effect requires further investigation.

In Chapter 5 we again examined perception of linear paths, this time with increasingly eccentric headings instead of simulated rotation. Here we found the expected centre screen bias, with judgements of heading tending towards the view direction, and doing so to a greater degree as heading eccentricity increased. We also found significant perception of curvature at heading eccentricities $\geq 10°s^{-1}$. Although perceived curvature for even the most eccentric paths ($\pm 20°$) was an order of magnitude lower than perceived curvature for linear paths with rotation perception of curvature closely corresponded to the degree of centre screen bias across all participants. Given how rotation affected heading in the previous experiment this indicates that eccentric heading stimuli are interpreted as containing a rotational component (Perrone, 2018). This seems reasonable given how increasingly eccentric headings bias flow in a similar manner as rotation, with extreme eccentricity (90°) approximating a rotation only stimulus, barring the effect of motion parallax.

During curvilinear motion with incongruent and congruent vestibular stimuli

Chapter 6 covered the examination of participant perception while they travelled on true curvilinear paths while physically remaining stationary. Here participants, on average, perceived paths only slightly more curved than they were. There were still large individual differences however, with some participants perceiving nearly straight paths while others perceived over-curved paths. The range of curvatures perceived by participants did not differ greatly from the range seen in the linear path with rotation experiments. Perceptions for any given curvature were more consistent when compared to perceptions of curvature in the linear motion with rotation experiments however. Perceived heading also differed from that seen in the linear motion with rotation experiment. Here, although participants still perceived heading error incorrectly the magnitude of the error was reduced. Furthermore, heading was perceived accurately for curves of radius ±34.38m and paths of zero curvature. Other than for these paths heading was misperceived.

Between the correctly perceived curved paths and the linear path heading was biased towards the inside of the curve. Outside of the correctly perceived curved paths heading was biased towards the outside of the curve.

Compared to the perceptions of curvilinear motion without physical rotation participants in the Chapter 8 experiment covering curvilinear motion with congruent physical rotation perceive substantially different paths. While it is not possible to draw strong conclusions from the experiment in this chapter due to the inadequacy of the rotating chair participants did perceived significantly straighter, although still not straight, paths when vestibular rotation matched visual rotation. This provides tentative support for the Perrone (2018) model, which predicts perception of straight paths following complete rotation compensation facilitated by the availability of a congruent rotation signal. Given the noisiness and bias of participant heading responses, and the limited range of rotation rates tested this does require further investigation however.

9.1.3 Modelling rotation perception

Chapter 7 covered the implementation of a subset of the Perrone (2018) model to compare the models ability to predict perceived rotation with actual participant performance. Overall, by varying the standard deviation of a vestibular estimate of rotation, the skew of a visual estimate of rotation, and a threshold for their combination the model accurately matched the majority of participant perceptions over a wide range of different response types. The model implantation did fall short in two aspects however. Due to how the visual distribution was implemented the model failed to match participant perceptions when participants greatly overestimated rotation rate for a given path curvature. Further, due to how the error function was implemented the model fitting mechanism treated imprecise participant estimates as equal in value to precise participant estimates. This means that the model fits found minimised absolute differences between predicted and observed perception, even where a larger absolute difference would have still been within the 95% confidence interval for the participants estimate. Solutions to these issues are discussed in Section 9.3, but even with these issues the model failed to provide a prediction within the 95% confidence intervals for

participant perception for three of the 27 participants.

9.1.4 Measuring curvilinear perceptions

Over the course of experiments covered in this thesis the new tool presented in Chapter 3 performed well. Participants reported finding the tool intuitive, with only a small number of trials required for participants to familiarise themselves with the novel hand-held controllers. This meant that participants could respond quickly and precisely over a range of perceived motions. It appears that the world immersion and stereoscopic depth provided by viewing responses and stimuli in the virtual reality headsets facilitated this intuitiveness by allowing the line tool to clearly project out into the virtual world instead of appearing to be drawn on a flat screen.

As mentioned previously the tool, in its current iteration, is somewhat limited in the range of paths that it can test. The tool can only record paths on a single fixed plane, although this plane can be varied between experiments and trials if required. Further, it cannot record paths of non-constant curvature. Fixing these issues is largely a matter of finding and implementing intuitive inputs for participants to interact with the tool however, and not a fundamental limitation of the display devices or line design. Recording responses on arbitrary planes should not be especially difficult. This could be done using current controllers by allowing participants to rotate the response plane by physically rotating their hand. A solution for paths of non-constant curvature is more elusive however. 'Online' testing during trials using compensation/nulling tasks (e.g. Li, Sweet, & Stone, 2006; Souman & Freeman, 2008) can test perception of complex paths using relatively simple inputs doing so makes it difficult to be sure of stimulus as the process of responding alters what the participant is responding to. On the other hand, measuring perception of increasingly complex curves post-trial requires increasingly large numbers of parameters and/or parameters that are unintuitive to manipulate with hand controls. This does not mean such paths cannot be tested however, just that some thought needs to go into the response mechanism.

9.2 The limitations of current generation VR

The currently available virtual reality systems eliminate many of the shortcomings of previous equipment as discussed in Sections 1.4, 1.5, and 4.1.2. Like most emerging technologies however these systems do have some limitations of their own. Most of these limitations are minor. For example, the comparatively low angular pixel density of HMD displays compared to concurrently available computer monitors and the screen door effect for example. These issues are already being rectified as new systems are developed and in any case are unlikely to have significant impact on participant perception.

Other limitations do have potential to impact perception however, and their solutions are less clear. The lenses required to view a screen so close to the eyes scale depth relative to the real world so that distance perception in any given VR headset does not necessarily correspond one to one with distance perception in either reality (Wann, Rushton, & Mon-Williams, 1995; Zhang & Yang, 2018) or in other headsets of different optical design. Furthermore, drawing the virtual world stereoscopically on a single plane introduces a mismatch between accommodation and convergence further compounding any potential issues with depth perception.

As such, some caution is warranted when interpreting reported perceptions of virtual worlds. Potential difficulties with depth perception suggest that responses made while wearing head-mounted virtual reality devices should not be taken as absolute but rather relative measurements. In particular, this caution applies to estimates of perceived rotation, which can be calculated from perceived curvature as the accuracy of these estimates depends on assumptions made about the participants perception of tangential speed.

In practice, however, these concerns are minor. Users typically reach directly and accurately for real objects that are also rendered in the virtual world (e.g. the hand-held controllers) indicating accurate depth perception corresponding well to the real world. Any depth perception errors should not affect heading judgements. Depth perception errors should also have no major effect on path judgements as judgements are made in the virtual world where while the participant may perceive a point as closer or further away than it really is in reality they make their judgement of path in the same distorted frame as they saw the movement.

Furthermore, these relatively minor limitations are far outweighed in practice by the advantages of these virtual reality systems. The ability to collect complex responses in a fast and intuitive manner saves time for the participants and the researcher. The ability to use tools that do not confound errors in heading and curvature judgements simplifies analysis of results. The ease of integrating the head-mounted display into motion platforms due to the tracked nature of the headset increases the range of experiments that can be considered.

9.3 Future research

The first question, raised in Chapter 4, concerned the effect of response delay have on memory of path and heading. During experiments using the line response tool participants reported forgetting what path they were on if there responding was delay by a few seconds for any of a variety of reasons. These reports suggest that slower response methods may be at a disadvantage when it comes to accurately recording perceptions. An experiment systematically manipulating a forced delay between stimulus presentation and response could quantify the magnitude and range of this effect. If the delay does turn out to be of consequence then we would expect to see greater variance in participant responses as delay time increases, perhaps with a lower bound defined by the minimum time it takes a participant to respond and upper bound defined by complete forgetting of the path.

The second question, raised in Chapter 7, was when during trials do participants make their judgements of path and heading. Related to this was the question of how long participants take to make such judgements. Many models of human self-motion perception assume either instantaneous heading extraction or heading extraction over very short time scales. This does not necessarily correspond with human behaviour however and it does not match experimental conditions when trials are longer than half a second. This mismatch adds an element of uncertainty to comparisons between model predictions and human behaviour and as such knowing exactly when participants make heading judgements could improve either experiment design or model structure. While this could be tested by manipulating the duration of trials this seems more likely to determine the minimum time it takes to make a heading judgement. To assess when heading judgements

are made it may be of more use to test perception of smoothly changing curvature. For example, if a path starts strongly curved and over the course of the trial straightens out then the perceived curvature tells the researcher something about when the judgement was made.

The third question does not concern a future experiment so much as the best way to implement the skewed visual distributions presented in Chapter 7. In its current form the implementation fails to accurately predict human performance when participants greatly overestimate heading. The visual distribution seems to be an important determinant of the model implementations ability to match over-estimators but its form was largely chosen for convenience and simplicity while still maintaining the skew. Considering its failure to capture the behaviour of extreme over-estimators but given the ability of the model to do so in principle suggests that further examination of the distribution is in order. A good starting point may be an analysis of the distribution of vector directions in the flow field across a range of rotations and headings to determine physically plausible tail lengths for the distribution.

The key work of interest, however, is a full scale experiment based on the real rotation pilot presented in Chapter 8. Perrone (2018) predicts that participants should perceive a linear path of accurate heading during curvilinear motion when provided with a rough congruent vestibular signal. An indication that this may in fact be the case was provided by the pilot study when it was found that participants perceived significantly straighter paths when provided with congruent vestibular input. As noted, however, the rotating chair used in the experiment had some serve deficiencies with regards to maintaining the correct speed, accurately returning to the starting position, and accelerating/decelerating at the correct time. Potentially as a result of this heading perception was heavily biased and individual curvature responses were quite noisy. We expect that an improved motion platform should reduce noise in the responses and eliminate the bias in heading perception and would like to know if a similar reduction in overall curvature perception can be obtained using more reliable equipment and a larger number of participants.

9.4 Final comments

Overall, the availability of modern virtual reality systems and their continued development appear to promise improvements in ease of development and testing for human self-motion perception experiments. This thesis has made use of such virtual reality devices to confirm historical reports of curved path perception and test perception of heading under a variety of circumstances. While confirming historical experiments we also uncovered the presence of large individual differences in perception and the grouping of these individual differences into two broad response styles, along with a persistent well defined plateau in path and heading perception near zero rotation and the misperception of curvature when travelling on eccentric headings. We then tested the capabilities of the rotation estimation stage from Perrone (2018) against participant performance and determined that it was largely successful in predicting human perception. The research presented here raised as many questions as it answered, however, indicating that there are still a great number of avenues to explore when it comes to human self-motion perception.

References

Aarts, S., Winkens, B., & van Den Akker, M. (2012). The insignificance of statistical significance. *The European journal of general practice*, *18*(1), 50–52.

Angelaki, D. E. (2004). Eyes on target: what neurons must do for the vestibuloocular reflex during linear motion. *Journal of neurophysiology*, *92*(1), 20–35.

Angelaki, D. E., & Cullen, K. E. (2008). Vestibular system: the many facets of a multimodal sense. *Annu. Rev. Neurosci.*, *31*, 125–150.

Azzalini, A. (2013). *The skew-normal and related families* (Vol. 3). Cambridge University Press.

Banks, M. S., Ehrlich, S. M., Backus, B. T., & Crowell, J. A. (1996). Estimating heading during real and simulated eye movements. *Vision research*, *36*(3), 431–443.

Beintema, J. A., & Van den Berg, A. (1998). Heading detection using motion templates and eye velocity gain fields. *Vision research*, *38*(14), 2155–2179.

Bertin, R., Israël, I., & Lappe, M. (2000). Perception of two-dimensional, simulated ego-motion trajectories from optic flow. *Vision Research*, *40*(21), 2951–2971.

Bridgeman, B. (2007). Efference copy and its limitations. *Computers in biology and medicine*, *37*(7), 924–929.

Britten, K. H. (2008). Mechanisms of self-motion perception. *Annu. Rev. Neurosci.*, *31*, 389–410.

Britten, K. H., Shadlen, M. N., Newsome, W. T., & Movshon, J. A. (1992). The analysis of visual motion: a comparison of neuronal and psychophysical performance. *Journal of Neuroscience*, *12*(12), 4745–4765.

Britten, K. H., & van Wezel, R. J. (1998). Electrical microstimulation of cortical area mst biases heading perception in monkeys. *Nature neuroscience*, *1*(1), 59.

Browning, N. A., Grossberg, S., & Mingolla, E. (2009). A neural model of how the brain computes heading from optic flow in realistic scenes. *Cognitive psychology*, *59*(4), 320–356.

Chen, A., DeAngelis, G. C., & Angelaki, D. E. (2011a). Convergence of vestibular and visual self-motion signals in an area of the posterior sylvian fissure. *Journal of Neuroscience*, *31*(32), 11617–11627.

Chen, A., DeAngelis, G. C., & Angelaki, D. E. (2011b). Representation of vestibular and visual cues to self-motion in ventral intraparietal cortex. *Journal of Neuroscience*, *31*(33), 12036–12052.

Cheng, Z., & Gu, Y. (2016). Distributed representation of curvilinear self-motion in the macaque parietal cortex. *Cell reports*, *15*(5), 1013–1023.

Crowell, J. A., Banks, M. S., & Royden, C. S. (1989). A physiologically plausible model of optic flow perception. *Invest. Ophthalmol. Visual Sci. Suppl.*, *30*, 427.

Crowell, J. A., Banks, M. S., Shenoy, K. V., & Andersen, R. A. (1998). Visual self-motion perception during head turns. *Nature neuroscience*, *1*(8), 732.

Cutting, J. E. (1986). *Perception with an eye for motion* (Vol. 1). Mit Press Cambridge, MA.

Cuturi, L. F., & MacNeilage, P. R. (2013). Systematic biases in human heading estimation. *PloS one*, *8*(2), e56862.

D'Avossa, G., & Kersten, D. (1996). Evidence in human subjects for independent coding of azimuth and elevation for direction of heading from optic flow. *Vision research*, *36*(18), 2915–2924.

Duffy, C. J., & Wurtz, R. H. (1991). Sensitivity of mst neurons to optic flow stimuli. i. a continuum of response selectivity to large-field stimuli. *Journal of neurophysiology*, *65*(6), 1329–1345.

Ehrlich, S. M., Beck, D. M., Crowell, J. A., Freeman, T. C., & Banks, M. S. (1998). Depth information and perceived self-motion during simulated gaze rotations. *Vision Research*, *38*(20), 3129 - 3145.

Eriksson, E. S. (1974). Movement parallax during locomotion. *Perception &*

Psychophysics, *16*(1), 197–200.

Ernst, M. O., & Banks, M. S. (2002). Humans integrate visual and haptic information in a statistically optimal fashion. *Nature*, *415*(6870), 429.

Fetsch, C. R., DeAngelis, G. C., & Angelaki, D. E. (2010). Visual–vestibular cue integration for heading perception: applications of optimal cue integration theory. *European Journal of Neuroscience*, *31*(10), 1721–1729.

Fitzpatrick, R. C., Butler, J. E., & Day, B. L. (2006). Resolving head rotation for human bipedalism. *Current Biology*, *16*(15), 1509–1514.

Gibson, J. J. (1950). *The perception of the visual world.* Boston, Massachusetts: Houghton Mifflin.

Gibson, J. J. (1966). The senses considered as perceptual systems.

Green, D. M., Swets, J. A., et al. (1974). *Signal detection theory and psychophysics* (Vol. 1). Huntington New York.

Gu, Y., Watkins, P. V., Angelaki, D. E., & DeAngelis, G. C. (2006). Visual and nonvisual contributions to three-dimensional heading selectivity in the medial superior temporal area. *Journal of Neuroscience*, *26*(1), 73–85.

Hanada, M., & Ejima, Y. (2000). A model of human heading judgement in forward motion. *Vision Research*, *40*(2), 243–263.

Heeger, D. J., & Jepson, A. D. (1992). Subspace methods for recovering rigid motion i: Algorithm and implementation. *International Journal of Computer Vision*, *7*(2), 95–117.

Hildreth, E. C. (1992). Recovering heading for visually-guided navigation. *Vision research*, *32*(6), 1177–1192.

Holst, E., & Mittelstaedt, H. (1950). Das reafferenzprinzip. *Naturwissenschaften*, *37*(20), 464–476.

Ivanenko, Y., Grasso, R., Israël, I., & Berthoz, A. (1997). The contribution of otoliths and semicircular canals to the perception of two-dimensional passive whole-body motion in humans. *The Journal of physiology*, *502*(1), 223–233.

Johnston, I. R., White, G. R., & Cumming, R. W. (1973). The role of optical expansion patterns in locomotor control. *The American Journal of Psychology*.

Kreylos, O. (2015). Optical Properties of Current VR HMDs. `http://doc-ok.org/?author=1`.

Lagarias, J. C., Reeds, J. A., Wright, M. H., & Wright, P. E. (1998). Convergence properties of the nelder–mead simplex method in low dimensions. *SIAM Journal on optimization*, *9*(1), 112–147.

Landy, M. S., Maloney, L. T., Johnston, E. B., & Young, M. (1995). Measurement and modeling of depth cue combination: In defense of weak fusion. *Vision research*, *35*(3), 389–412.

Lang, J. M., Rothman, K. J., & Cann, C. I. (1998). That confounded p-value. *Epidemiology (Cambridge, Mass.)*, *9*(1), 7–8.

Lepecq, J.-C., De Waele, C., Mertz-Josse, S., Teyssedre, C., Huy, P. T. B., Baudonniere, P.-M., & Vidal, P.-P. (2006). Galvanic vestibular stimulation modifies vection paths in healthy subjects. *Journal of neurophysiology*, *95*(5), 3199–3207.

Li, L., Sweet, B. T., & Stone, L. S. (2006). Humans can perceive heading without visual path information. *Journal of Vision*, *6*(9), 2–2.

Li, L., & Warren, W. H. (2000). Perception of heading during rotation: sufficiency of dense motion parallax and reference objects. *Vision Research*, *40*(28), 3873 - 3894.

Li, L., & Warren, W. H. (2004). Path perception during rotation: influence of instructions, depth range, and dot density. *Vision Research*, *44*(16), 1879 - 1889.

Llewellyn, K. R. (1971). Visual guidance of locomotion. *Journal of Experimental Psychology*, *91*(2), 245.

Longuet-Higgins, H. C. (1981). A computer algorithm for reconstructing a scene from two projections. *Nature*, *293*(5828), 133.

Maciokas, J. B., & Britten, K. H. (2010). Extrastriate area MST and parietal area VIP similarly represent forward headings. *Journal of neurophysiology*, *104*(1), 239–247.

MacNeilage, P. R., Banks, M. S., DeAngelis, G. C., & Angelaki, D. E. (2010). Vestibular heading discrimination and sensitivity to linear acceleration in head and world coordinates. *Journal of Neuroscience*, *30*(27), 9084–9094.

MacNeilage, P. R., Turner, A. H., & Angelaki, D. E. (2010). Canal–otolith interactions and detection thresholds of linear and angular components during curved-path self-motion. *Journal of neurophysiology*, *104*(2), 765–773.

Nooij, S. A., Nesti, A., Bülthoff, H. H., & Pretto, P. (2016). Perception of rotation, path, and heading in circular trajectories. *Experimental brain research*, *234*(8), 2323–2337.

Oculus Rift DK2 specifications. (2018). `https://xinreality.com/wiki/Oculus_Rift_DK2`.

Oculus Rift specifications. (2018). `https://xinreality.com/wiki/Oculus_Rift`.

Perrone, J. A. (1992). Model for the computation of self-motion in biological systems. *JOSA A*, *9*(2), 177–194.

Perrone, J. A. (2004). A visual motion sensor based on the properties of V1 and MT neurons. *Vision research*, *44*(15), 1733–1755.

Perrone, J. A. (2012). A neural-based code for computing image velocity from small sets of middle temporal (mt/v5) neuron inputs. *Journal of Vision*, *12*(8), 1–1.

Perrone, J. A. (2018). Visual–vestibular estimation of the body's curvilinear motion through the world: A computational model. *Journal of vision*, *18*(4), 1–1.

Perrone, J. A., & Krauzlis, R. J. (2008). Vector subtraction using visual and extraretinal motion signals: A new look at efference copy and corollary discharge theories. *Journal of Vision*, *8*(14), 24–24.

Perrone, J. A., & Stone, L. S. (1994). A model of self-motion estimation within primate extrastriate visual cortex. *Vision research*, *34*(21), 2917–2938.

Poole, C. (2001). Low p-values or narrow confidence intervals: which are more durable? *Epidemiology*, *12*(3), 291–294.

Priest, H. F., Cutting, J. E., Torrey, C. C., & Regan, D. (1985). Visual flow and direction of locomotion. *Science*, *227*(4690), 1063–1064.

Regan, D., & Beverley, K. (1982). How do we avoid confounding the direction we are looking and the direction we are moving? *Science*, *215*(4529), 194–196.

Rieger, J. (1983). Information in optical flows induced by curved paths of observation. *JOSA*, *73*(3), 339–344.

Rieger, J., & Toet, L. (1985). Human visual navigation in the presence of 3-d rotations. *Biological cybernetics*, *52*(6), 377–381.

Rohde, M., van Dam, L. C., & Ernst, M. O. (2016). Statistically optimal multi-

sensory cue integration: a practical tutorial. *Multisensory research*, *29*(4-5), 279–317.

Royden, C. S. (1994). Analysis of misperceived observer motion during simulated eye rotations. *Vision research*, *34*(23), 3215–3222.

Royden, C. S. (1997). Mathematical analysis of motion-opponent mechanisms used in the determination of heading and depth. *JOSA A*, *14*(9), 2128–2143.

Royden, C. S., Banks, M. S., & Crowell, J. A. (1992). The perception of heading during eye movements. *Nature*, *360*(6404), 583.

Royden, C. S., Cahill, J. M., & Conti, D. M. (2006). Factors affecting curved versus straight path heading perception. *Perception & psychophysics*, *68*(2), 184–193.

Royden, C. S., Crowell, J. A., & Banks, M. S. (1994). Estimating heading during eye movements. *Vision Research*, *34*(23), 3197 - 3214.

Souman, J. L., & Freeman, T. C. (2008). Motion perception during sinusoidal smooth pursuit eye movements: Signal latencies and non-linearities. *Journal of Vision*, *8*(14), 10–10.

Sperry, R. W. (1950). Neural basis of the spontaneous optokinetic response produced by visual inversion. *Journal of comparative and physiological psychology*, *43*(6), 482.

Stang, A., Poole, C., & Kuss, O. (2010). The ongoing tyranny of statistical significance testing in biomedical research. *European journal of epidemiology*, *25*(4), 225–230.

Stang, A., & Rothman, K. J. (2011). That confounded p-value revisited. *Journal of Clinical Epidemiology*, *64*(9), 1047–1048.

Stone, L. S., & Perrone, J. A. (1997). Human heading estimation during visually simulated curvilinear motion. *Vision research*, *37*(5), 573–590.

Takahashi, K., Gu, Y., May, P. J., Newlands, S. D., DeAngelis, G. C., & Angelaki, D. E. (2007). Multimodal coding of three-dimensional rotation and translation in area mstd: comparison of visual and vestibular selectivity. *Journal of Neuroscience*, *27*(36), 9742–9756.

Tanaka, K., Fukada, Y., & Saito, H. (1989). Underlying mechanisms of the response specificity of expansion/contraction and rotation cells in the dorsal

part of the medial superior temporal area of the macaque monkey. *Journal of Neurophysiology*, *62*(3), 642–656.

Tanaka, K., Hikosaka, K., Saito, H.-a., Yukie, M., Fukada, Y., & Iwai, E. (1986). Analysis of local and wide-field movements in the superior temporal visual areas of the macaque monkey. *Journal of Neuroscience*, *6*(1), 134–144.

Telford, L., Howard, I. P., & Ohmi, M. (1995). Heading judgments during active and passive self-motion. *Experimental Brain Research*, *104*(3), 502–510.

Tsai, R., & Huang, T. (1981). Estimating three-dimensional motion parameters of a rigid planar patch. *IEEE Transactions on Acoustics, Speech, and Signal Processing*, *29*(6), 1147–1152.

Van den Berg, A. (1992). Robustness of perception of heading from optic flow. *Vision research*, *32*(7), 1285–1296.

van den Berg, A. (1996). Judgements of heading. *Vision Research*, *36*(15), 2337 - 2350.

van den Berg, A. V., & Beintema, J. A. (1997). Motion templates with eye velocity gain fields for transformation of retinal to head centric flow. *Neuroreport*, *8*(4), 835–840.

VIVE Specs. (2018). `https://www.vive.com/us/product/vive-virtual-reality-system/`.

Wann, J. P., Rushton, S., & Mon-Williams, M. (1995). Natural problems for stereoscopic depth perception in virtual environments. *Vision research*, *35*(19), 2731–2736.

Warren, R. (1976). The perception of egomotion. *Journal of Experimental Psychology: Human Perception and Performance*, *2*(3), 448.

Warren, W. H. (2003). Optic flow. In L. M. Chalupa & J. S. Werner (Eds.), *The visual neurosciences* (Vol. 2, p. 1247-1259). Cambridge, MA: Bradford.

Warren, W. H., Blackwell, A. W., Kurtz, K. J., Hatsopoulos, N. G., & Kalish, M. L. (1991). On the sufficiency of the velocity field for perception of heading. *Biological cybernetics*, *65*(5), 311–320.

Warren, W. H., & Hannon, D. J. (1988). Direction of self-motion is perceived from optical flow. *Nature*, *336*(6195), 162–163.

Warren, W. H., & Hannon, D. J. (1990). Eye movements and optical flow. *JOSA A*, *7*(1), 160–169.

Warren, W. H., Mestre, D. R., Blackwell, A. W., & Morris, M. W. (1991). Perception of circular heading from optical flow. *Journal of Experimental Psychology: Human Perception and Performance*, *17*(1), 28.

Warren, W. H., Morris, M. W., & Kalish, M. (1988). Perception of translational heading from optical flow. *Journal of Experimental Psychology: Human Perception and Performance*, *14*(4), 646.

Warren, W. H., & Saunders, J. A. (1995). Perceiving heading in the presence of moving objects. *Perception*, *24*(3), 315–331.

Watson, A. B., Ahumada, A. J., & Farrell, J. E. (1986). Window of visibility: a psychophysical theory of fidelity in time-sampled visual motion displays. *JOSA A*, *3*(3), 300–307.

Weng, J., Huang, T. S., & Ahuja, N. (1989). Motion and structure from two perspective views: Algorithms, error analysis, and error estimation. *IEEE transactions on pattern analysis and machine intelligence*, *11*(5), 451–476.

Whittaker, E. T. (1988). *A treatise on the analytical dynamics of particles and rigid bodies*. Cambridge University Press.

Zhang, J., & Yang, X. (2018). Distance perception in the vr was determined by where you virtually are and where you really are. *VSS conference Tampa Florida*.